ASM Handbook, Volume 9: Metallography and Microstructures
G.F. Vander Voort, editor, p670–700
DOI: 10.1361/asmhba0003767

Metallography and Microstructures of Stainless Steels and Maraging Steels

George F. Vander Voort and Gabriel M. Lucas, Buehler Ltd.
Elena P. Manilova, Polzunov Central Boiler and Turbine Institute, St. Petersburg, Russia

STAINLESS STEELS are complex alloys containing a minimum of 11% Cr plus other elements to produce ferritic, martensitic, austenitic, duplex, or precipitation-hardenable grades. Procedures used to prepare stainless steels for macroscopic and microscopic examination are similar to those used for carbon, alloy, and tool steels. However, certain types require careful attention to prevent artifacts. Because the austenitic grades work harden readily, cutting and grinding must be carefully executed to minimize deformation. The high-hardness martensitic grades that contain substantial undissolved chromium carbide are difficult to polish while fully retaining the carbides. The most difficult to such grades to prepare is AISI 440C. For the most part, preparation of stainless steels is reasonably simple if the basic rules for metallographic preparation are followed. However, unlike carbon, alloy, and tool steels, etching techniques are more difficult due to the high corrosion resistance of stainless steels and the various second phases that may be encountered. Nominal compositions of standard wrought grades illustrated in this article are given in Table 1. Compositions of some nonstandard alloys mentioned in this article are given in Table 2. Nominal compositions of cast stainless steel, in accordance with designations of the Alloy Casting Institute, are given in Tables 3 and 4 for corrosion-resistant and heat-resistant grades, respectively. Heat-resistant grades tend to have higher carbon contents for strengthening relative to corrosion-resistant grades of steel castings.

Macroexamination

The procedures used to select and prepare stainless steel disks for macroetching are identical to those used for carbon, alloy, and tool steels. Because these grades are more difficult to etch, however, all surfaces to be etched must be smooth ground or polished. Saw-cut surfaces will yield little useful information if they are macroetched.

Macroetchants for stainless steels are listed in Table 5. Heated macroetchants are used with stainless steels in the same manner as carbon, alloy, or tool steels. Etchant compositions are often more complex and more aggressive. In the study of weld macrostructures, it is quite common to polish the section and use one of the general-purpose microetchants.

The standard sulfur print technique (Ref 1) can be used to reveal the distribution of manganese sulfide (MnS) inclusions in stainless steels. However, if the manganese content of the grade is low, chromium will substitute for manganese in the sulfides, and the sulfur print intensity will decrease. As the manganese content decreases below approximately 0.60%, chromium substitutes for manganese. At manganese contents below approximately 0.20%, pure chromium sulfides will form. These produce no image in the sulfur print test.

Microexamination

Sectioning techniques for stainless steels are identical to those used for carbon, alloy, or tool steels. Grades softer than approximately 35 HRC can be cut using a band saw or power hacksaw. However, such cutting produces substantial deformation and should be avoided, especially for the deformation-sensitive austenitic grades. Deformation will be greatly reduced if cutting is performed using abrasive cutoff wheels with the proper degree of bonding. Shearing can be used with the ferritic grades but should be avoided with the austenitic grades. Shearing does produce substantial damage, and the plane-of-polish may be within this layer at the end of the preparation cycle. If this happens, the true microstructure will not be observed. Metallographic preparation is more successful, and easier, if an abrasive cutoff wheel designed for metallographic work with stainless steels is used. Figure 1 illustrates the damage that results when an austenitic stainless steel is sectioned using different procedures. Figure 2 shows sectioning damage in a 26Cr-1Mo ferritic stainless steel.

Mounting procedures, when required, are also identical to those used for carbon, alloy, and tool steels. If edge preservation is required for

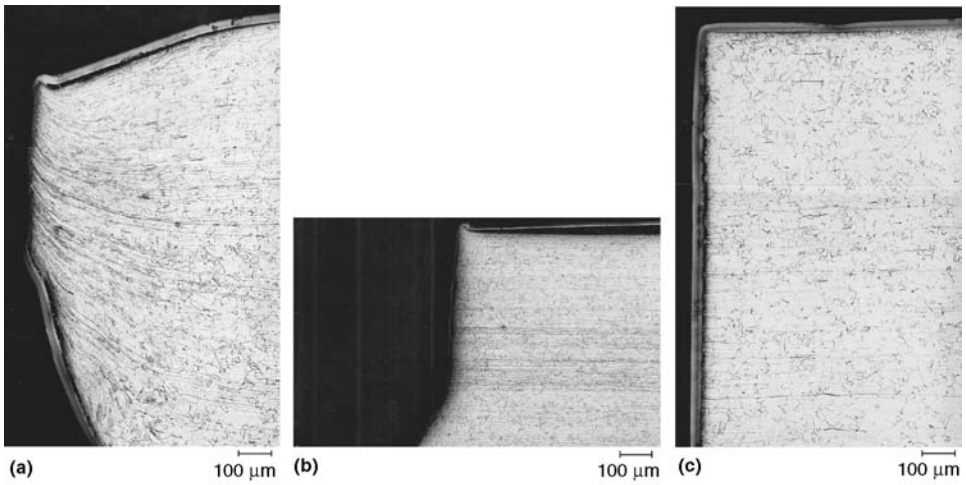

Fig. 1 Damage produced in sectioning austenitic 304 stainless steel using (a) metal shear, (b) band saw, and (c) abrasive cutoff saw. Glyceregia etch (electroless nickel plating used for the sheared and abrasive cutoff specimens)

Table 1 Compositions of standard wrought stainless steels

Type	UNS designation	Composition(a), %							
		C	Mn	Si	Cr	Ni	P	S	Other
Austenitic types									
201	S20100	0.15	5.5–7.5	1.00	16.0–18.0	3.5–5.5	0.06	0.03	0.25 N
202	S20200	0.15	7.5–10.0	1.00	17.0–19.0	4.0–6.0	0.06	0.03	0.25 N
205	S20500	0.12–0.25	14.0–15.5	1.00	16.5–18.0	1.0–1.75	0.06	0.03	0.32–0.40 N
301	S30100	0.15	2.00	1.00	16.0–18.0	6.0–8.0	0.045	0.03	. . .
302	S30200	0.15	2.00	1.00	17.0–19.0	8.0–10.0	0.045	0.03	. . .
302B	S30215	0.15	2.00	2.0–3.0	17.0–19.0	8.0–10.0	0.045	0.03	. . .
303	S30300	0.15	2.00	1.00	17.0–19.0	8.0–10.0	0.20	0.15 min	0.6 Mo(b)
303Se	S30323	0.15	2.00	1.00	17.0–19.0	8.0–10.0	0.20	0.06	0.15 min Se
304	S30400	0.08	2.00	1.00	18.0–20.0	8.0–10.5	0.045	0.03	. . .
304H	S30409	0.04–0.10	2.00	1.00	18.0–20.0	8.0–10.5	0.045	0.03	. . .
304L	S30403	0.03	2.00	1.00	18.0–20.0	8.0–12.0	0.045	0.03	. . .
304LN	S30453	0.03	2.00	1.00	18.0–20.0	8.0–12.0	0.045	0.03	0.10–0.16 N
302Cu	S30430	0.08	2.00	1.00	17.0–19.0	8.0–10.0	0.045	0.03	3.0–4.0 Cu
304N	S30451	0.08	2.00	1.00	18.0–20.0	8.0–10.5	0.045	0.03	0.10–0.16 N
305	S30500	0.12	2.00	1.00	17.0–19.0	10.5–13.0	0.045	0.03	. . .
308	S30800	0.08	2.00	1.00	19.0–21.0	10.0–12.0	0.045	0.03	. . .
309	S30900	0.20	2.00	1.00	22.0–24.0	12.0–15.0	0.045	0.03	. . .
309S	S30908	0.08	2.00	1.00	22.0–24.0	12.0–15.0	0.045	0.03	. . .
310	S31000	0.25	2.00	1.50	24.0–26.0	19.0–22.0	0.045	0.03	. . .
310S	S31008	0.08	2.00	1.50	24.0–26.0	19.0–22.0	0.045	0.03	. . .
314	S31400	0.25	2.00	1.5–3.0	23.0–26.0	19.0–22.0	0.045	0.03	. . .
316	S31600	0.08	2.00	1.00	16.0–18.0	10.0–14.0	0.045	0.03	2.0–3.0 Mo
316F	S31620	0.08	2.00	1.00	16.0–18.0	10.0–14.0	0.20	0.10 min	1.75–2.5 Mo
316H	S31609	0.04–0.10	2.00	1.00	16.0–18.0	10.0–14.0	0.045	0.03	2.0–3.0 Mo
316L	S31603	0.03	2.00	1.00	16.0–18.0	10.0–14.0	0.045	0.03	2.0–3.0 Mo
316LN	S31653	0.03	2.00	1.00	16.0–18.0	10.0–14.0	0.045	0.03	2.0–3.0 Mo; 0.10–0.16 N
316N	S31651	0.08	2.00	1.00	16.0–18.0	10.0–14.0	0.045	0.03	2.0–3.0 Mo; 0.10–0.16 N
317	S31700	0.08	2.00	1.00	18.0–20.0	11.0–15.0	0.045	0.03	3.0–4.0 Mo
317L	S31703	0.03	2.00	1.00	18.0–20.0	11.0–15.0	0.045	0.03	3.0–4.0 Mo
321	S32100	0.08	2.00	1.00	17.0–19.0	9.0–12.0	0.045	0.03	5 × %C min Ti
321H	S32109	0.04–0.10	2.00	1.00	17.0–19.0	9.0–12.0	0.045	0.03	5 × %C min Ti
330	N08330	0.08	2.00	0.75–1.5	17.0–20.0	34.0–37.0	0.04	0.03	. . .
347	S34700	0.08	2.00	1.00	17.0–19.0	9.0–13.0	0.045	0.03	10 × %C min Nb
347H	S34709	0.04–0.10	2.00	1.00	17.0–19.0	9.0–13.0	0.045	0.03	8 × %C min–1.0 max Nb
348	S34800	0.08	2.00	1.00	17.0–19.0	9.0–13.0	0.045	0.03	0.2 Co; 10 × %C min Nb; 0.10 Ta
348H	S34809	0.04–0.10	2.00	1.00	17.0–19.0	9.0–13.0	0.045	0.03	0.2 Co; 8 × %C min–1.0 max Nb; 0.10 Ta
384	S38400	0.08	2.00	1.00	15.0–17.0	17.0–19.0	0.045	0.03	. . .
Ferritic types									
405	S40500	0.08	1.00	1.00	11.5–14.5	. . .	0.04	0.03	0.10–0.30 Al
409	S40900	0.08	1.00	1.00	10.5–11.75	0.50	0.045	0.045	6 × %C min–0.75 max Ti
429	S42900	0.12	1.00	1.00	14.0–16.0	. . .	0.04	0.03	. . .
430	S43000	0.12	1.00	1.00	16.0–18.0	. . .	0.04	0.03	. . .
430F	S43020	0.12	1.25	1.00	16.0–18.0	. . .	0.06	0.15 min	0.6 Mo(b)
430FSe	S43023	0.12	1.25	1.00	16.0–18.0	. . .	0.06	0.06	0.15 min Se
434	S43400	0.12	1.00	1.00	16.0–18.0	. . .	0.04	0.03	0.75–1.25 Mo
436	S43600	0.12	1.00	1.00	16.0–18.0	. . .	0.04	0.03	0.75–1.25 Mo; 5 × %C min–0.70 max Nb
439	S43035	0.07	1.00	1.00	17.0–19.0	0.50	0.04	0.03	0.15 Al; 12 × %C min–1.10 Ti
442	S44200	0.20	1.00	1.00	18.0–23.0	. . .	0.04	0.03	. . .
444	S44400	0.025	1.00	1.00	17.5–19.5	1.00	0.04	0.03	1.75–2.50 Mo; 0.025 N; 0.2 + 4 (%C + %N) min–0.8 max (Ti + Nb)
446	S44600	0.20	1.50	1.00	23.0–27.0	. . .	0.04	0.03	0.25 N
Duplex (ferritic-austenitic) type									
329	S32900	0.20	1.00	0.75	23.0–28.0	2.50–5.00	0.040	0.030	1.00–2.00 Mo
Martensitic types									
403	S40300	0.15	1.00	0.50	11.5–13.0	. . .	0.04	0.03	. . .
410	S41000	0.15	1.00	1.00	11.5–13.5	. . .	0.04	0.03	. . .
414	S41400	0.15	1.00	1.00	11.5–13.5	1.25–2.50	0.04	0.03	. . .
416	S41600	0.15	1.25	1.00	12.0–14.0	. . .	0.06	0.15 min	0.6 Mo(b)
416Se	S41623	0.15	1.25	1.00	12.0–14.0	. . .	0.06	0.06	0.15 min Se
420	S42000	0.15 min	1.00	1.00	12.0–14.0	. . .	0.04	0.03	. . .
420F	S42020	0.15 min	1.25	1.00	12.0–14.0	. . .	0.06	0.15 min	0.6 Mo(b)
422	S42200	0.20–0.25	1.00	0.75	11.5–13.5	0.5–1.0	0.04	0.03	0.75–1.25 Mo; 0.75–1.25 W; 0.15–0.3 V
431	S43100	0.20	1.00	1.00	15.0–17.0	1.25–2.50	0.04	0.03	. . .
440A	S44002	0.60–0.75	1.00	1.00	16.0–18.0	. . .	0.04	0.03	0.75 Mo
440B	S44003	0.75–0.95	1.00	1.00	16.0–18.0	. . .	0.04	0.03	0.75 Mo
440C	S44004	0.95–1.20	1.00	1.00	16.0–18.0	. . .	0.04	0.03	0.75 Mo
Precipitation-hardening types									
PH 13-8 Mo	S13800	0.05	0.20	0.10	12.25–13.25	7.5–8.5	0.01	0.008	2.0–2.5 Mo; 0.90–1.35 Al; 0.01 N
15-5 PH	S15500	0.07	1.00	1.00	14.0–15.5	3.5–5.5	0.04	0.03	2.5–4.5 Cu; 0.15–0.45 Nb
17-4 PH	S17400	0.07	1.00	1.00	15.5–17.5	3.0–5.0	0.04	0.03	3.0–5.0 Cu; 0.15–0.45 Nb
17-7 PH	S17700	0.09	1.00	1.00	16.0–18.0	6.5–7.75	0.04	0.04	0.75–1.5 Al

(a) Single values are maximum values unless otherwise indicated. (b) Optional

near-surface examination, compression-mounting epoxy can be used, or specimens can be plated with electroless nickel. For specimens with surface cracks, it may be useful to vacuum impregnate the specimen in cold-setting epoxy; epoxy will be drawn into the cracks, minimizing bleed-out problems after etching.

Grinding has traditionally been performed using 120-, 240-, 320-, 400-, then 600-grit (P120-, P280-, P400-, P600-, and P1200-grit) water-cooled silicon carbide (SiC) papers. Care must be taken, particularly when grinding austenitic grades, to remove the cold work from cutting and from each grinding step. In general, speeds of 240 to 300 rpm and moderate, firm pressure are used. Grinding times are 1 to 2 min per step. If grinding is carried out by hand, the specimen should be rotated 45 to 90° between each step. Automatic grinding devices produce omnidirectional grinding patterns.

Polishing. After grinding, in the traditional method, specimens were usually rough polished using 6 or 3 μm diamond as a paste, spray, or slurry on napless, low-nap, or medium-nap cloths. Edge flatness and inclusion retention are improved by using napless cloths, although scratch removal may not be as complete as with medium-nap cloths. A lubricant extender compatible with the diamond abrasive should be used to moisten the cloth and reduce drag. A wheel speed of 120 to 150 rpm is usually adequate. Pressure should be moderate and firm; specimen rocking should be avoided if polishing is carried out by hand.

For hand polishing, rotate the specimen around the wheel in the direction opposite to the wheel rotation direction (contra rotation) while moving from center to edge. Automatic devices produce better edge flatness than hand polishing. After this step, the specimen may be polished using 1 μm diamond abrasive on a medium-nap cloth. For routine examination, a 1 μm diamond finish may be adequate, particularly for the hardened grades.

To produce high-quality, scratch-free surfaces suitable for photomicroscopy, specimens should be final polished using one or more fine abrasives. The most commonly used final abrasives are 0.3 μm α-alumina (Al_2O_3) or 0.05 μm γ-Al_2O_3. Medium-nap cloths are usually used. Polishing with these abrasives, mixed as a water slurry, is performed in the same manner as diamond polishing. Specimens should be carefully cleaned between each rough and final polishing step to avoid contamination at the next step. Colloidal silica is a highly suitable final abrasive for stainless steels. However, its use is more complicated, because cleaning is more difficult. Also, if colloidal silica is used, and the etchant contains Cl^- ions, such as Vilella's reagent or glyceregia, an unusual etch reaction often occurs as soon as the etch touches the specimen surface. Examination reveals a heavy scratch pattern that can only be removed by going back to SiC paper. This problem has been called flashing and is illustrated in Fig. 3. Consequently, many metallographers avoid using colloidal silica. Electrolytic reagents do not flash, even if colloidal silica is used. The alumina powders and suspensions do exhibit agglomeration of particles, even in the deagglomerated grades (better, but still has agglomerates). Sol-gel processed alumina suspensions are free from this problem and produce excellent polished surfaces without staining or flashing problems.

Modern preparation procedures use only one grinding step and fewer overall steps. Further, they employ napless surfaces in all but the final step. This yields more efficient procedures, better edge retention, better flatness and relief control, and fewer artifact problems. Table 6 lists a contemporary procedure excellent for all stain-

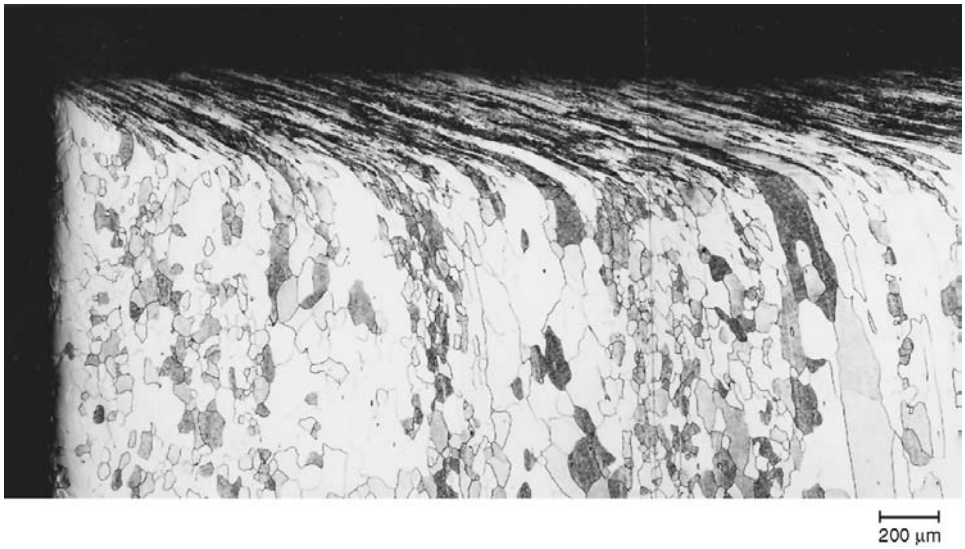

Fig. 2 Damage produced when 26Cr-1Mo ferritic stainless steel was cut with a band saw. Acetic glyceregia etch

Table 2 Compositions of nonstandard wrought stainless steels

Grade	UNS No.	Composition, wt%								
		C	Mn	Si	Cr	Ni	Mo	Cu	N	Other
Austenitic types										
Nitronic 50(a)	...	<0.06	5.0	...	22	13	2.25	...	0.3	0.2 Nb, 0.2 V
20 Mo-6 HS	NO8036	<0.06	<1.0	...	24	35	5.75	2	0.3	...
AL-6XN	NO8067	<0.03	<2	<1	21	24.5	6.5	<0.75	0.2	...
SCF-23	...	0.02	4.25	0.45	22.75	17.75	5.5	...	0.4	...
NeutraSorb PLUS	...	<0.08	<2	<0.75	19	13.5	...	...	<0.1	≤2.25 B
18-18 PLUS	...	<0.15	18	<1	18	...	1	1	0.5	...
Ferritic types										
Monit	44635	<0.025	<1	<0.75	25	4	4	...	<0.035	Nb + Ta = 0.2 + 4(C + N)
Seacure	44660	<0.025	0.5	...	27.5	1.2	3.5	...	0.025	0.5 Ti
Martensitic types										
EP 428	...	0.2	0.6	<0.4	11.5	0.65	0.6	...	...	0.9 W, 0.22 V
Trimrite	S42012	0.02	...	...	14.25	0.6	0.7	...	...	...
5F(b)	S41600	<0.1	...	...	13.25	...	...	...	...	>0.3 S
Maraging types										
Vascomax T-250 (cobalt-free grade)	...	<0.03	<0.1	<0.1	...	18.5	3	...	...	0.1 Al, 1.4 Ti

(a) Trade name for 22-13-5 (generic name). (b) Modified 416

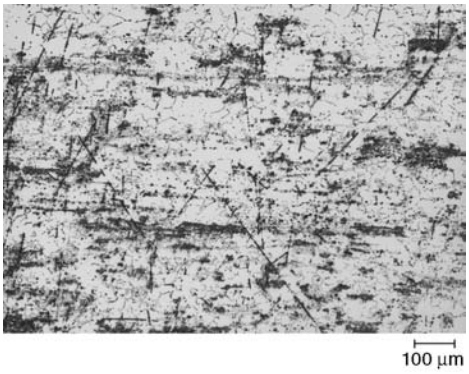

Fig. 3 Example of flashing when a stainless steel (duplex stainless steel in this case), polished with colloidal silica, is etched with a reagent containing chlorine ions. Glyceregia etch

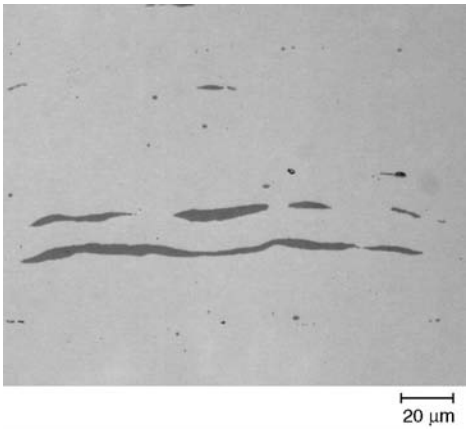

Fig. 4 Manganese sulfides (some chromium substitutes for manganese) in type 416 stainless steel

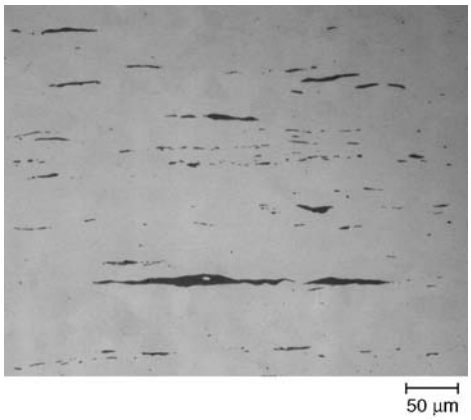

Fig. 5 Manganese sulfides in type 203 stainless steel

Table 3 Compositions and typical microstructures of Alloy Casting Institute (ACI) corrosion-resistant cast stainless steels

ACI type	Wrought alloy type(a)	ASTM specifications	Most common end-use microstructure	Composition(b), %					
				C	Mn	Si	Cr	Ni	Others(c)
Chromium steels									
CA-15	410	A 743, A 217, A 487	Martensite	0.15	1.00	1.50	11.5–14.0	1.0	0.50 Mo(d)
CA-15M	. . .	A 743	Martensite	0.15	1.00	0.65	11.5–14.0	1.0	0.15–1.00 Mo
CA-40	420	A 743	Martensite	0.40	1.00	1.50	11.5–14.0	1.0	0.5 Mo(d)
CA-40F	. . .	A 743	Martensite	0.2–0.4	1.00	1.50	11.5–14.0	1.0	. . .
CB-30	431, 442	A 743	Ferrite and carbides	0.30	1.00	1.50	18.0–22.0	2.0	. . .
CC-50	446	A 743	Ferrite and carbides	0.30	1.00	1.50	26.0–30.0	4.0	. . .
Chromium-nickel steels									
CA-6N	. . .	A 743	Martensite	0.06	0.50	1.00	10.5–12.5	6.0–8.0	. . .
CA-6NM	. . .	A 743, A 487	Martensite	0.06	1.00	1.00	11.5–14.0	3.5–4.5	0.4–1.0 Mo
CA-28MWV	. . .	A 743	Martensite	0.20–0.28	0.50–1.00	1.00	11.0–12.5	0.50–1.00	0.9–1.25 Mo; 0.9–1.25 W; 0.2–0.3 V
CB-7Cu-1	. . .	A 747	Martensite, age hardenable	0.07	0.70	1.00	15.5–17.7	3.6–4.6	2.5–3.2 Cu; 0.20–0.35 Nb; 0.05 N max
CB-7Cu-2	. . .	A 747	Martensite, age hardenable	0.07	0.70	1.00	14.0–15.5	4.5–5.5	2.5–3.2 Cu; 0.20–0.35 Nb; 0.05 N max
CD-4MCu	. . .	A 351, A 743, A 744, A 890	Austenite in ferrite, age hardenable	0.04	1.00	1.00	25.0–26.5	4.75–6.0	1.75–2.25 Mo; 2.75–3.25 Cu
CE-30	312	A 743	Ferrite in austenite	0.30	1.50	2.00	26.0–30.0	8.0–11.0	. . .
CF-3(e)	304L	A 351, A 743, A 744	Ferrite in austenite	0.03	1.50	2.00	17.0–21.0	8.0–12.0	. . .
CF-3M(e)	316L	A 351, A 743, A 744	Ferrite in austenite	0.03	1.50	2.00	17.0–21.0	8.0–12.0	2.0–3.0 Mo
CF-3MN	. . .	A 743	Ferrite in austenite	0.03	1.50	1.50	17.0–21.0	9.0–13.0	2.0–3.0 Mo; 0.10–0.20 N
CF-8(e)	304	A 351, A 743, A 744	Ferrite in austenite	0.08	1.50	2.00	18.0–21.0	8.0–11.0	. . .
CF-8C	347	A 351, A 743, A 744	Ferrite in austenite	0.08	1.50	2.00	18.0–21.0	9.0–12.0	Nb(f)
CF-8M	316	A 351, A 743, A 744	Ferrite in austenite	0.08	1.50	2.00	18.0–21.0	9.0–12.0	2.0–3.0 Mo
CF-10	. . .	A 351	Ferrite in austenite	0.04–0.10	1.50	2.00	18.0–21.0	8.0–11.0	. . .
CF-10M	. . .	A 351	Ferrite in austenite	0.04–0.10	1.50	1.50	18.0–21.0	9.0–12.0	2.0–3.0 Mo
CF-10MC	. . .	A 351	Ferrite in austenite	0.10	1.50	1.50	15.0–18.0	13.0–16.0	1.75–2.25 Mo
CF-10SMnN	. . .	A 351, A 743	Ferrite in austenite	0.10	7.00–9.00	3.50–4.50	16.0–18.0	8.0–9.0	0.08–0.18 N
CF-12M	316	. . .	Ferrite in austenite or austenite	0.12	1.50	2.00	18.0–21.0	9.0–12.0	2.0–3.0 Mo
CF-16F	303	A 743	Austenite	0.16	1.50	2.00	18.0–21.0	9.0–12.0	1.50 Mo max; 0.20–0.35 Se
CF-20	302	A 743	Austenite	0.20	1.50	2.00	18.0–21.0	8.0–11.0	. . .
CG-6MMN	. . .	A 351, A 743	Ferrite in austenite	0.06	4.00–6.00	1.00	20.5–23.5	11.5–13.5	1.50–3.00 Mo; 0.10–0.30 Nb; 0.10–30 V; 0.20–40 N
CG-8M	317	A 351, A 743, A 744	Ferrite in austenite	0.08	1.50	1.50	18.0–21.0	9.0–13.0	3.0–4.0 Mo
CG-12	. . .	A 743	Ferrite in austenite	0.12	1.50	2.00	20.0–23.0	10.0–13.0	. . .
CH-8	. . .	A 351	Ferrite in austenite	0.08	1.50	1.50	22.0–26.0	12.0–15.0	. . .
CH-10	. . .	A 351	Ferrite in austenite	0.04–0.10	1.50	2.00	22.0–26.0	12.0–15.0	. . .
CH-20	309	A 351, A 743	Austenite	0.20	1.50	2.00	22.0–26.0	12.0–15.0	. . .
CK-3MCuN	. . .	A 351, A 743, A 744	Ferrite in austenite	0.025	1.20	1.00	19.5–20.5	17.5–19.5	6.0–7.0 V; 0.18–0.24 N; 0.50–1.00 Cu
CK-20	310	A 743	Austenite	0.20	2.00	2.00	23.0–27.0	19.0–22.0	. . .
Nickel-chromium steel									
CN-3M	. . .	A 743	Austenite	0.03	2.00	1.00	20.0–22.0	23.0–27.0	4.5–5.5 Mo
CN-7M	. . .	A 351, A 743, A 744	Austenite	0.07	1.50	1.50	19.0–22.0	27.5–30.5	2.0–3.0 Mo; 3.0–4.0 Cu
CN-7MS	. . .	A 743, A 744	Austenite	0.07	1.50	3.50(g)	18.0–20.0	22.0–25.0	2.5–3.0 Mo; 1.5–2.0 Cu
CT-15C	. . .	A 351	Austenite	0.05–0.15	0.15–1.50	0.50–1.50	19.0–21.0	31.0–34.0	0.5–1.5 V

(a) Type numbers of wrought alloys are listed only for nominal identification of corresponding wrought and cast grades. Composition ranges of cast alloys are not the same as for corresponding wrought alloys; cast alloy designations should be used for castings only. (b) Maximum unless a range is given. The balance of all compositions is iron. (c) Sulfur content is 0.04% in all grades except: CG-6MMN, 0.030% S (max); CF-10SMnN, 0.03% S (max); CT-15C, 0.03% S (max); CK-3MCuN, 0.010% S (max); CN-3M, 0.030% S (max), CA-6N, 0.020% S (max); CA-28MWV, 0.030% S (max); CA-40F, 0.20–0.40% S; CB-7Cu-1 and -2, 0.03% S (max). Phosphorus content is 0.04% (max) in all grades except: CF-16F, 0.17% P (max); CF-10SMnN, 0.060% P (max); CT-15C, 0.030% P (max); CK-3MCuN, 0.045% P (max); CN-3M, 0.030% P (max); CA-6N, 0.020% P (max); CA-28MWV, 0.030% P (max); CB-7Cu-1 and -2, 0.035% P (max). (d) Molybdenum not intentionally added. (e) CF-3A, CF-3MA, and CF-8A have the same composition ranges as CF-3, CF-3M, and CF-8, respectively, but have balanced compositions so that ferrite contents are at levels that permit higher mechanical property specifications than those for related grades. They are covered by ASTM A 351. (f) Nb, 8 × %C min (1.0% max); or Nb + Ta × %C (1.1% max). (g) For CN-7MS, silicon ranges from 2.50 to 3.50%.

Table 4 Compositions of Alloy Casting Institute (ACI) heat-resistant casting alloys

ACI designation	UNS number	ASTM specifications(a)	Composition(b), % C	Cr	Ni	Si (max)
HA	. . .	A 217	0.20 max	8–10	. . .	1.00
HC	J92605	A 297, A 608	0.50 max	26–30	4 max	2.00
HD	J93005	A 297, A 608	0.50 max	26–30	4–7	2.00
HE	J93403	A 297, A 608	0.20–0.50	26–30	8–11	2.00
HF	J92603	A 297, A 608	0.20–0.40	19–23	9–12	2.00
HH	J93503	A 297, A 608, A 447	0.20–0.50	24–28	11–14	2.00
HI	J94003	A 297, A 567, A 608	0.20–0.50	26–30	14–18	2.00
HK	J94224	A 297, A 351, A 567, A 608	0.20–0.60	24–28	18–22	2.00
HK30	. . .	A 351	0.25–0.35	23.0–27.0	19.0–22.0	1.75
HK40	. . .	A 351	0.35–0.45	23.0–27.0	19.0–22.0	1.75
HL	J94604	A 297, A 608	0.20–0.60	28–32	18–22	2.00
HN	J94213	A 297, A 608	0.20–0.50	19–23	23–27	2.00
HP	. . .	A 297	0.35–0.75	24–28	33–37	2.00
HP-50WZ(c)	. . .	. . .	0.45–0.55	24–28	33–37	2.50
HT	J94605	A 297, A 351, A 567, A 608	0.35–0.75	13–17	33–37	2.50
HT30	. . .	A 351	0.25–0.35	13.0–17.0	33.0–37.0	2.50
HU	. . .	A 297, A 608	0.35–0.75	17–21	37–41	2.50
HW	. . .	A 297, A 608	0.35–0.75	10–14	58–62	2.50
HX	. . .	A 297, A 608	0.35–0.75	15–19	64–68	2.50

(a) ASTM designations are the same as ACI designations. (b) Bal Fe in all compositions. Manganese content: 0.35 to 0.65% for HA, 1% for HC, 1.5% for HD, and 2% for the other alloys. Phosphorus and sulfur contents: 0.04% (max) for all but HP-50WZ. Molybdenum is intentionally added only to HA, which has 0.90 to 1.20% Mo; maximum for other alloys is set at 0.5% Mo. HH also contains 0.2% N (max). (c) Also contains 4 to 6% W, 0.1 to 1.0% Zr, and 0.035% S (max) and P (max)

Table 5 Macroetchants for stainless steels

Etchant	Comments
1. 50 mL HCl, 10 g $CuSO_4$ (copper sulfate), 50 mL H_2O(a)	Marble's reagent. General-purpose macroetch; can be heated
2. 50 mL HCl, 50 mL H_2O, 20 mL 30% H_2O_2	Mix HCl and H_2O, heat to 70–75 °C (160–170 °F). Immerse specimen and add H_2O_2 in steps when foaming stops; do not mix
3. (a) 15 g $(NH_4)_2S_2O_8$ (ammonium persulfate) and 75 mL H_2O (b) 250 g $FeCl_3$ and 100 mL H_2O (c) 30 mL HNO_3	Lepito's No. 1 etch. Combine (a) and (b), then add (c); immerse specimen at room temperature; use fresh
4. 1 part HCl and 1 part H_2O	Standard hot etch. Use at 70–80 °C (160–180 °F), 15–45 min; desmut by dipping in warm 20% aqueous HNO_3 solution to produce a bright surface
5. 10–40 mL HNO_3, 3–10 mL 48% HF, 25–50 mL H_2O	Use at 70–80 °C (160–180 °F); immerse until the desired degree of contrast is obtained
6. 50 mL HCl and 25 mL saturated $CuSO_4$ in H_2O	Use at 75 °C (170 °F); immerse until the desired degree of contrast is obtained

(a) When water is specified, use distilled water.

Table 6 Contemporary procedure for preparing stainless steels and maraging alloys

Step	Surface	Abrasive/size	Load per specimen N	lbf	Base speed, rpm Direction	Time, min
1.	Waterproof abrasive paper	120–320 grit (P120–P400), water cooled	27	6	240–300 Complementary	Until planar
2.	Silk	9 μm diamond with lubricant	27	6	120–150 Complementary or contra	5
3.	Silk, polyester, or synthetic chemotextile	3 μm diamond with lubricant	27	6	120–150 Complementary or contra	4
4.	Silk, polyester, or synthetic chemotextile	1 μm diamond with lubricant	27	6	120–150 Complementary or contra	3
5.	Medium-nap synthetic rayon or polyurethane	0.05 μm sol-gel alumina suspension	27	6	100–150 Complementary or contra	1–3

Notes: 1) Step 4 is optional and is used for the more difficult grades and heat treatment conditions. 2) Use a sectioning technique that produces minimal damage. Then, choose the finest possible SiC grit size that will remove this damage in a short time. Surfaces cut with band saws and power hacksaws, or that are sheared, will exhibit substantial damage depths that must be removed. 3) Use pressure-sensitive adhesive-backed surfaces for best results, especially when using automated equipment. 4) In step 1, do not use one sheet of SiC paper longer than 60 s when preparing several specimens in a holder. Use more than one sheet, if needed. Other types of abrasive surfaces with a similar abrasive particle size may be substituted but should be evaluated to be sure that they do not produce excessive damage. 5) Complementary rotation means that the head and platen both rotate in the same (counterclockwise) direction. Contra means that the head rotates clockwise, opposite the platen direction, which is slightly more aggressive. If the head speed is <100 rpm, one can use contra, and liquid abrasives will stay on the polishing surface longer. If the head speed is >100 rpm, the abrasive will be splattered all over the operator and the walls. Contra rotation in step 5 may cause excessive relief around MnS particles. If that happens, repeat step 5 using complementary rotation. 6) Colloidal silica can lead to the flashing problem, as described in text, when using etchings containing chlorine ions. 7) In step 5, when polyurethane is used, increase the load to 31 or 36 N (7 or 8 lbf). 8) When using diamond abrasive, charge the cloth with paste and press the paste into the cloth surface. Then, add the appropriate lubricant. During the cycle, add diamond of the same size in slurry form to maintain a high cutting rate.

less steels and maraging steels. Some substitution can be made at each step, depending on personal preference.

Stainless steels, particularly the austenitic grades, are often polished electrolytically. In most cases, electropolishing is performed after grinding to a 600-grit silicon carbide finish. Table 7 lists recommended procedures. Electropolishing usually produces high-quality, deformation-free surfaces; however, inclusion attack is encountered, and second phases, cracks, and edges may be attacked preferentially.

Etching. For inclusion examination, etching is not required, although it is necessary for examining the microstructure. Figures 4 to 7 illustrate sulfide inclusions in several common stainless steels designed for improved machinability. Although the stainless steels are reasonably easy to polish, etching is generally a more difficult step. The corrosion resistance of stainless steels and the potential microstructural complexity of these alloys make selection of the best etchant a more difficult problem than for carbon and alloy steels. In general, no one etchant will be suitable for a wide range of compositions. As the corrosion resistance of the alloys increases, stronger and stronger etchants must be used. Many of these etchants will attack the sulfide inclusions in resulfurized steels with improved machinability.

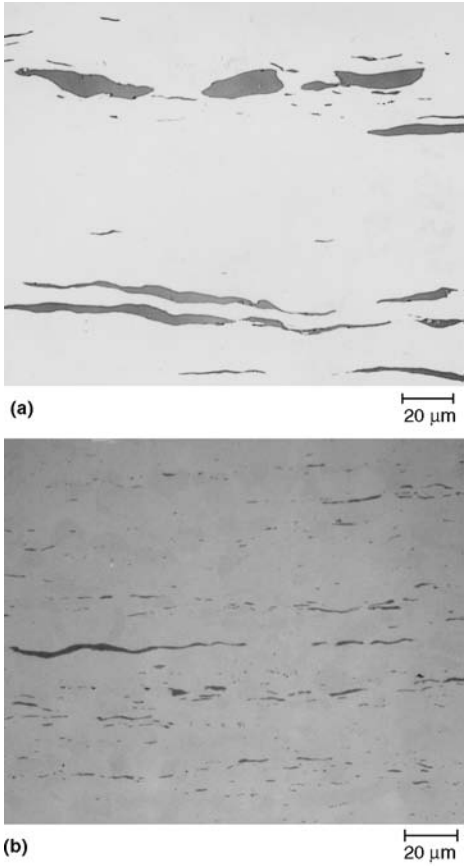

Fig. 6 Manganese sulfides in (a) a billet of ingot-cast type 303 stainless steel and (b) a bar of continuously cast 303 stainless steel

Stainless steel etchant ingredients are dissolved in water, methanol or ethanol, glycerol, or a mixture of these solvents. Reagents with alcohol or glycerol as the solvent provide better wetting of the surface than water-based reagents and generally provide more uniform etching. Because alcohol reduces dissociation, alcohol-based reagents can be made more concentrated without becoming too powerful for controlled etching. Stainless steel surfaces passivate; therefore, reducing conditions are preferred to oxidizing conditions that promote passivity. Consequently, stainless steel etchants often contain hydrochloric (HCl), sulfuric (H_2SO_4), or hydrofluoric (HF) acid, although nitric acid (HNO_3) may be used alone or mixed with HCl to produce aqua regia or a modified aqua regia. Swabbing, instead of immersion, may be desired to obtain more uniform etch results. Electrolytic etching is also very popular, because it produces uniform etching, is easier to control, and gives reproducible results. Numerous etchants have been proposed for stainless steels; each has advantages and disadvantages.

Etching the 400-series ferritic or martensitic grades is simpler than the 200- or 300-series austenitic grades or the 600-series precipitation-hardenable grades. Vilella's reagent (or 4% picral + HCl), superpicral, modified Fry's reagent, or Ralph's reagent (does not attack sulfide inclusions) are commonly used with ferritic, martensitic, and precipitation-hardenable stainless steels and maraging steel grades. However, these reagents will not be suitable for the most corrosion-resistant precipitation-hardenable grades, and a stronger etch must be used, such as glyceregia or waterless Kalling's. Etching of the extra low-interstitial-content ferritic grades to observe the grain boundaries, however, is much more difficult than the ordinary ferritic grades. The best etchant for ferritic grades is electrolytic 60% HNO_3, as illustrated in Fig. 8. Additional examples are given elsewhere in this article. Microetchants for stainless steels are listed in Table 8.

Etching of the austenitic grades to examine the grain structure is difficult with most standard reagents. As shown in the illustrations, most of the standard reagents reveal only a portion of the grain and twin boundaries. Tint etching, which requires a high-quality polish for good results, reveals all of the grains by color contrast. Figure 9(a) shows the grain structure of 316L austenitic stainless steel etched with waterless Kalling's (Kalling's No. 2) reagent, where many, but not all, of the grain boundaries and twin boundaries are revealed. This is inadequate for an actual measurement of grain size. Figure 9(b) shows the same specimen after tint etching with a Beraha reagent that colors all of the grains (shown in black and white). Additional examples of tint-etched stainless steels, but in color, can be found in the article "Color Metallography" in this Volume. To measure the grain size when a more accurate value is required than can be obtained by a comparison chart rating, all the boundaries must be revealed. Twin boundaries are ignored.

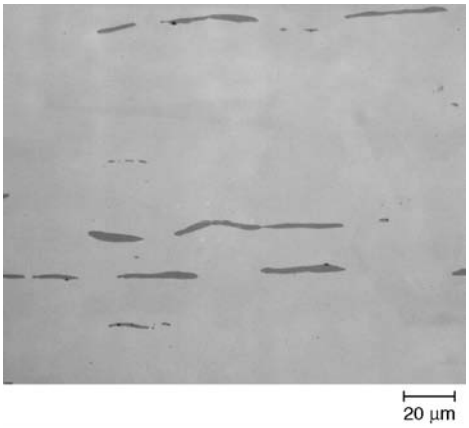

Fig. 7 Manganese selenides in type 303Se stainless steel

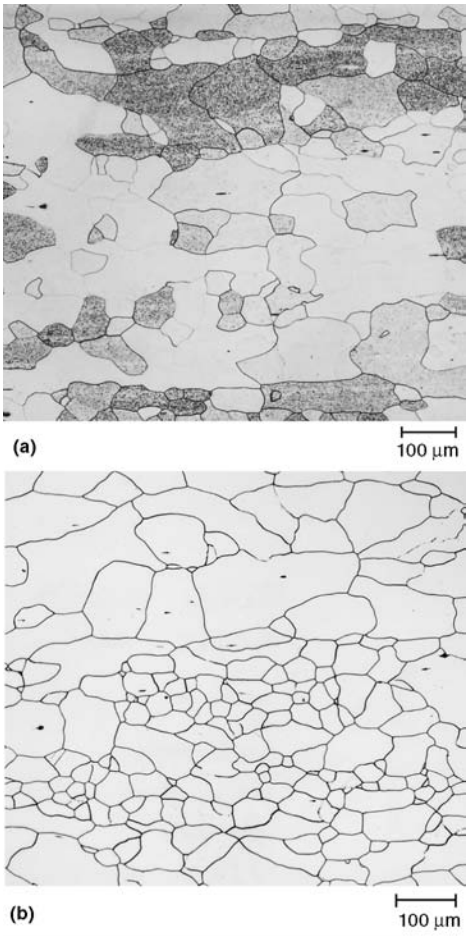

Fig. 8 Microstructure of annealed 26Cr-1Mo E-Brite ferritic stainless steel, revealed using (a) acetic glyceregia and (b) aqueous 60% HNO_3 at 1.2 V dc for 120 s

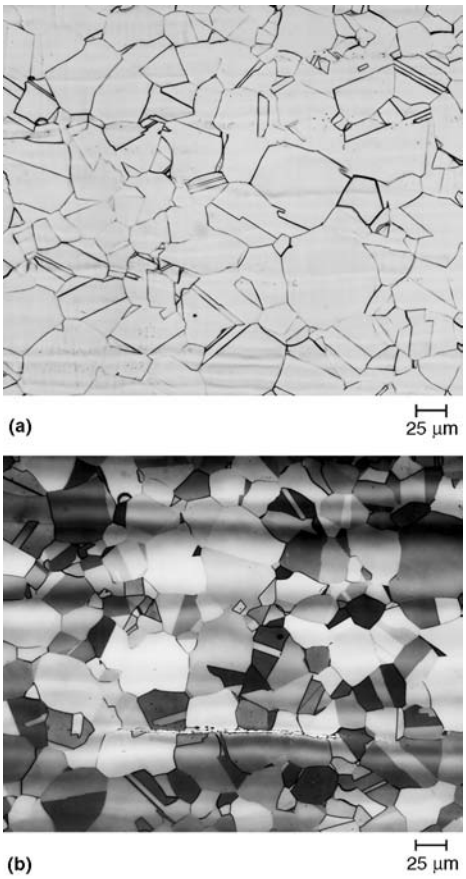

Fig. 9 Grain structure of austenitic type 316L, solution annealed at 954 °C (1750 °F) and etched with (a) waterless Kalling's and (b) Beraha's tint etch

Table 7 Electropolishing procedures for stainless steels

Electrolyte composition	Comments
1. 50 mL $HClO_4$ (perchloric acid), 750 mL ethanol, 140 mL H_2O(a)	Add $HClO_4$ last, with care. Use at 8–20 V dc, 0.3–1.3 A/cm^2 (1.9–8.4 A/in.^{2}), 20 °C (70 °F), 20–60 s. Rinse immediately after polishing
2. 78 mL $HClO_4$, 90 mL H_2O, 730 mL ethanol, 100 mL butyl cellusolve	Add $HClO_4$ last, with care. Use at 0.5–1.5 A/cm^2 (3.2–9.7 A/in.^{2}), 20 °C (70 °F) max
3. 62 mL $HClO_4$, 700 mL ethanol, 100 mL butyl cellusolve, 137 mL H_2O	Add $HClO_4$ last, with care. Use at 1.2 A/cm^2 (7.7 A/in.^{2}), 20 °C (70 °F), 20–25 s
4. 25 g CrO_3, 133 mL acetic acid, 7 mL H_2O	Use at 20 V dc, 0.09–0.22 A/cm^2 (0.58–1.4 A/in.^{2}), 17–19 °C (63–66 °F), 6 min. Dissolve CrO_3 in solution heated to 60–70 °C (140–160 °F)
5. 37 mL H_3PO_4, 56 mL glycerol, 7 mL H_2O	Use at 0.78 A/cm^2 (5.0 A/in.^{2}), 100–120 °C (210–250 °F), 5–10 min
6. 6 mL $HClO_4$ and 94 mL ethanol	Use at 35–40 V dc, 24 °C (75 °F), 15–60 s

(a) When water is specified, use distilled water.

Sensitizing the specimen by heating it for 1 to 6 h at 650 °C (1200 °F) will facilitate revealing the grain boundaries. However, the carbon content must be >0.03% to develop enough grain-boundary carbides to reveal the grains. Examples are shown in Fig. 10 and 11. Electrolytic 10% ammonium persulfate is an excellent etchant for sensitized stainless steels, because it colors the chromium carbides brown. Today, most steelmakers are melting to the L-carbon requirement, regardless of whether the grade being purchased is the standard carbon level or the L version for weldability, to save inventory costs. This method is not as successful for the low-carbon versions, because less $M_{23}C_6$ carbide can be precipitated at the grain boundaries.

An alternate technique (Ref 2, 3) that does not depend on the carbon content involves electrolytically etching the solution-annealed specimen with aqueous 60% HNO_3 (Table 8). With this procedure, twin boundaries are not revealed as long as the voltage is kept low. Figure 12 shows the 316L specimen previously shown in Fig. 9 after electrolytic etching with 60% nitric acid in water. Note that virtually all of the grain boundaries are revealed. A few minor problems can be seen within certain grains, but these can be removed with image-editing techniques and are easily ignored in manual measurements. Figure 13 shows an additional example where a solution-annealed specimen of 316 grade has been etched with three standard reagents and two electrolytic reagents, including 60% nitric acid in water. The clear superiority of this etchant is evident in these micrographs. This etchant will also bring out prior-austenite grain boundaries in solution-annealed, but not aged, precipitation-hardened grades, including maraging grades. For structure-property correlations, the mean lineal intercept value for grain and twin boundaries should be measured, because the twin boundaries also contribute to strengthening. Such a measurement should not be converted to a grain size value.

Various alkaline ferricyanide reagents, such as Murakami's reagent and its numerous modifications, have been widely used to etch austenitic stainless steels for phase identification. The col-

Table 8 Microetchants for stainless steel

Etchants	Comments
1. 1 g picric acid, 5 mL HCl, 100 mL ethanol	Vilella's reagent. Use at room temperature to 1 min. Outlines second-phase particles (carbides, σ phase, δ-ferrite); etches martensite. Can be stored
2. 1.5 g $CuCl_2$ (cupric chloride), 33 mL HCl, 33 mL ethanol, 33 mL H_2O(a)	Kalling's No. 1 reagent for martensitic stainless steels. Use at room temperature. Martensite dark, ferrite colored, austenite not attacked. Can be stored
3. 5 g $CuCl_2$, 100 mL HCl, 100 mL ethanol	Kalling's No. 2 reagent. Use at room temperature. Ferrite attacked rapidly, austenite slightly attacked, carbides not attacked. Can be stored
4. 5 g $CuCl_2$, 40 mL HCl, 30 mL H_2O, 25 mL ethanol	Fry's reagent. For martensitic and precipitation-hardenable grades. Use at room temperature. Can be stored
5. 1 g $CuCl_2$, 50 mL HCl, 150 mL H_2O, 50 mL HNO_3	Modified Fry's (Spaeder) for martensitic stainless steels, precipitation-hardenable stainless steels, and maraging steels. Use at room temperature. Can be stored
6. 4 g $CuSO_4$, 20 mL HCl, 20 mL H_2O	Marble's reagent. Used primarily with austenitic grades. Use at room temperature to 10 s. Attacks σ phase
7. 3 parts HCl, 2 parts glycerol, 1 part HNO_3	Glyceregia. Popular etch for all stainless grades. Use fresh; never store. Discard when reagent is orange colored. Use with care under a hood. Add HNO_3 last. Swab a few seconds to a few minutes. Attacks σ phase, outlines carbides. Substitution of water for glycerol increases attack rate.
8. 3 parts HCl, 2 parts acetic acid, 1 part HNO_3, 2 drops glycerol	Acetic glyceregia. Use as glyceregia (stronger).
9. 3 parts HCl, 2 parts acetic acid, 2 parts HNO_3	15-10-10 reagent. Use as glyceregia (more aggressive). Good for grades such as alloy 625 that are difficult to etch
10. 45 mL HCl, 15 mL HNO_3, 20 mL methanol	Methanolic aqua regia. Used with austenitic grades to reveal grain structure, outline ferrite and σ phase
11. 15 mL HCl, 5 mL HNO_3, 100 mL H_2O	Dilute aqua regia for austenitic grades. Uniform etching of austenite; outlines carbides, σ phase, and ferrite (sometimes attacked)
12. 4 g $KMnO_4$ (potassium permanganate), 4 g NaOH, 100 mL H_2O	Groesbeck's reagent. Use at 60–90 °C (140–195 °F) to 10 min. Colors carbides dark, σ phase gray, ferrite and austenite not affected
13. 30 g $KMnO_4$, 30 g NaOH, 100 mL H_2O	Modified Groesbeck's reagent. Use at 90–100 °C (195–210 °F) for 20 s to 10 min to color ferrite dark in duplex alloys. Austenite not affected
14. 10 g $K_3Fe(CN)_6$, 10 g KOH or NaOH, 100 mL H_2O	Murakami's reagent. Use at room temperature to 60 s to reveal carbides; σ phase faintly revealed by etching to 3 min. Use at 80 °C (175 °F) to boiling up to 60 min to darken carbides. Sigma may be colored blue, ferrite yellow to yellow-brown, austenite not attacked. Use under a hood.
15. 30 g KOH (or NaOH), 30 g $K_3Fe(CN)_6$, 100 mL H_2O; or 20 g KOH (or NaOH), 20 g $K_3Fe(CN)_6$, 100 mL H_2O	Two modifications of Murakami's reagent. Use at 95 °C (205 °F). Second modification etches faster than the first modification, and it etches faster than etch 14. Colors σ phase reddish-brown, ferrite dark-gray, austenite not attacked, carbide black. Use under a hood.
16. 10 g oxalic acid and 100 mL H_2O	Popular electrolytic etch; 6 V dc, 25 mm (1.0 in.) spacing. 15–30 s reveals carbides; grain boundaries revealed after 45–60 s; σ phase outlined after 6 s. Lower voltages (1–3 V dc) can be used. Dissolves carbides. Sigma strongly attacked, austenite moderately attacked, ferrite not attacked
17. 10 g NaCN (sodium cyanide) and 100 mL H_2O	Electrolytic etch at 6 V dc, 25 mm (1.0 in.) spacing, 5 min, platinum cathode. Sigma darkened, carbides light, ferrite outlined, austenite not attacked. Good for revealing carbides. Use with care under a hood. Dangerous!
18. 10 mL HCl and 90 mL methanol	Electrolytic etch at 1.5 V dc, 20 °C (70 °F) to attack σ phase. Use at 6 V dc for 3–5 s to reveal structure.
19. 60 mL HNO_3 and 40 mL H_2O	Electrolytic etch to reveal austenite grain boundaries (but not twins) in austenitic grades. With stainless steel cathode, use at 1.1 V dc, 0.075–0.14 A/cm^2 (0.48–0.90 A/in.^{2}), 120 s. With platinum cathode, use at 0.4 V dc, 0.055–0.066 A/cm^2 (0.35–0.43 A/in.^{2}), 45 s. Will reveal prior-austenite grain boundaries in solution-treated (but not aged) martensitic precipitation-hardenable alloys and maraging steels
20. 50 g NaOH and 100 mL H_2O	Electrolytic etch at 2–6 V dc, 5–10 s to reveal σ phase in austenitic grades
21. 56 g KOH and 100 mL H_2O	Electrolytic etch at 1.5–3 V dc for 3 s to reveal σ phase (red-brown) and ferrite (bluish). Chi colored same as sigma
22. 20 g NaOH and 100 mL H_2O	Electrolytic etch at 20 V dc for 5–20 s to outline and color δ-ferrite tan
23. NH_4OH (conc)	Electrolytic etch at 1.5–6 V dc for 10–60 s. Very selective. At 1.5 V, carbide completely etched in 40 s; sigma unaffected after 180 s. At 6 V, σ phase etched after 40 s
24. 10 g $(NH_4)_2S_2O_8$ and 100 mL H_2O	Use at 6 V dc for 10 s to color $M_{23}C_6$ carbide dark brown
25. 200 mL HCl and 1000 mL H_2O	Beraha's tint etch for austenitic, duplex, and precipitation-hardenable grades. Add 0.5–1.0 g $K_2S_20_5$ per 100 mL of solution (if etching is too rapid, use a 10% aqueous HCl solution). Immerse at room temperature (never swab) for 30–120 s until surface is reddish. Austenite colored, carbides not colored. Longer immersion colors ferrite lightly. If coloration is inadequate, add 24 g $NH_4F{\cdot}HF$ (ammonium bifluoride) to stock reagent at left.
26. 20 g picric acid and 100 mL HCl	Etch by immersion. Develops grain boundaries in austenite and δ-ferrite in duplex alloys
27. Saturated aqueous $Ba(OH)_2$ (barium hydroxide)	Attacks carbides well before σ phase in austenitic grades when used at 1.5 V dc, but attacks both equally when used at 3–6 V dc. Has been used to differentiate χ phase and Laves phase (use at 4.3 V dc, platinum cathode, 20 s). Chi is stained mottled-purple, Laves is not colored, ferrite is stained tan.
28. 50 mL each H_2O, ethanol, methanol, and HCl; plus 1 g $CuCl_2$, 3.5 g $FeCl_3$, 2.5 mL HNO_3	Ralph's reagent. Use by swabbing. Can be stored. General-purpose etch for most stainless steels. Does not attack sulfides in free-machining grades
29. 150 mL HCl, 50 mL lactic acid, 3 g oxalic acid	Lucas's reagent. Etches less corrosion-resistant grades by immersion, more corrosion-resistant grades electrolytically, at 0.3 to 1.2 V dc for 10–30 s. The reagent can be stored.
30. 15 mL HCl, 85 mL ethanol	Immerse for 15–45 min to reveal all phase/grain boundaries in duplex stainless steel.

(a) When water is specified, use distilled water.

ors produced by these etchants vary with etchant composition, temperature, time, and phase orientation. When using a particular reagent in the prescribed manner, the colors obtained may differ from those reported in the literature. However, the etch response, that is, what is attacked and what is not attacked at either room temperature or with a boiling solution, is highly reproducible.

When using the standard formulation of Murakami's reagent at room temperature, for example, the carbides will be attacked in 7 to 15 s, and σ phase will be only lightly attacked after 3 min. If higher concentrations of potassium hydroxide (KOH) or sodium hydroxide (NaOH) and potassium ferricyanide ($K_3Fe(CN)_6$) are used at room temperature, σ phase will be attacked instead of the carbides. Used boiling, the standard formulation attacks ferrite, carbide, and

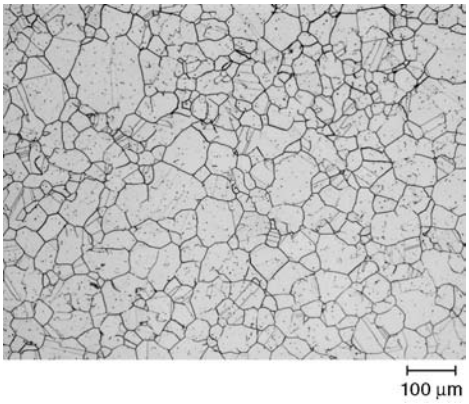

Fig. 10 Solution-annealed and sensitized (1038 °C, or 1900 °F, for 1 h, water quenched, aged at 650 °C, or 1200 °F, for 2 h, air cooled) type 304 stainless steel etched with aqueous 10% ammonium persulfate at 6 V dc for 10 s to color the $M_{23}C_6$ grain-boundary carbides

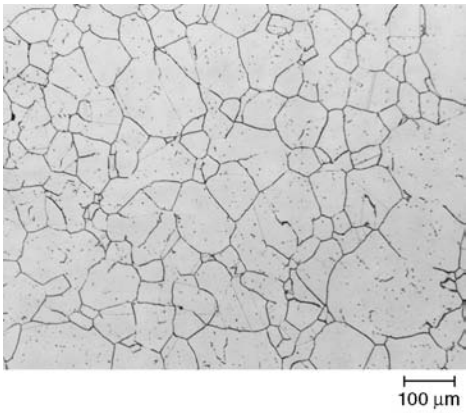

Fig. 11 Solution-annealed and sensitized type 316 stainless steel etched with waterless Kalling's reagent to reveal the $M_{23}C_6$ grain-boundary carbides

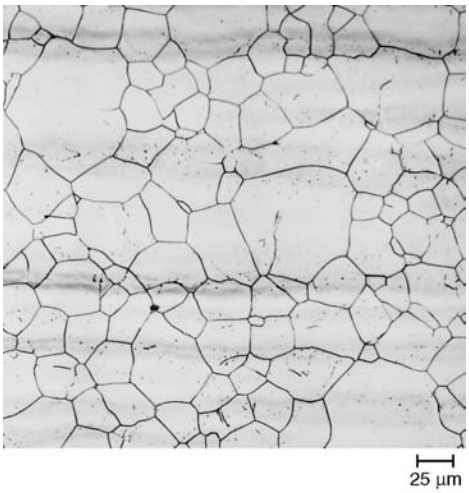

Fig. 12 Austenitic grain boundaries in solution-annealed (954 °C, or 1750 °F, water quenched) type 316L, revealed by electrolytic etching with aqueous 60% HNO_3 at 1 V dc for 120 s

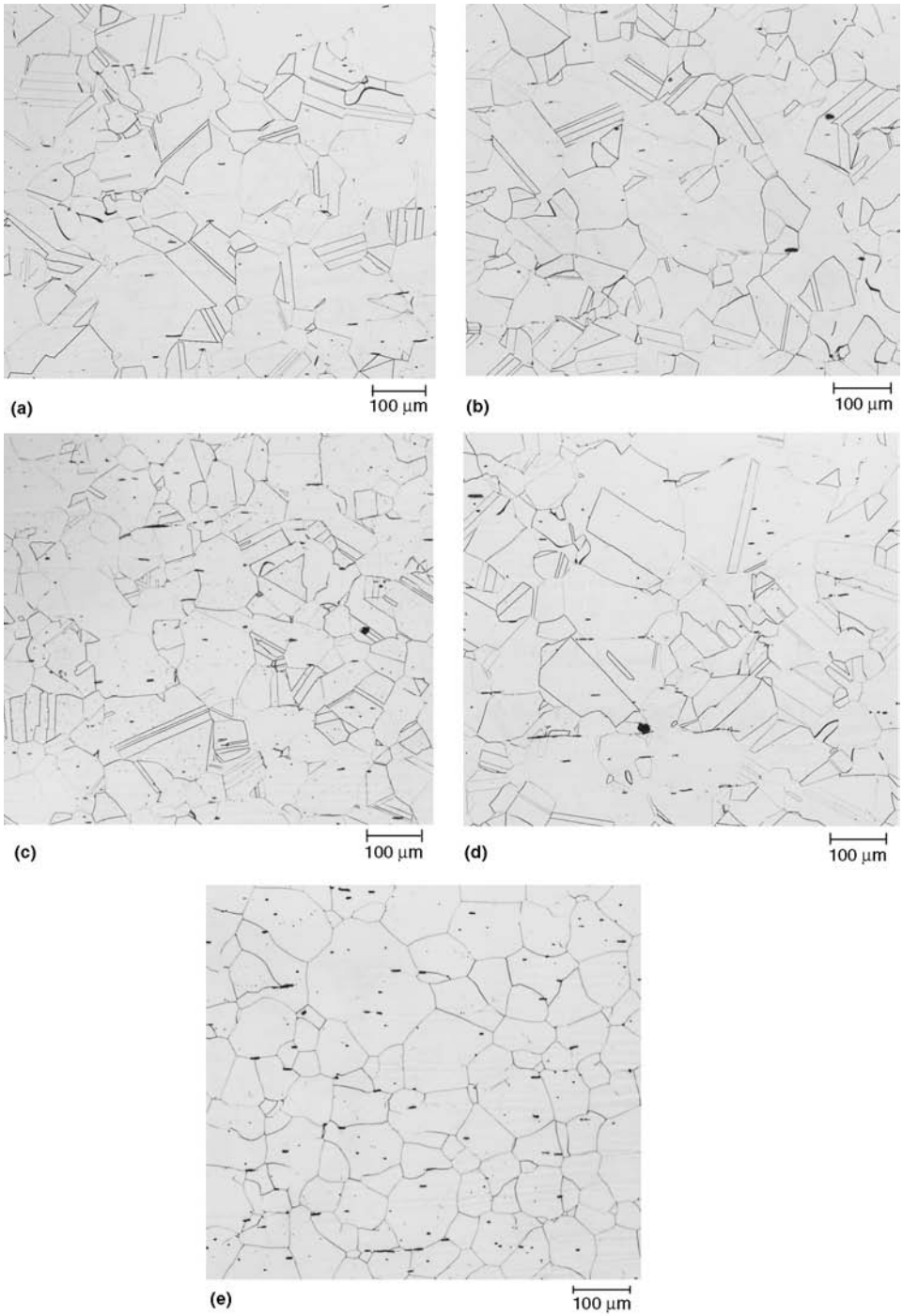

Fig. 13 Austenitic grain boundaries in solution-annealed type 316 stainless steel, revealed by (a) acetic glyceregia, (b) Marble's reagent, (c) equal parts HCl, HNO_3, and water, (d) aqueous 10% oxalic acid at 6 V dc, and (e) aqueous 60% HNO_3 at 0.6 V dc for 90 s

σ phase, although some evidence indicates that σ will not be attacked. Therefore, when using this reagent or one of its numerous modifications, directions should be followed carefully. Experimentation with specimens of known constitution is also recommended.

In some etchant compilations, the standard version of Murakami's reagent is listed as 10 g KOH (or 7 g NaOH) and 10 g $K_3Fe(CN)_6$ (po-

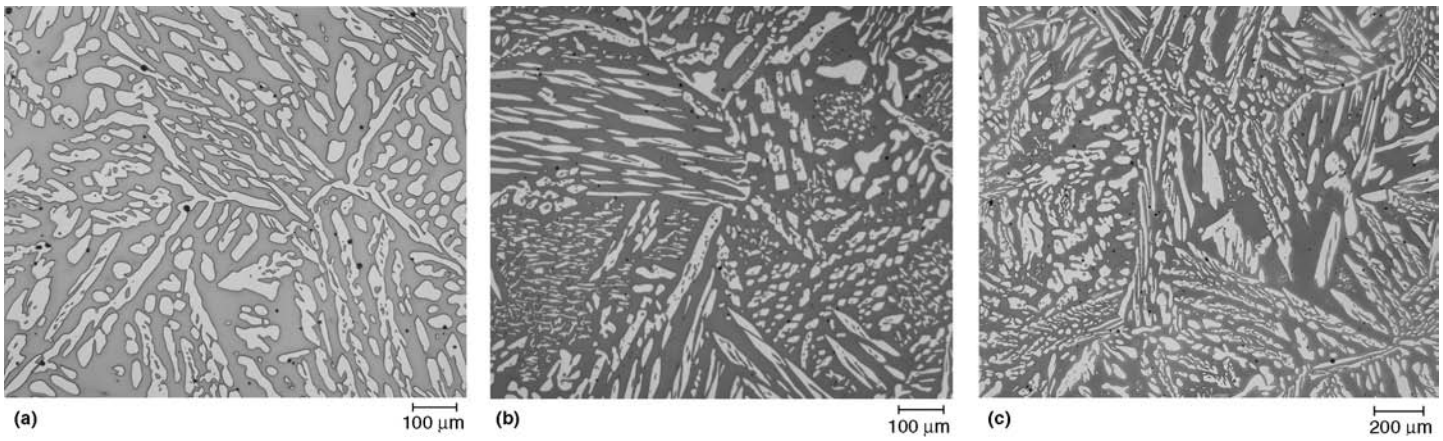

Fig. 14 Ferrite is colored preferentially when as-cast ASTM A 890, grade 5A, is etched with boiling Murakami's reagent using (a) 10 g NaOH 10 g $K_3Fe(CN)_6$ in 100 mL water for 90 s, (b) 20 g NaOH 20 g $K_3Fe(CN)_6$ in 100 mL water for 50 s, and (c) 30 g NaOH 30 g $K_3Fe(CN)_6$ in 100 mL water for 10 s

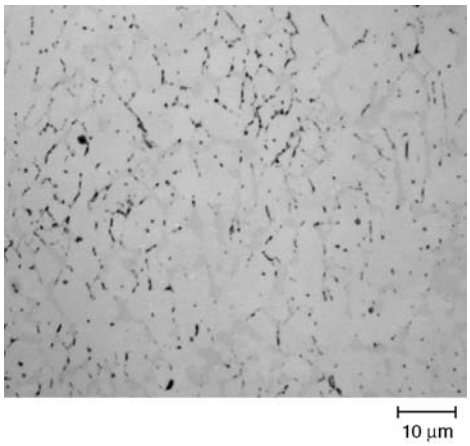

Fig. 15 Carbides in type 312 weld metal, aged at 816 °C (1500 °F) for 160 h, were revealed using standard Murakami's reagent at room temperature for 60 s.

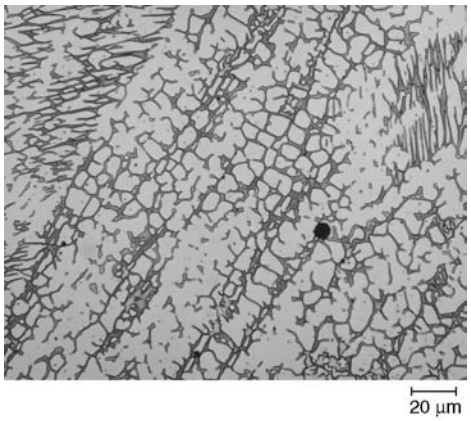

Fig. 16 Delta ferrite in type 312 weld metal revealed using modified Murakami's (30 g NaOH, 30 g $K_3Fe(CN)_6$, and 100 mL water) at 100 °C (210 °F) for 10 s

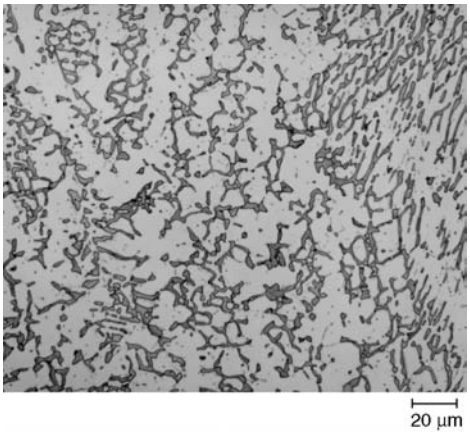

Fig. 17 Sigma phase in 312 weld metal, aged at 816 °C (1500 °F) for 160 h, was revealed using standard Murakami's reagent at 80 °C (175 °F) for 60 s.

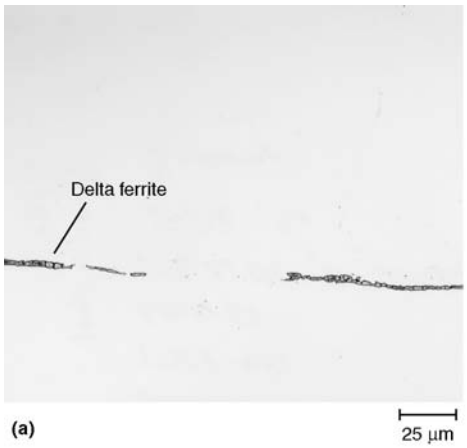

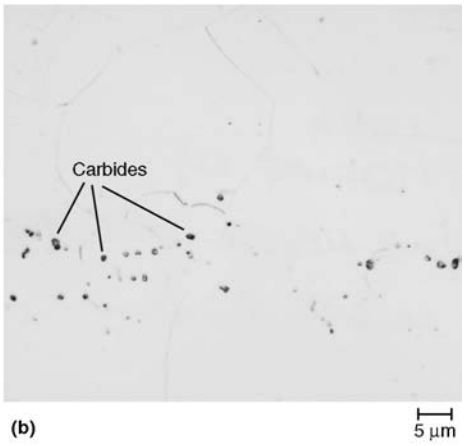

Fig. 18 Delta-ferrite stringer and carbides along the centerline in solution-annealed (954 °C, or 1750 °F, water quenched) type 316L were revealed using (a) aqueous 20% NaOH and (b) concentrated ammonium hydroxide (NH_4OH) at 5 V dc for 10 s.

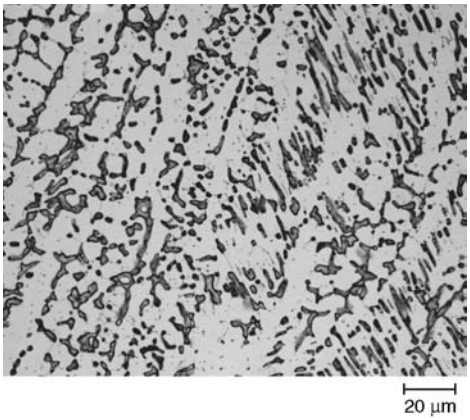

Fig. 19 Sigma phase in 312 weld metal, aged at 816 °C (1500 °F) for 160 h, was revealed using aqueous 20% NaOH at 3 V dc for 10 s.

tassium ferricyanide). Murakami's original publication in 1918 gave the formula as 10 g NaOH, 10 g $K_3Fe(CN)_6$, and 100 mL water and does not mention KOH. There are numerous modifications to this reagent, and several are quite useful. Useful modifications include 20 g NaOH (or KOH), 20 g $K_3Fe(CN)_6$, and 100 mL water, or 30 g NaOH (or KOH), 30 g $K_3Fe(CN)_6$, and 100 mL water. There is a slight variant of this last modification using only 60 mL water, but this solution is difficult to mix, because there is inadequate water to dissolve the two chemicals. In general, as the concentration of NaOH (or KOH) and $K_3Fe(CN)_6$ increases, etch time is reduced, which is very helpful when using a boiling reagent. The end results are the same, and there is little difference between using NaOH or KOH, although the authors prefer to use NaOH. Figure 14 shows how ferrite in a cast ASTM A 890, grade 5A, duplex stainless steel was revealed using the three versions of Murakami's reagent. Murakami's reagent etches carbides when used at room temperature but not ferrite or sigma. Figure 15 shows an example of the use of Murakami's at room temperature to reveal carbides in type 312 weld metal that was aged 160 h at 816 °C (1500 °F). There is σ in the weld also, but it was not darkened or colored. To color ferrite and

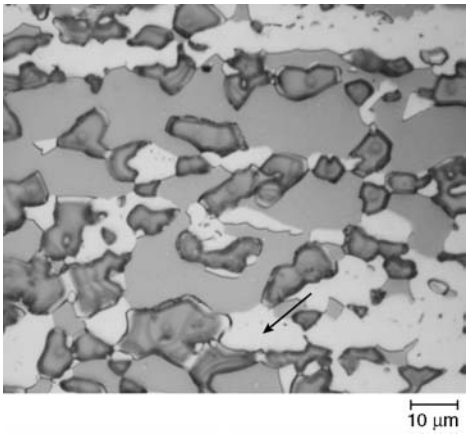

Fig. 20 Delta-ferrite and σ phase revealed in a modified type 329 duplex stainless steel, aged 48 h at 816 °C (1500 °F), using aqueous 20% NaOH at 3 V dc for 10 s. Austenite is not colored, ferrite is tan, and σ is orange. As the σ forms, new austenite (arrow) is also formed and can be seen around the σ particles.

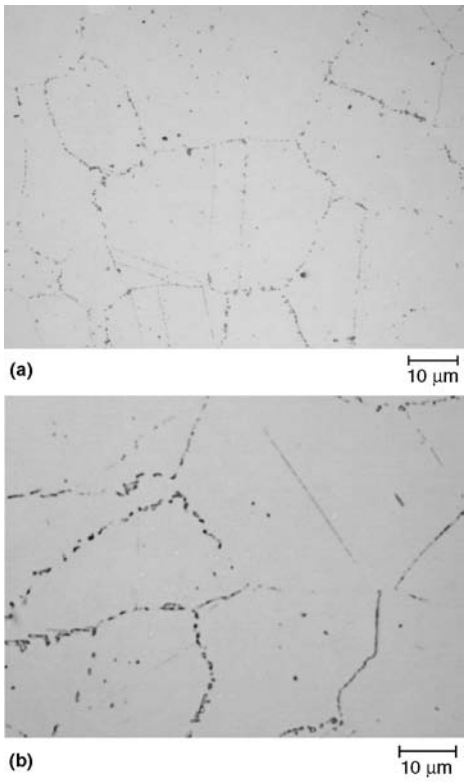

Fig. 21 Grain-boundary carbides in the heat-affected zone of a sensitized 316 stainless steel, revealed using (a) concentrated NH_4OH at 6 V dc for 60 s and (b) aqueous 10% ammonium persulfate at 6 V dc for 10 s

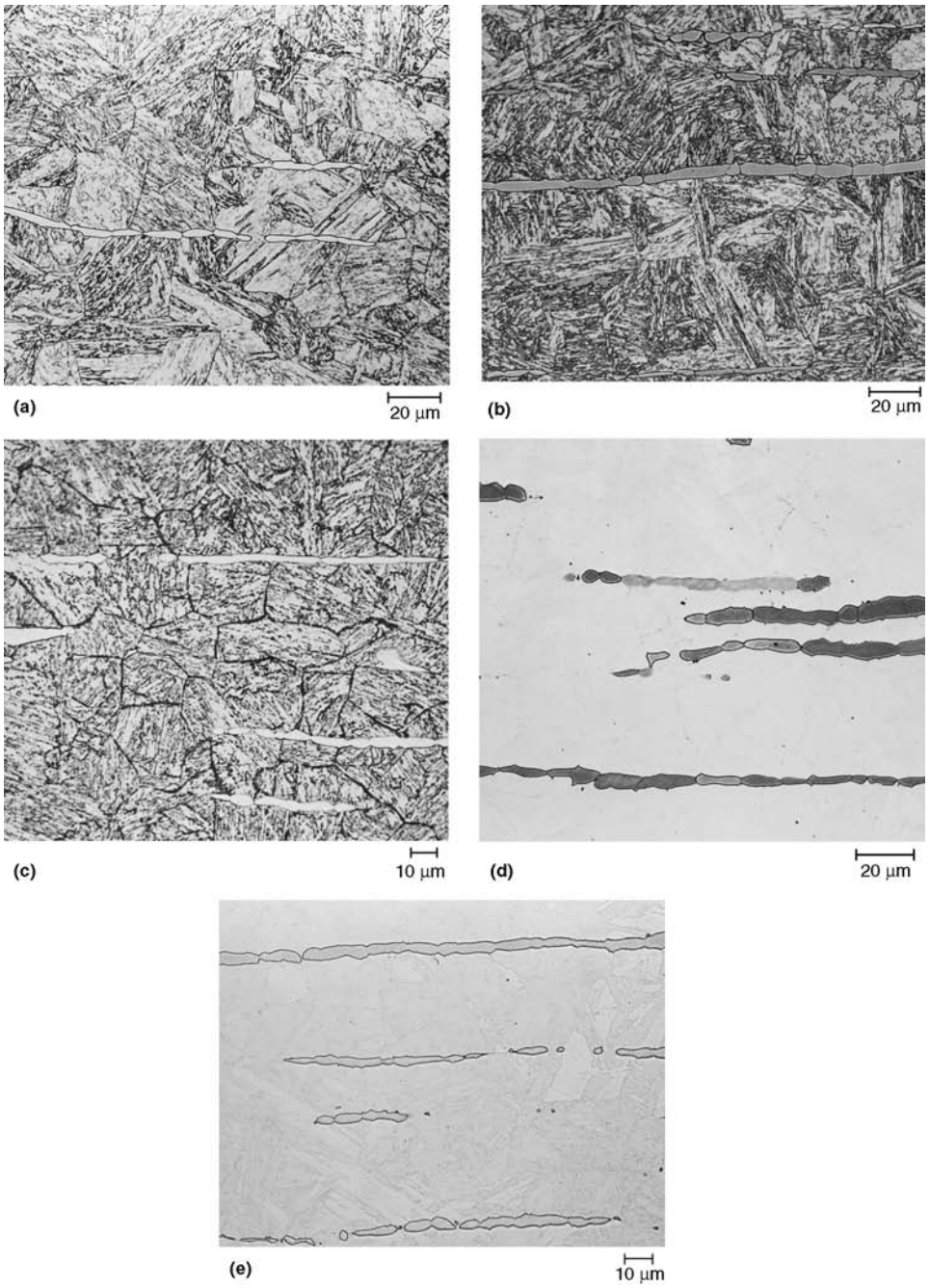

Fig. 22 Delta-ferrite in the martensitic matrix of solution-annealed and aged 17-4 PH stainless steel, revealed using (a) Fry's reagent, (b) Marble's reagent, (c) superpicral (which brought out the prior-austenite grain boundaries better than Fry's), (d) aqueous 10 *N* KOH at 2.5 V dc for 10 s, and (e) aqueous 20% NaOH at 20 V dc for 20 s

sigma, Murakami's must be used between approximately 80 and 100 °C (180 and 210 °F). Sigma is colored more readily than ferrite. For example, when coloring ferrite in type 312 weld metal (as-welded), the standard grade was used boiling for 180 s, while the 20-20-100 version required 60 s, and the 30-30-100 version required 10 s (Fig. 16). To color σ in the aged 312 weld metal (Fig. 15), the 10-10-100 (Fig. 17) version required immersion in the boiling solution for 60 s, while the 30-30-100 version required <10 s.

Electrolytic reagents, which are used often with austenitic and duplex grades, provide greater control of the etching process and are

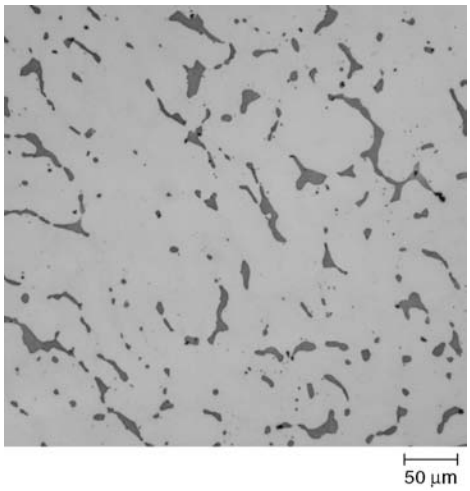

Fig. 23 Delta ferrite, colored brown in solution-annealed and aged (H900 temper) 17-4 PH stainless steel, revealed using the standard Murakami's reagent at 100 °C (210 °F) for 60 s

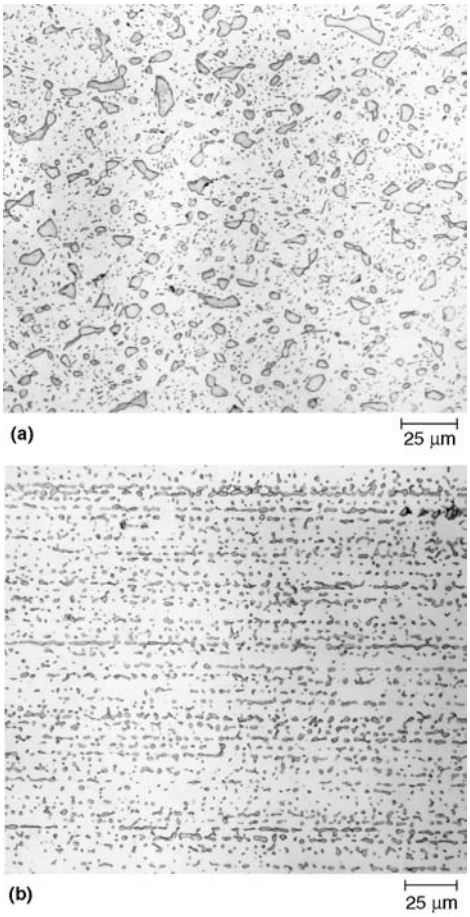

Fig. 24 Delta-ferrite revealed in (a) AM 350 and (b) PH 15-7 Mo stainless steels, using aqueous 20% NaOH at 3 V dc for 10 s

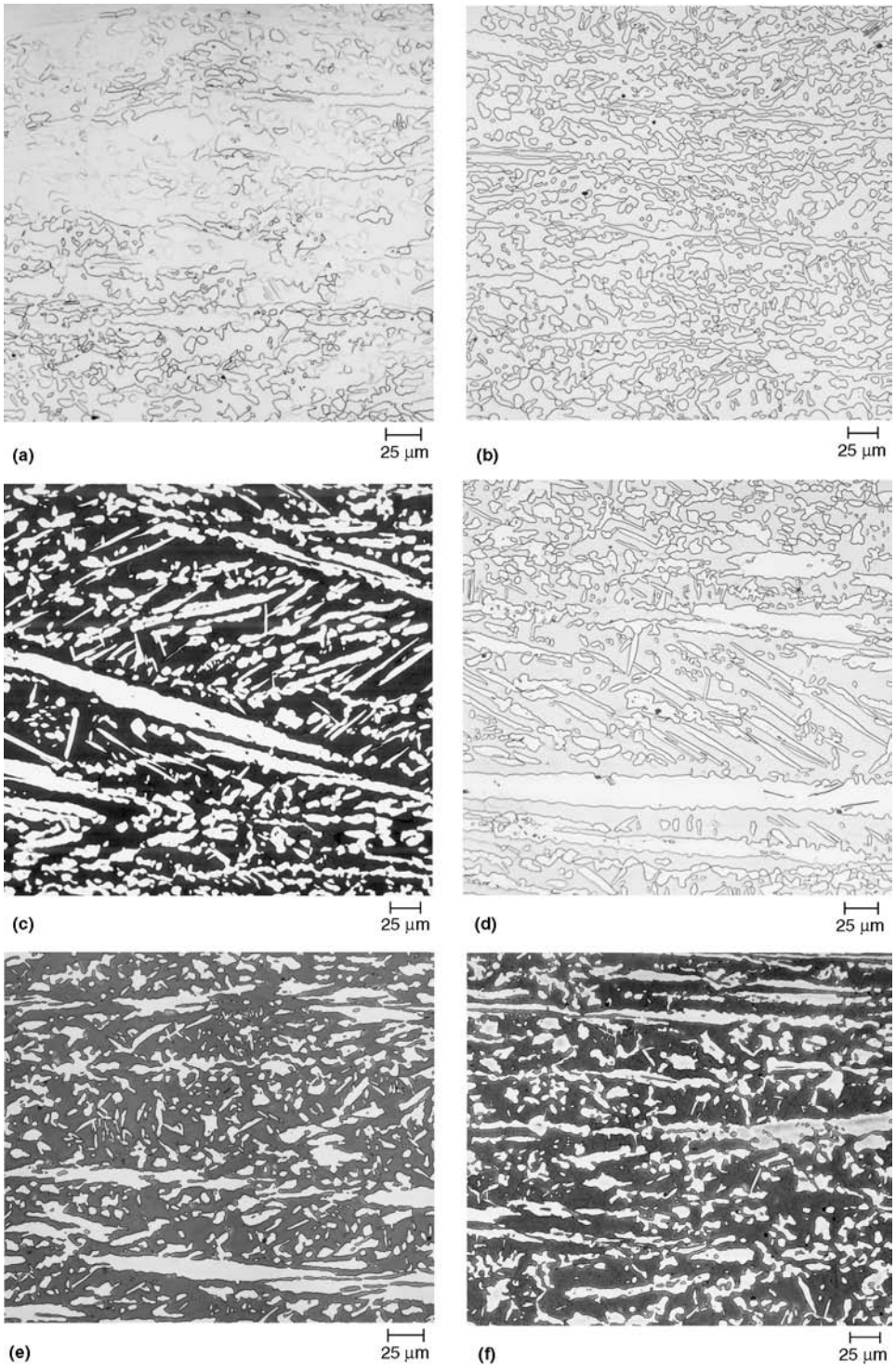

Fig. 25 Ferrite-austenite phase boundaries revealed in 7-Mo PLUS duplex stainless steel plate, using (a) glyceregia (poor results), (b) ethanol 15% HCl, (c) Beraha's tint etch, (d) aqueous 60% HNO_3 at 1 V dc for 60 s, (e) aqueous 20% NaOH at 4 V dc for 10 s, and (f) 10 *N* KOH at 3 V dc for 10 s

highly reproducible. One of the most commonly used electrolytic reagents is 10% aqueous oxalic acid, which will reveal carbides after a short etch, if they are present (Table 7). When carbides are not present, the austenite grain boundaries will be revealed in 15 to 60 s (Fig. 13d). If ferrite is present, it will be outlined after 10 to 15 s. Electrolytic 10% ammonium persulfate is highly reliable for coloring $Cr_{23}C_6$ carbides in stainless steels (6 V dc, 10 s) (Fig. 10).

Electrolytic reagents are generally quite simple in composition. The selectivity of electrolytic reagents based on various hydroxide solutions has been demonstrated (Ref 4). Strong hydroxide solutions attack σ phase preferentially to carbides; weak hydroxide solutions attack carbides much more readily than σ phase. Therefore, to reveal σ phase, 10 *N* KOH or 20% NaOH is employed, and to reveal carbides, concentrated ammonium hydroxide (NH_4OH) is used. For intermediate-strength hydroxide solutions, etching response is altered by a change in the applied potential. Strong hydroxides also darken ferrite and σ when used electrolytically but do not affect austenite.

Figure 18 shows the 316L specimen illustrated in Fig. 9 and 12 etched electrolytically, this time with 20% NaOH to color the fine δ-ferrite stringers and subsequently with concentrated ammonium hydroxide (NH_4OH) to color carbides not dissolved in solution annealing (954 °C or 1750 °F, was used—lower than normal to minimize grain growth). Figure 19 shows 20% NaOH used electrolytically to darken the σ phase in the aged 312 weld metal (compare with Fig. 17). Figure 20 shows ferrite and σ in a modified type 329 (experimental) alloy that was aged 48 h at 816 °C (1500 °F), revealed by electrolytic etching with 20% NaOH. The austenite was unaffected, the ferrite was colored light brown, and the σ was colored orange. Figure 21 compares the use of electrolytic 10% ammonium persulfate with concentrated ammonium hydroxide to reveal grain-boundary carbide precipitation (sensitization) in the heat-affected zone of a 316 weld.

Several sequential etching procedures have been suggested for phase identification in austenitic stainless steels. One procedure (Ref 4) involves etching first with Vilella's reagent to outline the phases present. Next, the specimen is electrolytically etched with 10 *N* KOH at 3 V dc for 0.4 s to color σ phase, if present, but not carbides. The specimen is then electrolytically etched with concentrated NH_4OH at 6 V dc for 30 s to color any carbides present. Another procedure (Ref 5) also begins with Vilella's reagent to reveal the constituents. Next, Murakami's reagent is used at room temperature to stain the carbides present. Any σ phase or δ-ferrite present is unaffected. Finally, the specimen is electrolytically etched with aqueous chromium trioxide (CrO_3), which will attack carbides and σ phase but not δ-ferrite. Murakami's reagent does not attack carbides in titanium- or niobium-stabilized stainless steels. These carbides are attacked slowly in electrolytic CrO_3.

Delta-ferrite in martensitic, austenitic, or precipitation-hardenable grades can be preferentially colored by electrolytic etching with 20% aqueous NaOH at 3 V dc for 5 to 20 s. This procedure outlines and uniformly colors tan the δ-ferrite. Although the color varies with orientation, 10 *N* KOH also colors δ-ferrite. Figure 22 illustrates the use of five different etchants to reveal δ-ferrite in solution-annealed and aged 17-4 PH stainless. Note that 10 *N* KOH produced color variations from grain to grain (orientation sensitivity), while 20% NaOH colored the δ-ferrite uniformly and generally exhibits sharper phase boundaries. Figure 23 shows δ-ferrite revealed in a different specimen of 17-4 PH, using boiling Murakami's reagent. Figure 24 shows 20% NaOH used to reveal δ-ferrite in AM 350 and 15-7 PH stainless steels. Figure 25 shows the microstructure of 7-Mo PLUS duplex stainless steel etched with two standard reagents: a Beraha tint etch (colors the ferrite) and three electrolytic reagents. Although glyceregia (Fig. 25a) is a popular general-purpose etchant for stainless steels, it is orientation-sensitive and did not reveal the structure well. Ethanolic 15% HCl (developed at Carpenter Technology Corp.) is a very interesting etchant. It is used by immersion, but the time is not too critical. Usually, specimens are immersed from 15 to 45 min; long times do not seem to cause overetching problems. However, while it reveals the phase boundaries very well and uniformly (Fig. 25b), one cannot tell ferrite from austenite. The tint etch (Fig. 25c) does a great job coloring the ferrite, but it is more challenging to get this quality of results than by using electrolytic 20% NaOH.

Table 9 Electropolishing procedures for preparing thin-foil stainless steel specimens

Solution composition	Comments
1. 5 or 10 mL $HClO_4$ and 95 or 90 mL acetic acid at 20 V dc	Popular electropolish for stainless steels. Used for window technique or for perforation of disk specimens. Keep solution cool
2. (a) 10 mL HNO_3 and 90 mL H_2O(a) at 50 V dc (b) 10 mL, $HClO_4$, 20 mL glycerol, 70 mL ethanol at 65 V dc	Popular procedures for austenitic grades. Use (a) to electrodish specimens, then (b) for perforation.
3. 10 mL $HClO_4$ and 90 mL ethanol at 12 V dc, 0 °C (32 °F)	Popular electropolish for stainless steels. Use for perforation.
4. 40 mL H_2SO_4 and 60 mL H_3PO_4 at 35 V dc, 0.3 A/cm^2 (1.9 A/in.^{2})	Electropolish for stainless steels for perforation
5. 25 g CrO_3, 133 mL acetic acid, 7 mL H_2O at 20 °C (70 °F)	Electropolish for stainless solution makes it difficult to use for jet perforation
6. (a) 40 mL acetic acid, 30 mL H_3PO_4, 20 mL HNO_3, 10 mL H_2O at 80–120 V dc, 0.1 A/cm^2 (0.65 A/in.^{2}) (b) 54 mL H_3PO_4, 36 mL H_2SO_4, 10 mL ethanol at 6 V dc	Procedure for austenitic grades. Jet electrodish disks with (a) prior to final thinning with (b) to perforation
7. 45 mL H_3PO_4, 30 mL H_2SO_4, 25 mL H_2O at 6 V dc	Procedure for austenitic grades for perforation

(a) When water is specified, use distilled water.

Table 10 Second-phase constituents observed in stainless steels

Phase	Crystal structure	Lattice parameters, nm	Reported compositions	Comments
$M_{23}C_6$	Face-centered cubic	a_0 = 1.057–1.068	$(Cr_{16}Fe_5Mo_2)C_6$ $(Cr_{17}Fe_{4.5}Mo_{1.5})C_6$ $(Fe,Cr)_{23}C_6$	Most commonly observed carbide in austenitic stainless steels. Precipitates from 500–950 °C (930–1740 °F), fastest at 650–700 °C (1200–1290 °F)
M_6C	Face-centered cubic	a_0 = 1.085–1.111	$(Cr,Co,Mo,Ni)_6C$ $(Fe_3Mo_3)C$ Fe_3Nb_3C $(Fe,Cr)_3Nb_3C$	Observed in austenitic grades containing substantial molybdenum or niobium after long time exposure
M_7C_3	Hexagonal	a_0 = 1.398 c_0 = 0.4523	Cr_7C_3	Observed in martensitic grades
MC	Cubic	a_0 = 0.430–0.470	TiC NbC	Observed in alloys with additions of titanium or niobium. Very stable carbide. Will usually contain some nitrogen
Sigma (σ)	Tetragonal	a_0 = 0.8799–0.9188 c_0 = 0.4544–0.4599	FeCr FeMo Fe(Cr,Mo) $(Fe,Ni)_x(Cr,Mo)_y$	Formation from δ-ferrite is much more rapid than from austenite. Potent embrittler below 595 °C (1105 °F). Forms with long time exposure from 650–900 °C (1200–1650 °F)
Chi (χ)	Body-centered cubic: (α-Mn structure)	a_0 = 0.8862–0.892	$Fe_{36}Cr_{12}Mo_{10}$ $(FeNi)_{36}Cr_{18}Mo_4$ $M_{18}C$	Observed in alloys containing substantial molybdenum. Chi precipitates with exposure to 730–1010 °C (1345–1850 °F) (varies with alloy composition).
Laves (η)	Hexagonal	a_0 = 0.470–0.4744 c_0 = 0.772–0.7725	Fe_2Mo $(Ti_{21}Mo_9)$ $(Fe_{50}Cr_5Si_5)$	Forms in austenitic alloys with substantial amounts of molybdenum, titanium, or niobium after long time exposure from 600–1100 °C (1110–2010 °F)

The very useful electrolytic aqueous 60% nitric acid etch also reveals the phase boundaries very well (Fig. 25d) and gives a slight gray color to the ferrite. Much stronger contrast, however, is obtained using electrolytic aqueous 20% NaOH or 10 *N* KOH (56%), as shown in Fig. 25(e) and (f). Note that the uniformity of the color and the sharpness of the phase boundaries are better with NaOH than with KOH.

Potentiostatic etching (Ref 1) is frequently used for selective etching of constituents in stainless steels. This technique is similar to electrolytic etching, except a third electrode is included to monitor the etch potential, which is controlled using a potentiostat. This technique affords the greatest possible control over etching.

Heat tinting is a useful technique with austenitic stainless steels. Phase delineation is improved by first etching with a general-purpose reagent, such as Vilella's. The specimen is then heated in air at 500 to 700 °C (930 to 1290 °F); 650 °C (1200 °F) has been most commonly used, with times to 20 min. Austenite is colored more readily than ferrite (Fig. 19), and carbides resist coloration longest. After 20 min at 650 °C (1200 °F), austenite is blue-green, σ phase is orange, ferrite is light cream, and carbides are uncolored.

Magnetic colloids have also been used to detect ferromagnetic constituents in austenitic stainless steels. This technique has been extensively applied using a ferromagnetic colloid solution containing very fine magnetic particles (Ref 6). Delta-ferrite and strain-induced martensite are readily identified by this method.

Electron Microscopy. Scanning electron microscopy and transmission electron microscopy are used to examine the fine structure of stainless steels and for phase identification. Scanning electron microscopy examination uses the same specimens as light optical microscopy. As-polished specimens often can be examined, although etching is more common. Many second-phase constituents can be observed using backscattered electron detectors, due to the adequate atomic number contrast between these phases and the matrix. However, secondary electron images produced from topographic contrast and atomic number contrast are most often used. Energy-dispersive x-ray analysis (EDXA) is prevalent for chemical analysis of second phases, although lightweight elements, such as carbon and nitrogen, cannot be detected unless thin-window or windowless EDXA detectors or wavelength-dispersive detectors are used.

Transmission electron microscopy requires preparation of replica or thin-foil specimens. Replicas may be made to reveal the outline and topography of the phases, or, if the specimen is deeply etched, second-phase particles may be extracted. Extraction replicas permit analysis of second phases by electron diffraction and by EDXA. Thin-foil specimens can also be analyzed by these methods, although interference from the matrix is possible. Table 9 lists electropolishing procedures for producing stainless steel thin foils.

Bulk Extractions. Although bulk samples can be directly analyzed by x-ray diffraction for phase identification, it is quite common to extract the second phases chemically and analyze the extracted particles. This eliminates the matrix and concentrates the second phase, facilitating identification of small amounts of the second-phase constituents. Bulk extraction of phases from stainless steels is performed using the same procedures as for heat-resistant grades (see the article "Metallography and Microstructures of Heat-Resistant Alloys" in this Volume).

Microstructures of Stainless Steels

The microstructures of stainless steels can be quite complex. Matrix structures vary according to the type of steel, such as ferritic, austenitic, martensitic, precipitation hardenable, or duplex. A wide range of second-phase constituents (Table 10) can be observed; welding or high-tem-

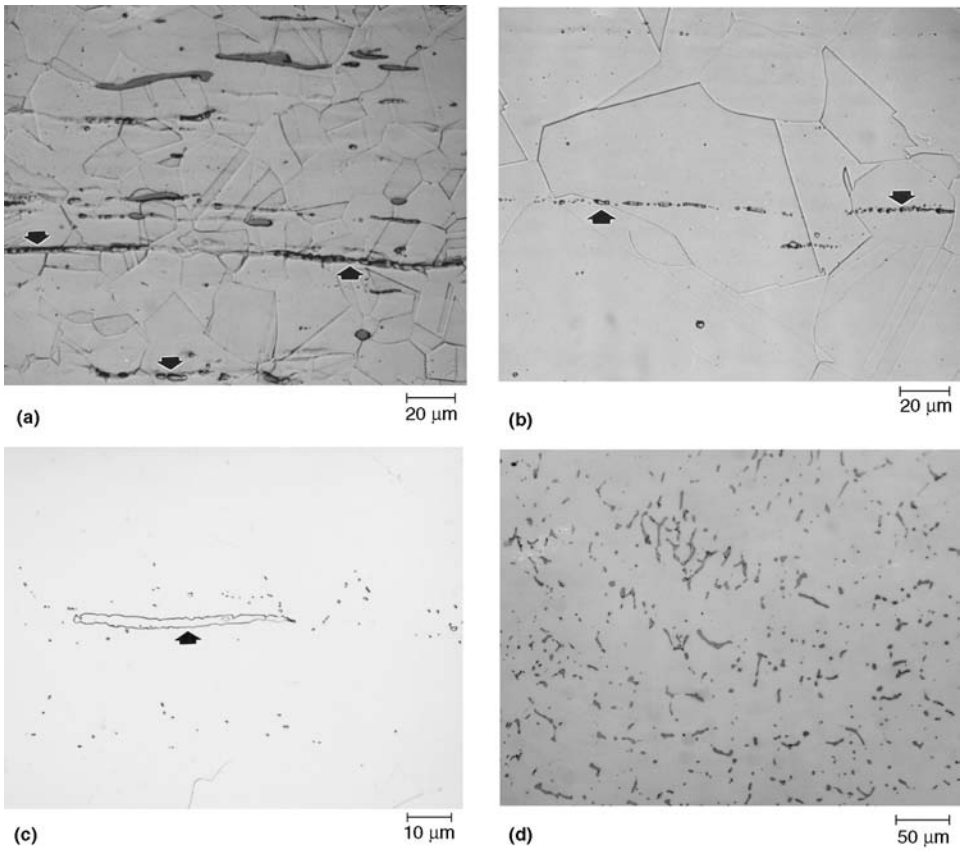

Fig. 26 Examples of δ-ferrite stringers (arrows) in austenitic stainless steels. (a) 203 etched with Ralph's reagent. (b) 302-HQ etched with waterless Kalling's reagent. (c) 316L etched with glyceregia. (d) 304 etched with aqueous 20% NaOH at 3 V dc for 20 s

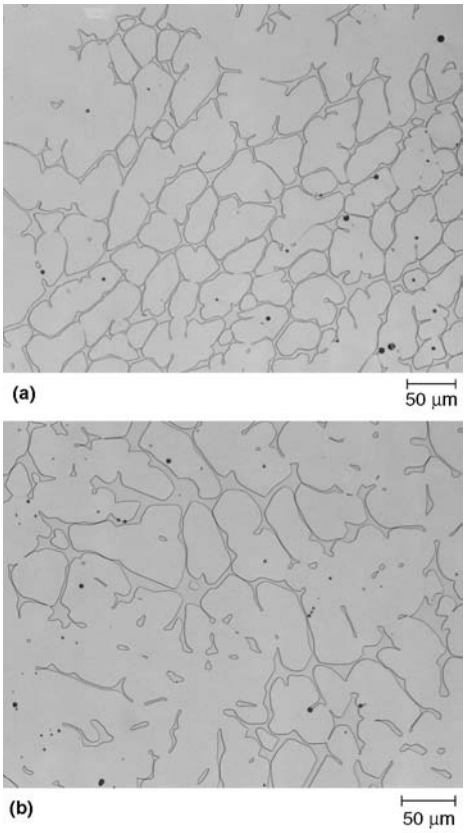

Fig. 27 Ferrite in CF-8M stainless steel in the (a) as-cast condition and (b) after solution annealing. Revealed using glyceregia

perature exposure increases the complexity. Additional information is available in Ref 7.

Austenitic Stainless Steels. The most commonly used stainless steels are the austenitic grades, of which AISI 302, 304, and 316 are the most popular wrought grades, and CF-8 and CF-8M are the most popular cast grades. These grades contain 16% or more chromium, a ferrite-stabilizing element, and sufficient austenite-stabilizing elements, such as carbon, nitrogen, nickel, and manganese, to render austenite stable at room temperature. The grades containing silicon, molybdenum, titanium, or niobium—AISI 302B, 316, 317, 321, and 347, for example—will sometimes include a minor amount of δ-ferrite because of the ferrite-stabilizing influence of these elements. Alloys with substantial nickel are fully austenitic, for example, AISI 310 or 330. For alloys susceptible to δ-ferrite stabilization, the amount present will depend on the composition, chemical homogeneity, and hot working. Alloys with especially low carbon contents to minimize susceptibility to sensitization during welding (AISI 304L, 316L, or 317L, for example) will have a greater tendency toward δ-ferrite stabilization. Figure 26 shows examples of δ-ferrite stringers in wrought 203, 302-HQ, 304, and 316L stainless steels.

Alloys CF-3 through CF-16F in Table 3 are austenitic, with limited amounts of ferrite; alloys CF-20, CK-20, and CN-7M are completely austenitic. They exhibit maximum corrosion resistance in the solution-treated condition. The corrosion resistance of certain alloys is enhanced by extralow carbon content (as in CF-3), a molybdenum addition (as in CF-3M and CF-8M), or the addition of niobium (as in CF-8C). Alloy CF-16F contains 0.20 to 0.35% Se for improved machinability. Figure 27 shows the microstructure of as-cast and as-cast and solution-annealed CF-8M. Figure 28 shows the microstructure of as-cast type 301, and Fig. 29 shows the microstructure of as-cast 316 stainless steel (wrought grades before hot working). Note that in the as-cast condition, both contain substantial ferrite. However, after hot working, they will be free or nearly free of ferrite.

Numerous studies have been conducted to predict matrix phases based on chemical composition. Most of these studies have concentrated on predicting weldment microstructures (Ref 8 to 15); others have concentrated on predicting cast microstructures (Ref 16 to 18) or predicting structures at the hot-working temperature (Ref 19) or after hot working (Ref 20). Measurement of the δ-ferrite content of stainless steels, particularly weldments, has been widely studied (Ref 21 to 24).

The austenite in these grades is not stable but metastable. Martensite can be formed, particularly in the leaner grades, by cooling specimens to very low temperatures or by extensive plastic deformation. Nonmagnetic, hexagonal close-packed ε-martensite and magnetic, body-centered cubic (bcc) α′-martensite have been observed. Empirical relationships have been developed to show how composition influences the resistance of such steel to deformation-induced martensite (Ref 25, 26). Figure 30 shows examples of martensite formed in cold-worked specimens of 203, 303, 303Se, and 304 stainless steels. In alloys where the austenite is more stable, cold working does not produce martensite. Because austenitic alloys are face-centered cubic, they have twelve well-developed slip systems, and only slip lines are observed, as shown in the examples for 302-HQ and 316L in Fig. 31. Figure 32 shows the slip in type 347 stainless steel, cold drawn with 5, 10, 15, and 30% reductions. Cold drawing affects the metal at the surface far more than in the interior; thus, the slip line density will be highest at the surface and lowest at the center.

Carbon content limits are generally 0.03, 0.08, or 0.15% in the austenitic grades. Solution annealing will usually dissolve all, or most of, the carbides present after hot rolling. Rapid quenching from the solution-annealing temperature of generally 1010 to 1065 °C (1850 to 1950 °F) will retain the carbon in solution, producing a strain-free, carbide-free austenitic microstructure. Some of these grades are water quenched from the hot working temperature. When properly performed, the solution-annealed structure should exhibit a single grain size distribution, with equiaxed grains containing annealing twins. Examples for a number of alloys are given in Fig. 33. The more highly alloyed grades can be quite difficult to etch and obtain full delineation of the grain structure. In such cases, use of Nomarski differential interference contrast illumination is very helpful in bringing out the grain structure as well as the alloy segregation, as shown in Fig. 33(i) to (l). However, grain structures are not always equiaxed and unimodal, especially in as-hot-worked specimens. Figure 34 shows examples of bimodal grain size distributions in austenitic stainless steels.

The most widely observed carbide type in austenitic stainless steels is $M_{23}C_6$, which is often referred to as $Cr_{23}C_6$, but more properly is $(Cr, Fe)_{23}C_6$ or $(Cr, Fe, Mo)_{23}C_6$. The precipitation of this carbide at grain boundaries during welding produces intergranular corrosion. To counter sensitization during welding, carbon contents are reduced or strong carbide formers are added, as in AISI 321 and 347.

Precipitation of $M_{23}C_6$ carbide occurs as a result of heating solution-annealed grades to 500 to 950 °C (930 to 1740 °F); the fastest rate of precipitation takes place from 650 to 700 °C (1200 to 1290 °F). Precipitation occurs first at

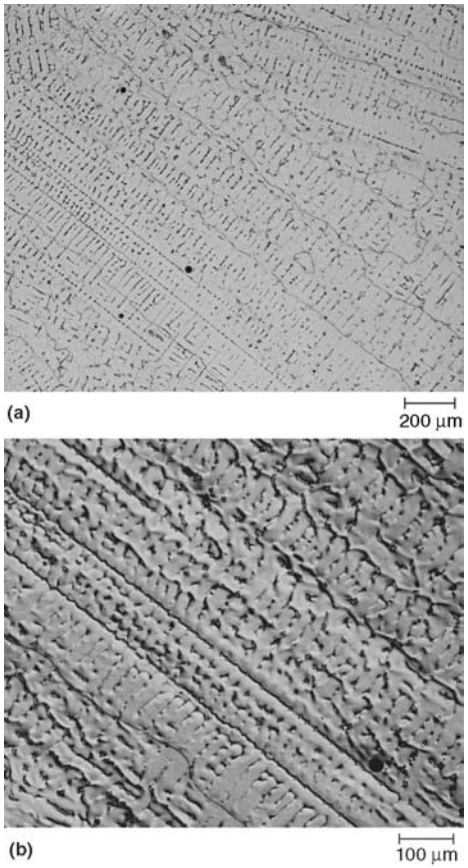

Fig. 28 As-cast microstructure of type 301 stainless steel, revealed using Ralph's reagent. (a) Bright field. (b) Nomarski differential interference contrast

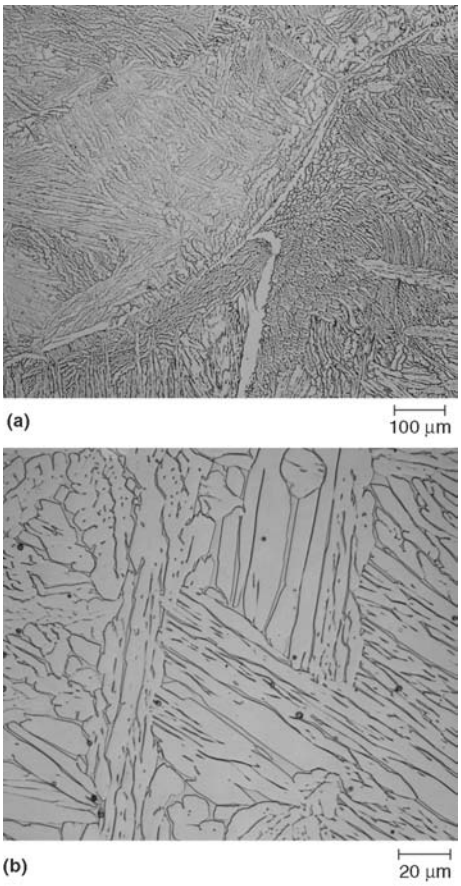

Fig. 29 As-cast microstructure of 316 stainless steel contains considerable δ-ferrite. Revealed using glyceregia.

austenite/δ-ferrite phase boundaries, when present, followed by precipitation at other noncoherent interfaces (grain and twin boundaries), and finally by precipitation at coherent twin boundaries. In addition, $M_{23}C_6$ may precipitate at inclusion/matrix-phase boundaries.

The appearance of $M_{23}C_6$ varies with the precipitation temperature and time. It is most easily studied using extraction replicas. At the lower precipitation temperatures, $M_{23}C_6$ has a thin, continuous, sheetlike morphology. When the precipitation temperature is 600 to 700 °C (1110 to 1290 °F), feathery dendritic particles form at boundary intersections. With time, these precipitates coarsen and thicken. At still higher precipitation temperatures, $M_{23}C_6$ forms at grain boundaries as discrete globular particles whose shape is influenced by the boundary orientation, degree of misfit, and temperature (Ref 27). The $M_{23}C_6$ that precipitates at noncoherent twin boundaries is lamellar or rodlike; that which precipitates at coherent twin boundaries is platelike. The $M_{23}C_6$ that forms at the lower precipitation temperatures is most detrimental to intergranular corrosion resistance. Examples of sensitized grain structures are shown in Fig. 35.

Alloys given deliberate minor additions of titanium or niobium—AISI 321 and 347, for example—form titanium or niobium carbides, rather than $M_{23}C_6$. To take full advantage of these additions, solution-annealed specimens are subjected to a stabilizing heat treatment to precipitate the excess carbon as titanium or niobium carbides. This treatment is commonly used with AISI 321 and involves holding the specimen several hours at 845 to 900 °C (1550 to 1650 °F). These MC-type carbides will precipitate intragranularly at dislocations or stacking faults within the matrix. Some may also precipitate on grain boundaries.

Additions of titanium or niobium must be carefully controlled to neutralize the carbon in solution. In practice, titanium and niobium carbides can contain some nitrogen, and both can form rather pure nitrides. Titanium nitrides usually appear as distinct, bright-yellow cubic particles. Titanium carbide is grayish, with a less regular shape. Titanium carbonitride will have an intermediate appearance that varies with the carbon/nitrogen ratio. Chromium nitrides are not usually observed in the austenitic grades, unless

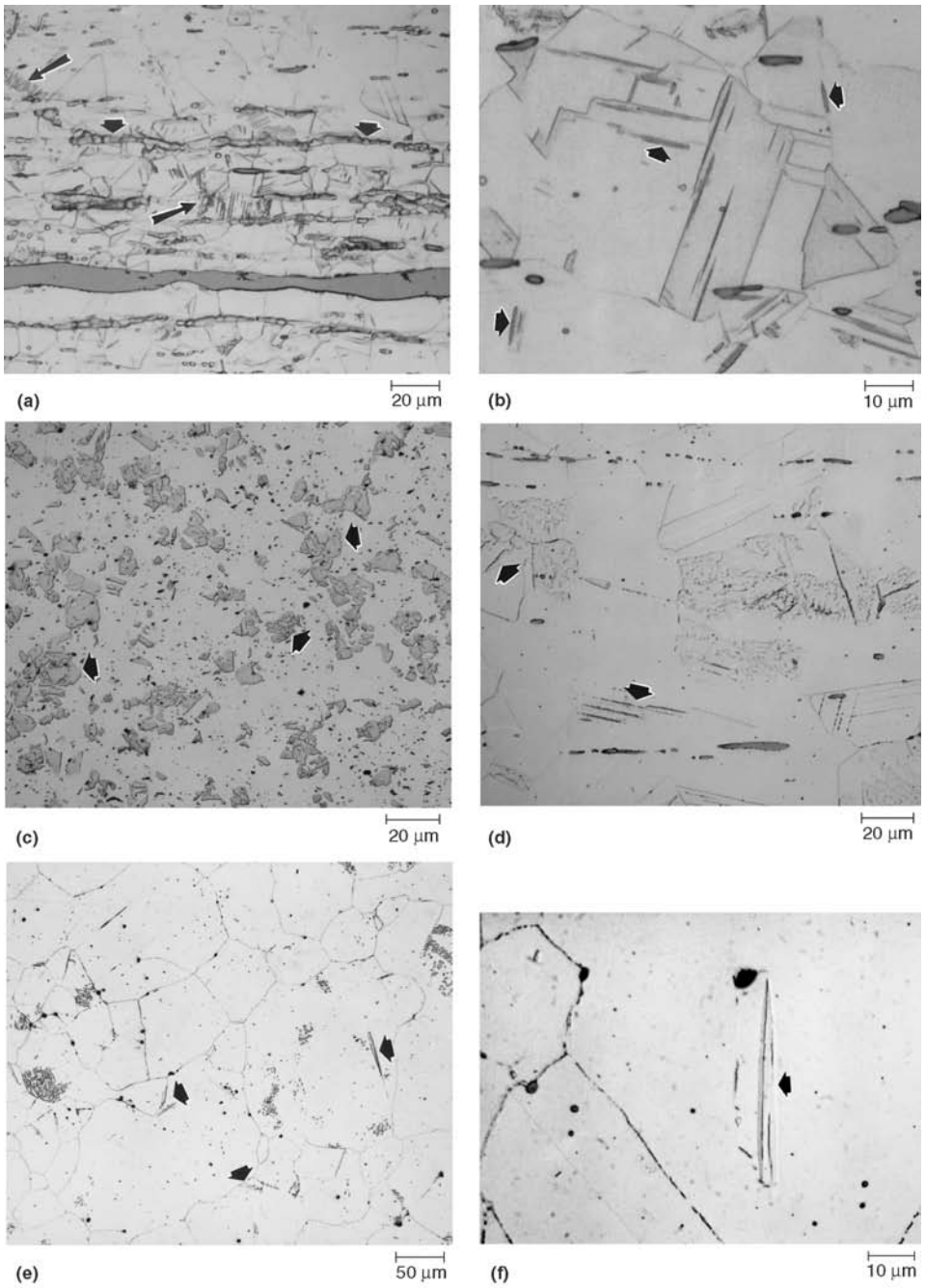

Fig. 30 Martensite (arrows) produced by cold working austenitic stainless steels. (a) 203 etched with Ralph's reagent. (b) 303 etched with Ralph's reagent. (c) 303 etched with Lucas reagent. (d) 303Se etched with waterless Kalling's reagent. (e) 304 etched with Vilella's reagent. (f) Same specimen as in (e) but higher magnification

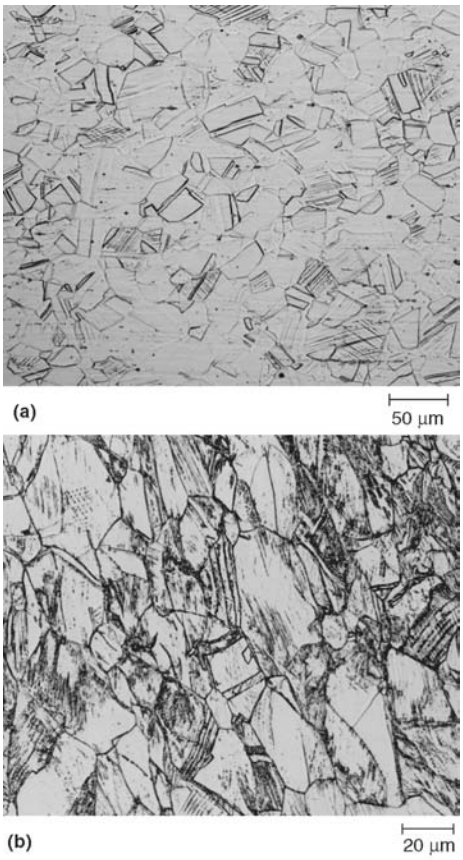

Fig. 31 Slip produced by cold working. (a) 302-HQ etched with waterless Kalling's reagent. (b) 316L stainless steel etched with glyceregia

the service environment causes substantial nitrogen surface enrichment or they are nitrogen strengthened.

Carbides of the M_6C type are observed in austenitic grades containing substantial molybdenum or niobium additions. It usually precipitates intragranularly. For example, in AISI 316 with 2 to 3% Mo, M_6C will form after approximately 1500 h at 650 °C (1200 °F). Several types of M_6C have been observed, including Fe_3Mo_3C, Fe_3Nb_3C, and $(Fe, Cr)_3Nb_3C$.

Several types of sulfides have been observed in austenitic grades. The most common form is MnS. However, if the manganese content is low, chromium will replace some of the manganese in the sulfide. At manganese contents less than approximately 0.20%, pure chromium sulfides will form. Because these are quite hard, machinability (tool life) will be poor. Figure 36 shows manganese sulfides in types 203 and 303 resulfurized austenitic grades. Some free-machining grades have additions of selenium and sulfur to form manganese selenides as well as manganese sulfides. Figure 30(d) shows the manganese selenides in 303Se. In grades with substantial titanium, several forms of titanium sulfides have been observed, including Ti_2S, Ti_2SC, and $Ti_4C_2S_2$.

Several intermetallic phases may be formed by high-temperature exposure. These phases form from titanium, vanadium, and chromium ("A" elements) and from manganese, iron, cobalt, and nickel ("B" elements). Some of these phases are stoichiometric compounds. Probably the most important is σ phase, first observed in 1927. The leaner austenitic grades free of δ-ferrite are relatively immune to σ-phase formation, but the higher alloy grades and those containing δ-ferrite are prone to its formation. Sigma is frequently described as FeCr, although its composition can be quite complex and variable, ranging from B_4A to BA_4.

Certain elements, such as silicon, promote σ-phase formation. Cold working also enhances subsequent σ-phase formation. Empirical equations based on composition have been developed to predict the tendency toward σ-phase formation (Ref 28, 29). Sigma is a very potent embrittler whose effects are observable at temperatures below approximately 595 °C (1100 °F). Sigma also reduces resistance to strong oxidizers. The morphology of σ phase varies substantially. Etching techniques (Ref 5, 30 to 32) have been widely used to identify σ phase in stainless steels (Fig. 19), but x-ray diffraction is more definitive. Although its crystal structure is tetragonal, σ phase does not respond to crossed-polarized light.

Chi phase (Ref 33 to 38) is observed in alloys containing substantial additions of molybdenum subjected to high-temperature exposure. Chi can dissolve carbon and exist as an intermetallic compound or as a carbide ($M_{18}C$). It is often observed in alloys susceptible to σ-phase formation and has a bcc, α-manganese-type crystal structure. Several forms of the intermetallic phase have been identified, as shown in Table 10. Chi nucleates first at grain boundaries, then at incoherent twin boundaries, and finally intragranularly (Ref 38). Chi varies in shape from rodlike to globular. As with σ phase, cold work accelerates nucleation of χ phase.

Laves phase (η phase) can also form in austenitic stainless steels after long-term high-temperature exposure (Ref 37, 38). Alloys containing molybdenum, titanium, and niobium are most susceptible to Laves formation. Precipitation occurs from 650 to 950 °C (1200 to 1740 °F). Laves is a hexagonal intermetallic compound of AB_2 form. Several types have been observed, as shown in Table 10. Laves phase precipitates intragranularly and exists as globular particles.

Other phases have been observed in stainless steels but less often than those discussed previously. Among these is R phase (Ref 39 to 41), which has been observed in an Fe-12Cr-CoMo alloy and in welded AISI 316. A globular nickel-titanium silicide, G phase, was observed in a 26Ni-15Cr heat-resistant A-286-type alloy and was attributed to grain-boundary segregation (Ref 42). A chromium-iron-niobide phase, Z phase (Ref 43), was detected in an 18Cr-12Ni-1Nb alloy after creep testing at 850 °C (1560 °F). Table 10 summarizes the more common second-phase constituents observed in stainless steels. Austenitic grades, chiefly 304, have been modified with additions of boron to produce chromium borides. These steels have been used as control rods (using boron enriched in the B^{10} isotope, Fig. 37), and for nuclear waste containment (Fig. 38). Etching with waterless Kalling's reagent will outline the borides, and a deeper etch will bring up the austenite grain structure.

The ferritic stainless steels (Ref 44) are basically iron-chromium alloys with enough chromium and other elements to stabilize bcc ferrite at all temperatures. Carbon and nitrogen contents must be minimized. The microstructure of these alloys consists of ferrite plus small amounts of finely dispersed $M_{23}C_6$, but other phases may form due to high-temperature exposure. However, because of severe embrittlement problems, these alloys are generally not used for elevated-temperature service.

The ferritic grades depend on solid-solution strengthening, because heat treatment cannot be used to harden the alloys or produce grain refinement. Quenching ferritic alloys from high temperatures produces only very slight increases in hardness. However, because many users desire higher strengths, steelmakers often make type 430 with a carbon content high in the allowable range (<0.12% C is specified), rather than keeping carbon as low as possible. This re-

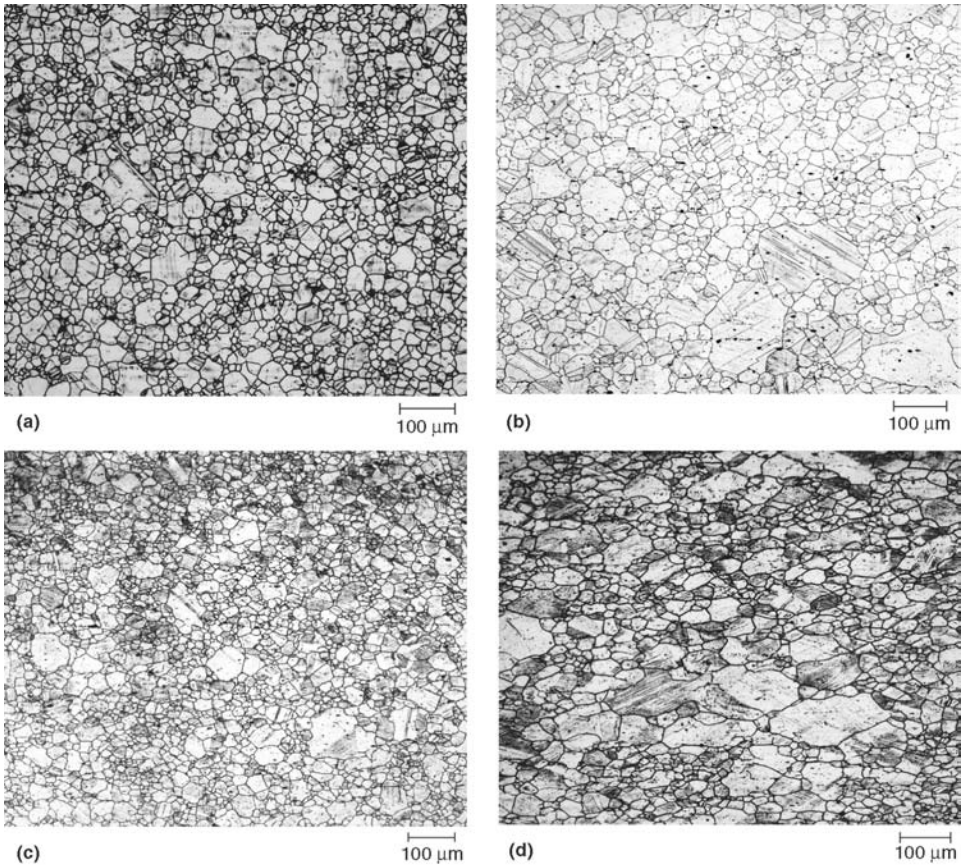

Fig. 32 Slip near the surface of cold-drawn 347 stainless steel reduced (a) 5%, (b) 10%, (c) 15%, and (d) 30% in diameter. Revealed using aqueous 60% HNO_3 at 4 V dc

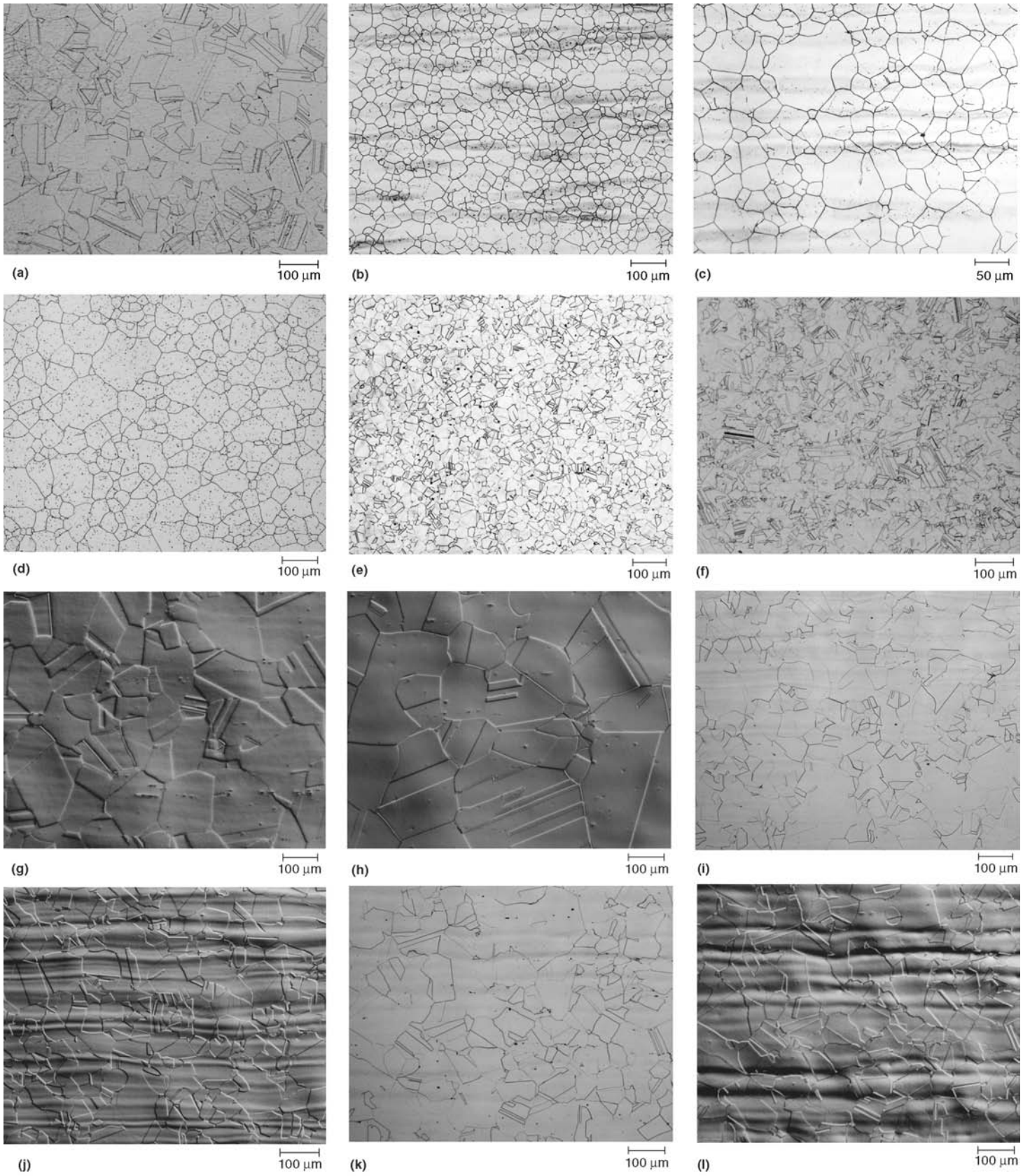

Fig. 33 Austenitic grain boundaries revealed in (a) 302-HQ etched with waterless Kalling's, (b) 304 Modified etched with aqueous 60% HNO_3 at 1 V dc for 90 s, (c) 316L etched as in (b) but for 20 s, (d) concast 316 etched with aqueous 60% HNO_3 at 1.5 V dc for 60 s, (e) 330 etched as in (d), (f) Nitronic 50 etched with glyceregia, (g) 18-18 PLUS etched with 15 HCl-10 HNO_3-10 acetic acid, (h) 20 Mo-6 etched as for (g), (i) AL-6XN plate etched as in (g), (j) same field as (i) but viewed with Nomarski differential interference contrast, (k) SCF-23 etched as in (g), and (l) same field as (k) but viewed with Nomarski differential interference contrast. (g) and (h) also viewed with Nomarski DIC.

sults in a duplex ferrite-martensite grade that can be heat treated to higher strength levels. Figure 39 illustrates the microstructure of a duplex 430 grade. Type 430 is also made with high sulfur for improved machinability (Fig. 40). However, the classic ferritic stainless steel contains only ferrite grains, as illustrated by the examples in Fig. 8 and 41. Figure 42 shows the microstructure of a weld in 29-4 ferritic stainless steel.

Three forms of embrittlement can occur in ferritic stainless steels: σ-phase embrittlement, 475 °C (885 °F) embrittlement, and high-temperature embrittlement. Sigma is difficult to form in alloys with less than 20% Cr but forms readily in alloys with 25 to 30% Cr when heated between 500 and 800 °C (930 and 1470 °F). Molybdenum, silicon, nickel, and manganese additions shift the σ-forming tendency to lower chromium contents. As with the austenitic grades, σ phase severely reduces ductility and toughness below approximately 600 °C (1110 °F). Sigma can be redissolved by holding for a few hours above 800 °C (1470 °F).

Ferritic stainless steels are susceptible to embrittlement when heated from 400 to 540 °C (750 to 1005 °F), a condition referred to as 475 °C (885 °F) embrittlement. Embrittlement, which increases with time at temperature, is caused by production of chromium-rich and iron-rich ferrites but can be removed by heating above approximately 550 °C (1020 °F). Under identical aging conditions, embrittlement increases with increasing chromium content.

High-temperature embrittlement occurs in alloys with moderate to high interstitial carbon and nitrogen contents heated above 950 °C (1740 °F) and cooled to room temperature, resulting in severe embrittlement and loss of corrosion resistance. This has been attributed to chromium depletion adjacent to precipitated carbides and nitrides. The properties of such a sensitized specimen can be improved by heating to 700 to 950 °C (1290 to 1740 °F), which allows chromium to diffuse to the depleted areas. A better procedure, however, is to reduce the carbon and nitrogen contents to very low levels, which also improves toughness and weldability. Strong carbide-forming elements, such as titanium and niobium, may also be added.

Martensitic Stainless Steels. The hardenable martensitic stainless steels contain more than 10.5% Cr plus other austenite-stabilizing elements, such as carbon, nitrogen, nickel, and manganese, to expand the austenite phase field and permit heat treatment. The composition must be carefully balanced to prevent δ-ferrite formation at the austenitizing temperature. Delta-ferrite in the hardened structure should be avoided to attain the best mechanical properties. Empirical formulas have been developed to predict δ-ferrite formation based on the composition (Ref 45, 46). Temperature control during austenitization is also important for preventing δ-ferrite formation. To enhance the machinability of type 416 stainless steel, steelmakers deliberately form δ-ferrite, as shown in Fig. 43. The martensitic grades are generally immune from σ-phase formation.

Increases in strength when martensitic stainless steels are heat treated depend primarily on the carbon content, which can vary widely in these grades, and on the stability of δ-ferrite at the austenitizing temperature. The hardenability of these grades is very high due to the high chromium content. All these grades can be martempered to reduce the risk of quench cracking in complex shapes. The heat treatment of these

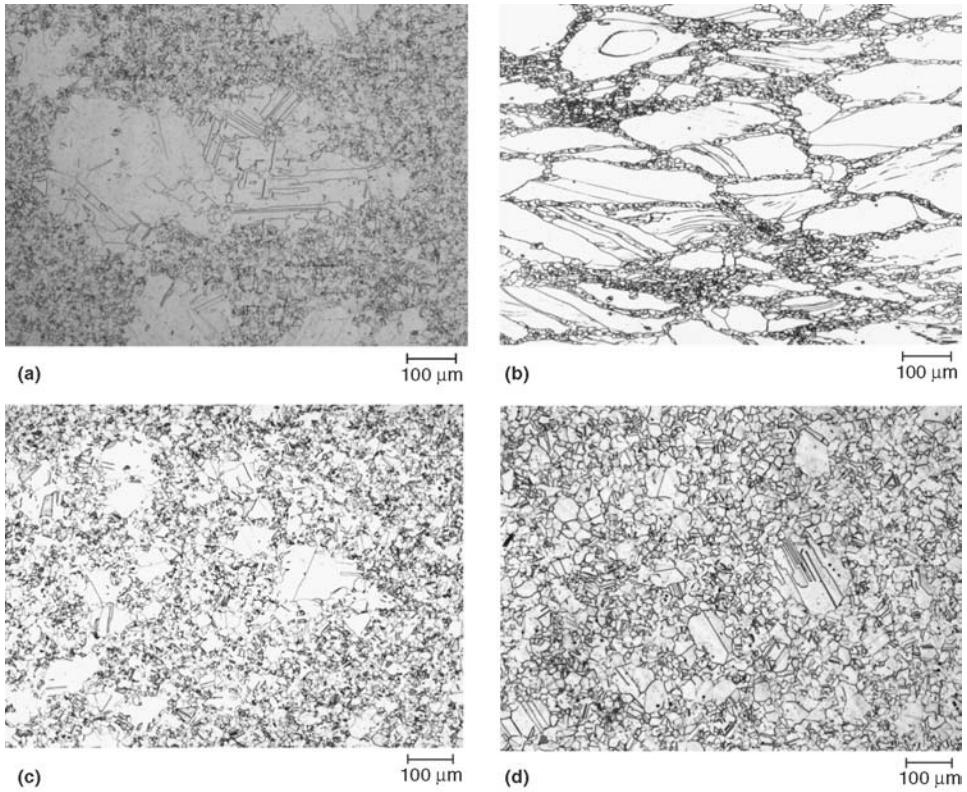

Fig. 34 Duplex grain structures observed in (a) Nitronic 50 etched with glyceregia, (b) SCF-19 etched with aqueous 60% HNO_3 at 1 V dc for 60 s ("necklace"-type condition), (c) 22-13-5 etched with waterless Kalling's reagent, and (d) 330 etched as in (b) but at 1.5 V dc

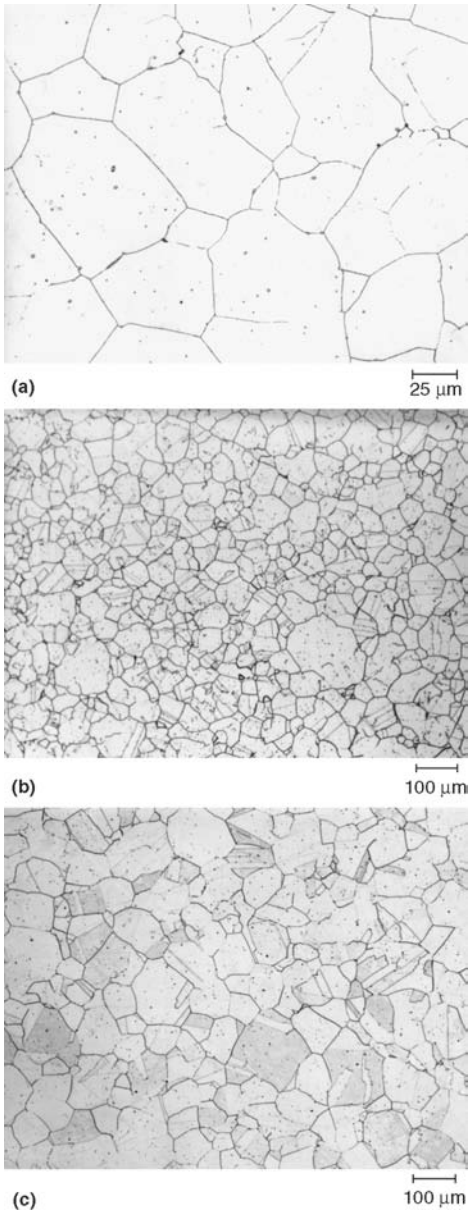

Fig. 35 Grain-boundary carbides in sensitized (a) 304 etched with Ralph's reagent, (b) 304 etched with aqueous 10% ammonium persulfate at 6 V dc for 10 s, and (c) 316 etched as in (a)

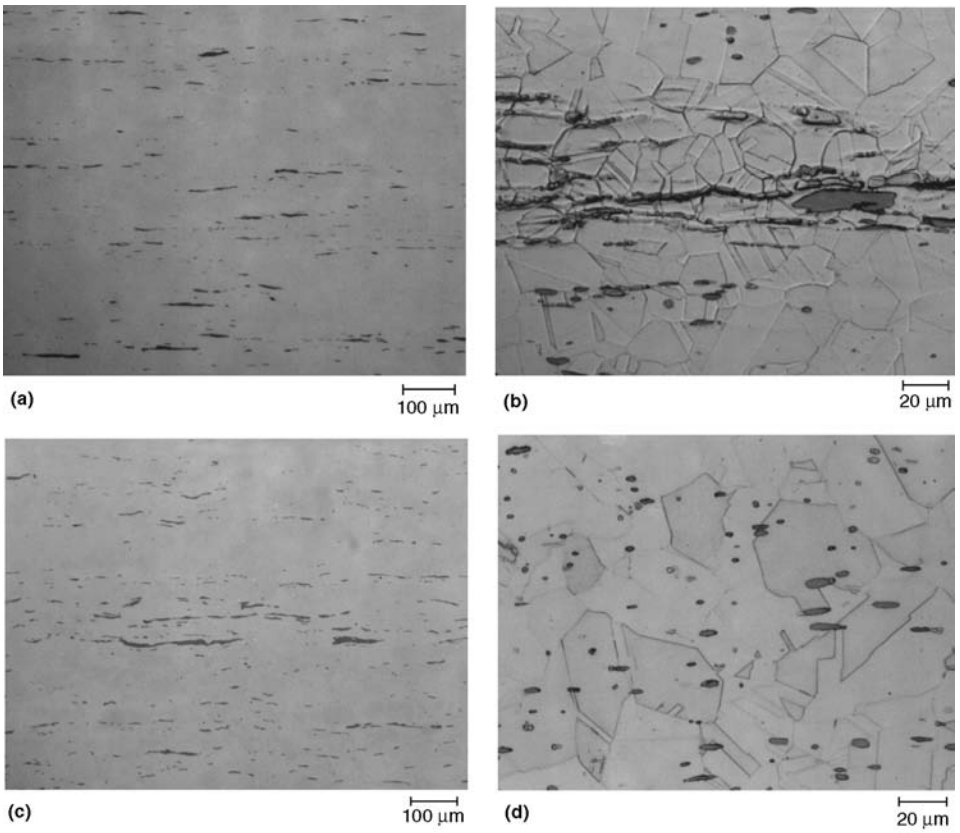

Fig. 36 Examples of the grain structures of resulfurized stainless steels revealed using Ralph's reagent. (a) and (b) 203. (c) and (d) 303

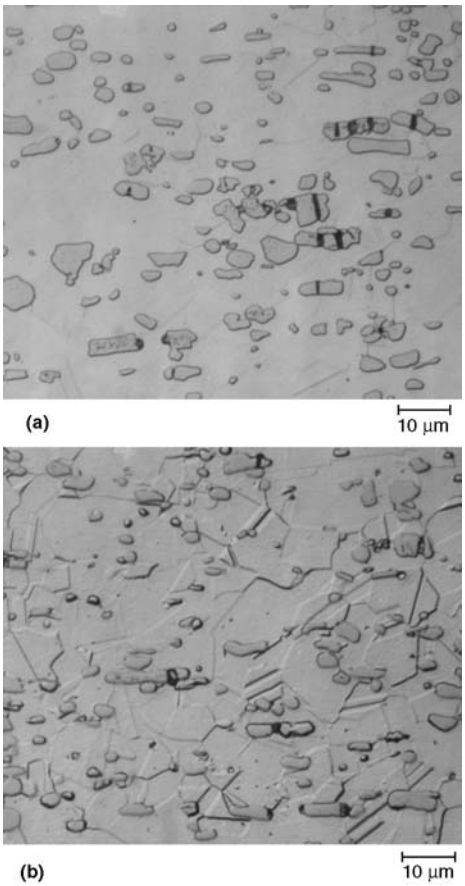

Fig. 37 The microstructure of 304 stainless steel plus boron enriched in the B^{10} isotope for nuclear reactors (Nautilus-class submarines). (a) Etched with waterless Kalling's reagent. (b) Etched with waterless Kalling's reagent but heavier than (a) to reveal the grain boundaries

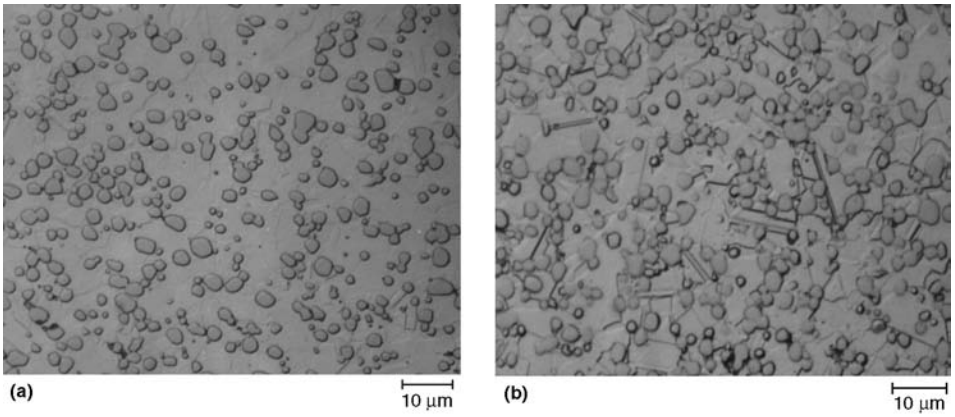

Fig. 38 The microstructure of powder metallurgy 304 stainless steel plus 1.75% B for nuclear waste containment. (a) Etched with waterless Kalling's reagent. (b) Etched with waterless Kaling's reagent but heavier than (a) to reveal the grain boundaries

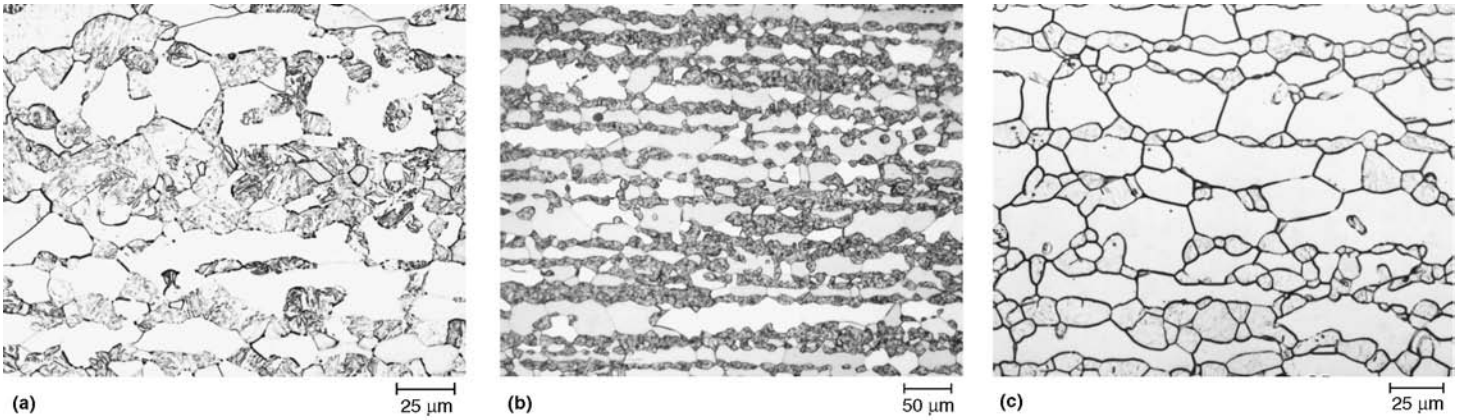

Fig. 39 Microstructure of high-carbon type 430 stainless steel with a duplex martensite-ferrite grain structure, revealed using (a) glyceregia, (b) Beraha's tint etch, and (c) aqueous 60% HNO_3 at 1 V dc for 60 s

grades is very similar to that of highly alloyed tool steels.

The appearance of martensite in these grades varies with carbon content. With increasing carbon content, the martensite becomes finer, changing from lath to plate morphology, and the amount of residual retained austenite increases but will not cause problems unless excessively high austenitizing temperatures are used. Figure 44 shows tempered martensite in martensitic stainless steels over the range of carbon contents encountered. This series also shows the structure of powder metallurgy (P/M) alloys versus ingot technology alloys of the same grade. The difference is more noticeable when comparing the P/M versus ingot technology 440C (Fig. 44f and g) than for the 422 grade (Fig. 44d and e), due to the marked difference in carbide size and segregation in P/M 440C versus the conventional product. In most cases, martensitic stainless steels are sold in the annealed condition. It is very important to control the carbide size and distribution in these alloys. If carbide is precipitated in the grain boundaries (Fig. 45), they will be present in the part after quenching and tempering (Fig. 46), which will drastically reduce toughness and ductility. Figure 47 shows examples of annealed martensitic stainless steel microstructures. A uniform dispersion of carbides in ferrite is desired. Coarse carbides in type 440C, made by conventional technology, have been a problem, because this limits cold formability and toughness. Figure 48 shows cracked primary carbides in 440B and 440C grades (compare Fig. 48b to Fig. 47e, which has large, noncracked primary carbides). Segregation can be a problem in any stainless grade. Figure 49 shows an example of alloy segregation that apparently caused δ-ferrite formation and then carbide precipitation at the δ-ferrite phase boundaries. Subsequent processing removed the δ-ferrite but not the carbides. Control of the austenitizing temperature is vitally important in martensitic stainless steels to avoid grain growth. In 440C, excessive austenitizing temperatures will dissolve more carbide, thus lowering the martensite start and finish temperatures, resulting in incomplete transformation of austenite to martensite during quenching, as illustrated in Fig. 50. Figure 51 shows the microstructure of EP 428, an alloy similar to type 422, used for turbine blades and disks in electric power-generation systems. Figure 51(a) shows the microstructure after the standard heat treatment, while Fig. 51(b) and (c) show the alloy after 100,000 h service at 350 and 500 °C (660 and 930 °F). The microstructure appears to be coarser after extended service. The carbide composition has changed with service exposure, but this cannot be detected by light microscopy.

Tempering reactions are similar to those observed in the high-alloy tool steels. For example, when as-quenched AISI 410 is tempered, M_3C is present at tempering temperatures to approximately 480 °C (900 °F) but is not present at approximately 650 °C (1200 °F). At approximately 480 °C (900 °F), $M_{23}C_6$ forms. It becomes the predominant carbide at 540 °C (1005 °F) and above. At approximately 480 °C (900 °F), M_7C_3 also forms but decreases in quantity with higher tempers. Because M_7C_3 seriously degrades corrosion resistance, its presence at tempering temperatures of 480 to 650 °C (900 to 1200 °F) precludes using this tempering range. Tempers below approximately 480 °C (900 °F) are also avoided due to low toughness. Overtempering must be avoided, particularly in those grades containing nickel, because of formation of reverted austenite.

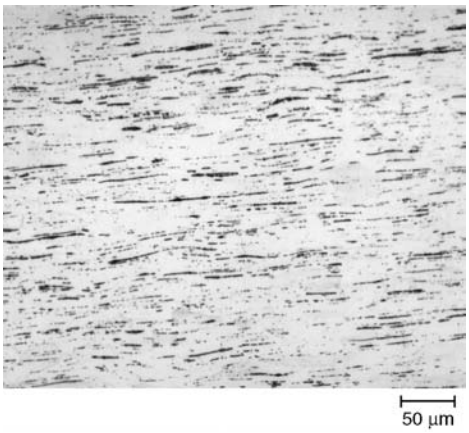

Fig. 40 Microstructure of 430F resulfurized steel etched lightly with Ralph's reagent

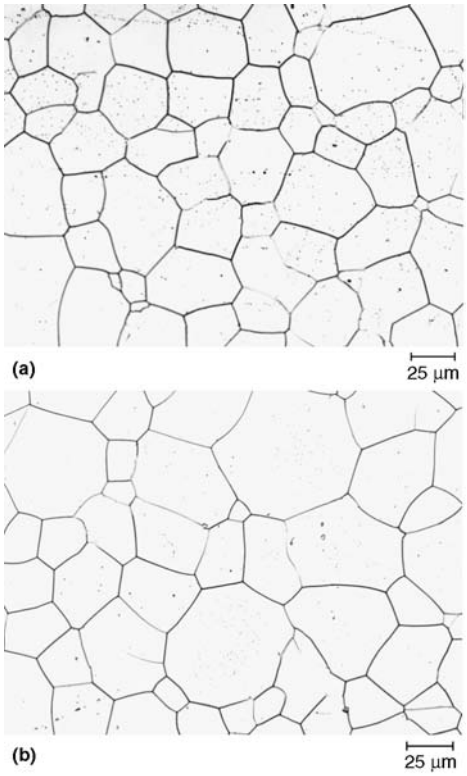

Fig. 41 Ferritic grain structure of (a) Monit and (b) Seacure stainless steels etched with aqueous 60% HNO_3 at 1.5 V dc for 120 s

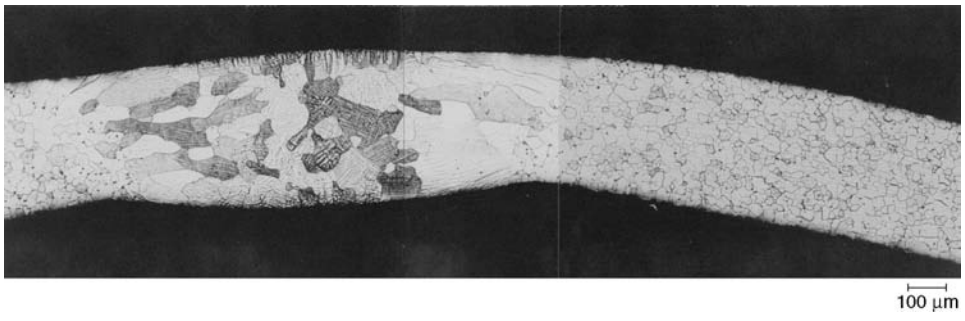

Fig. 42 Ferritic grain structure of a welded 29-4 ferritic tube etched with aqueous 60% HNO_3 at 1.5 V dc

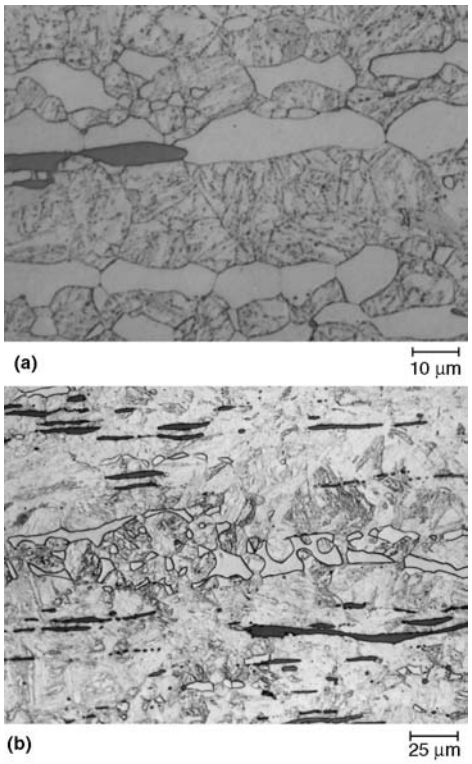

Fig. 43 Delta-ferrite and manganese sulfides in martensitic matrix of (a) 416 stainless steel etched with modified Fry's reagent and (b) 5F (modified 416) stainless steel etched with Ralph's reagent

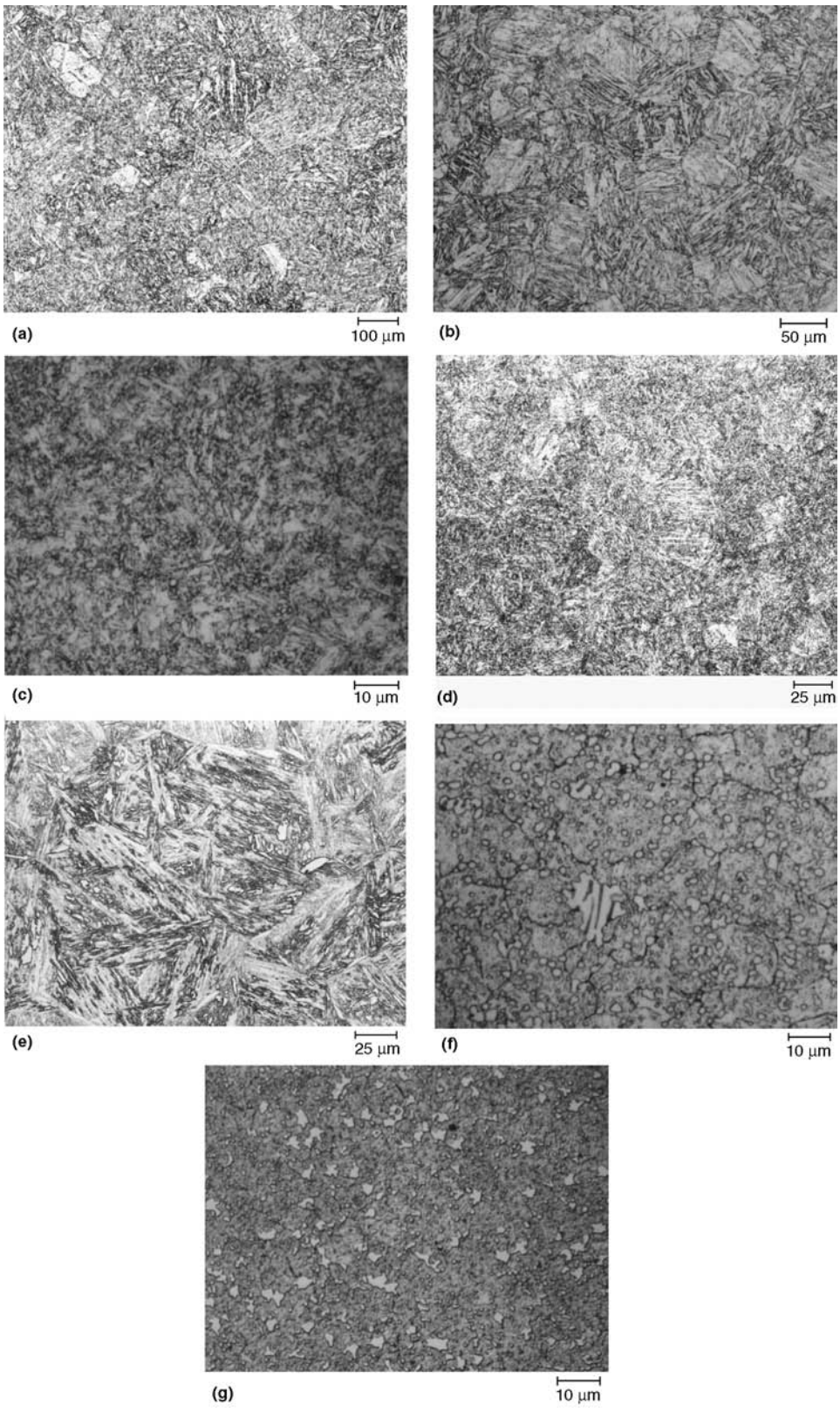

Fig. 44 Examples of the appearance of martensite in quenched and tempered martensitic stainless steels. (a) 403 etched with 4% picral plus HCl. (b) 410 etched with Vilella's reagent. (c) 420 etched with Ralph's reagent. (d) Powder metallurgy 422 etched with Ralph's reagent. (e) EF-AOD/ESR 422 etched with Ralph's reagent. (f) Ingot technology 440C etched with Vilella's reagent. (g) Powder metallurgy 440C etched with Ralph's reagent

Martensitic stainless steels are also susceptible to surface decarburization during heat treatment if the furnace atmosphere is not properly controlled. However, with their high chromium content, they are less susceptible than many of the low-alloy tool steels.

Of the cast alloys listed in Table 3, CA-6NM and CA-15 are essentially martensitic when cooled from the austenitizing temperature (approximately 980 °C, or 1800 °F). The martensitic structure of CA-6NM depends on a proper balance of low carbon content (0.06% maximum) and nickel content (nominally 4%). These alloys develop maximum strength and corrosion resistance in the hardened and tempered condition. They are normally tempered at a temperature safely above the maximum recommended service temperature—approximately 540 °C (1005 °F). Figure 52 shows the martensitic structure of cast CA-6NM (341 HV) etched with Ralph's reagent (note the small amount of δ-ferrite in Fig. 52b) and with 15 mL HCl-10 mL acetic acid-10 mL HNO_3. The latter etch, although quite strong,

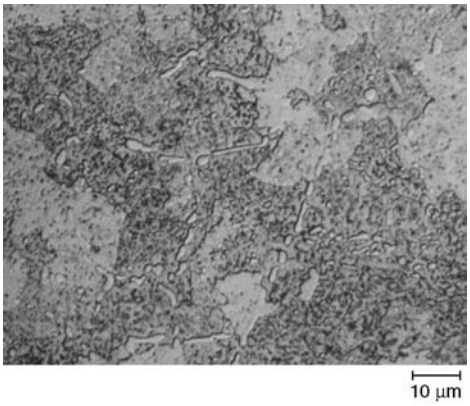

Fig. 45 Grain-boundary carbide networks in annealed 420 stainless steel etched with Ralph's reagent

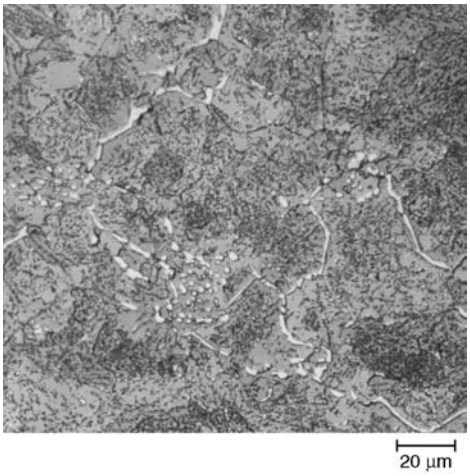

Fig. 46 Grain-boundary carbides in annealed 420 stainless steel tint etched with Beraha's sulfamic acid etch (No. 4)

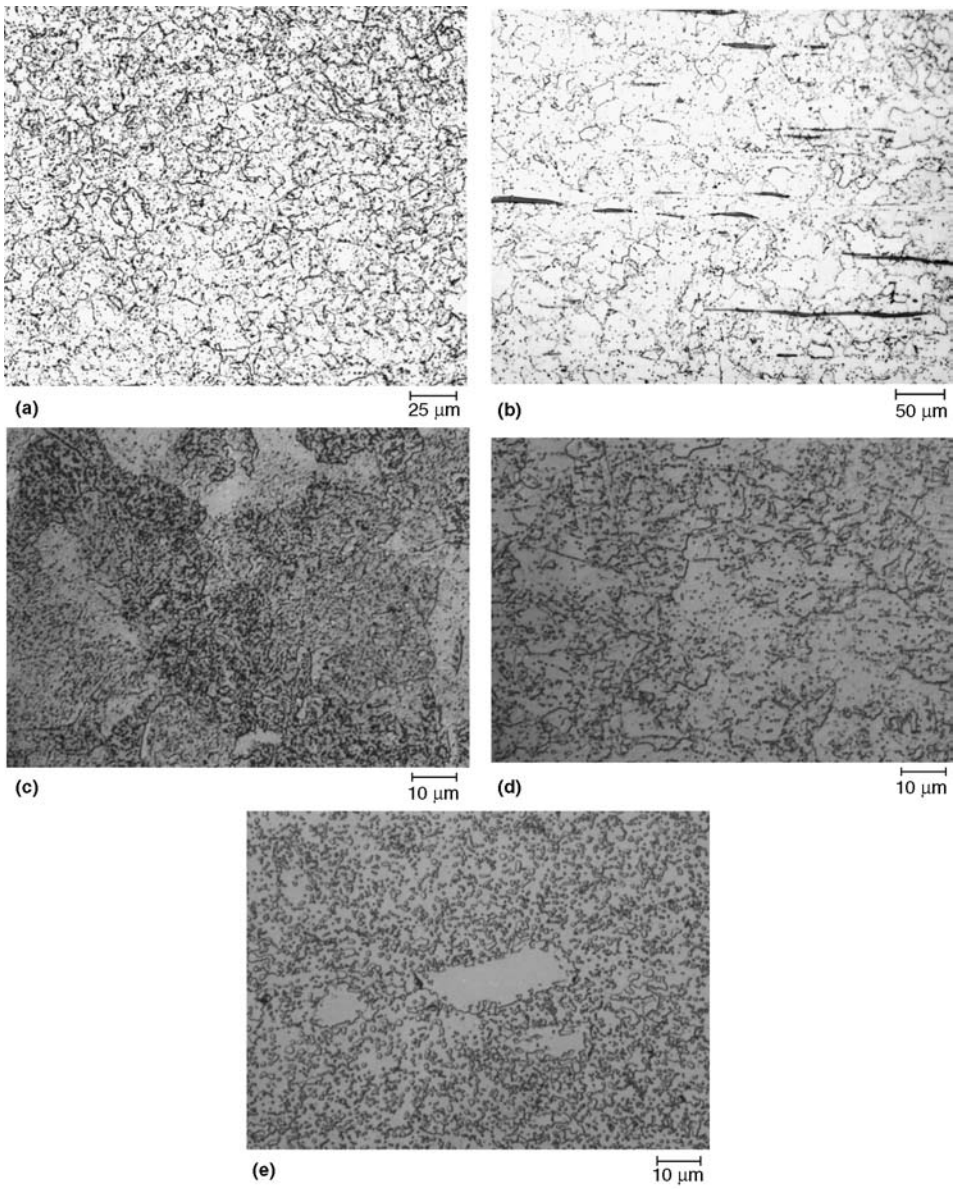

Fig. 47 Examples of annealed martensitic stainless steel microstructures. (a) 403 etched with 4% picral plus HCl. (b) Bushing-quality 416 etched with Vilella's reagent. (c) 420 etched with Ralph's reagent. (d) Trimrite etched with Vilella's reagent. (e) 440C etched with modified Fry's reagent

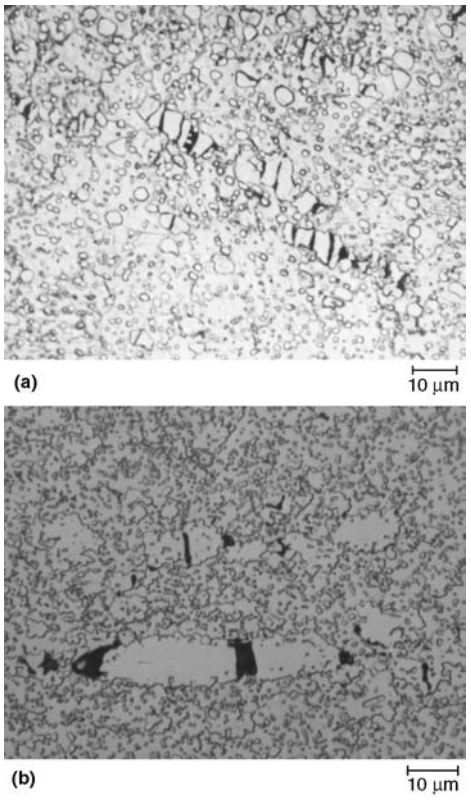

Fig. 48 Carbides cracked due to excessive cold deformation in (a) 440B etched with Vilella's reagent and (b) 440C martensitic stainless steel etched with modified Fry's reagent

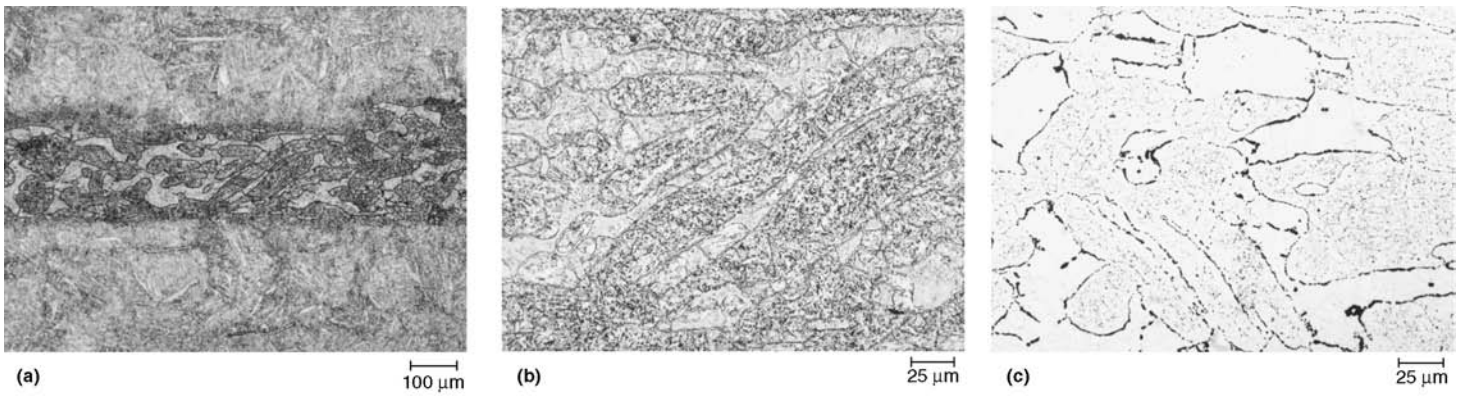

Fig. 49 Carbide segregation in a segregation streak in 422 martensitic stainless steel. (a) and (b) Etched with glyceregia. (c) Etched 30 s with Murakami's at room temperature to darken the carbides

did not reveal the structure fully, but by going to Nomarski differential interference contrast (Fig. 52d), details can be better revealed. Figure 53 shows the martensitic microstructure of as-cast CD-4MCu (295 HV), with ferrite in the interdendritic boundaries. Figure 54 shows the microstructure of cast high-carbon, high-chromium martensitic white cast irons. Note the substantial amount of primary carbide, mostly Cr_7C_3, in these alloys. Beraha's sulfamic acid (No. 4) tint etch (see the article "Color Metallography" in this Volume) did a much better job of revealing the carbide distribution than standard etchants, such as Vilella's reagent. Figure 55 shows the martensitic structure of as-cast 410 stainless steel, which contained patches of δ-ferrite, while Fig. 56 shows the microstructure of as-cast 440C, with segregation and primary carbide eutectics in the interdendritic region.

Precipitation-Hardenable Grades. The precipitation-hardenable stainless steels (Ref 47 to 50) were developed in the 1940s when the first alloy of this type, Stainless W, was introduced. Three types of precipitation-hardenable grades have been developed: austenitic, semiaustenitic, and martensitic. All are hardened by a final aging treatment that precipitates very fine second-phase particles from a supersaturated solid solution. Precipitation introduces strain into the lattice, which produces the strengthening. Maximum strengthening occurs well before visible precipitates are produced. Increasing the aging temperature reduces the aging time for maximum strength, but a lower strength is obtained. As shown in Table 1, precipitation-hardenable grades contain additions of aluminum, copper, titanium, and, occasionally, molybdenum and niobium to produce the precipitates.

The semiaustenitic grades have an austenitic matrix with up to 20% δ-ferrite that persists throughout heat treatment. These grades are austenitic (plus δ-ferrite) in the solution-annealed condition but can be transformed to martensite by a series of thermal or thermomechanical treatments. Because they are complex alloys, the chemical composition must be carefully balanced.

Heat treatment of the semiaustenitic grades requires conditioning of the austenite matrix, transformation to martensite, then precipitation hardening. The austenite conditioning treatment removes carbon from solution as $Cr_{23}C_6$, beginning at the austenite/δ-ferrite interfaces. This is accomplished by heating to between 705 and 815 °C (1300 and 1500 °F). The austenite is unstable and transforms to martensite on cooling. The martensite start temperature, M_s, is approximately 65 to 93 °C (150 to 200 °F); the martensite finish temperature, M_f, is approximately 15 °C (60 °F). The alloy is then aged, usually between 480 and 650 °C (900 and 1200 °F), to relieve stress produced during martensite formation and to increase toughness, ductility, and corrosion resistance. Aging at 565 °C (1050 °F) or above results in overaging, with the occurrence of precipitation of the strengthening intermetallic second phase, tempering of the martensite, and partial reversion of martensite to austenite (reverted austenite). Cold working can also be used to produce martensite, which is followed by aging.

Commercial examples of semiaustenitic precipitation-hardenable stainless steels include types 17-7 PH, PH 15-7 Mo, and PH 14-8 Mo. Also classed as semiaustenitic precipitation-hardenable grades are AM 350 and AM 355, but they do not have true precipitation reactions. These grades are embrittled by long-term exposure above approximately 550 °C (1020 °F), due to continued precipitation of the intermetallic-strengthening phase. Figure 57(a) shows nitrides in 17-7 PH, while Fig. 57(b) shows the etched microstructure of this specimen with isolated patches of ferrite. Figure 57(c) shows heavier δ-ferrite stringers in a different specimen of 17-7 PH. Figure 58(a) shows δ-ferrite stringers in PH 15-7 Mo. Etching longer with waterless Kalling's reagent brought up the martensitic matrix,

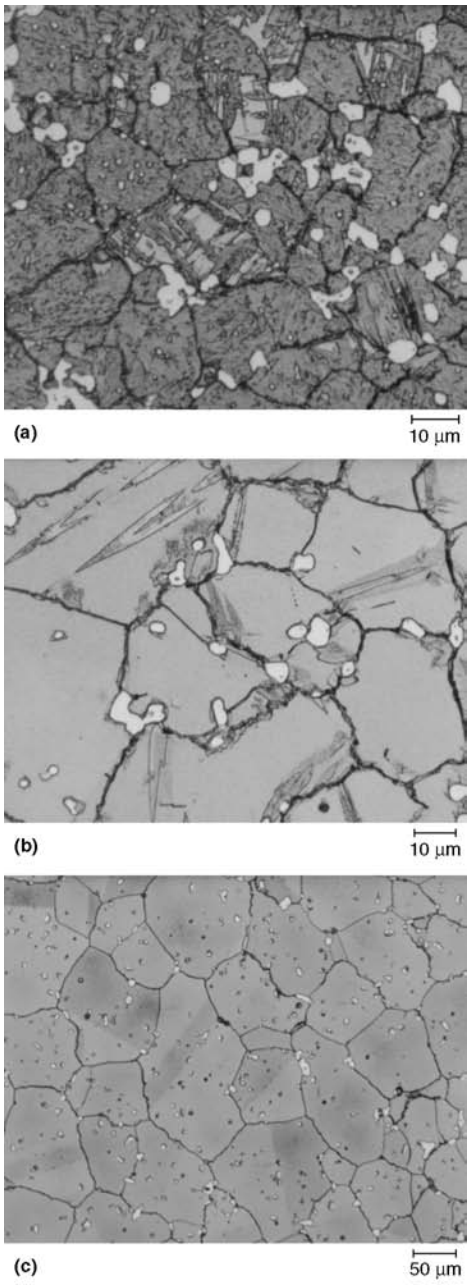

Fig. 50 Raising the austenitizing temperature during the heat treatment of type 440C stainless steel from (a) 1150 °C (2100 °F) to (b) 1204 °C (2200 °F) to (c) 1260 °C (2300 °F) caused the as-quenched microstructure to go from mainly martensite with some retained austenite (a) to mostly retained austenite with a few martensite plates (b) to nearly all retained austenite (c). Note that the carbide content also decreases and the grain size increases. Revealed using Beraha's sulfamic acid No. 4 tint etch

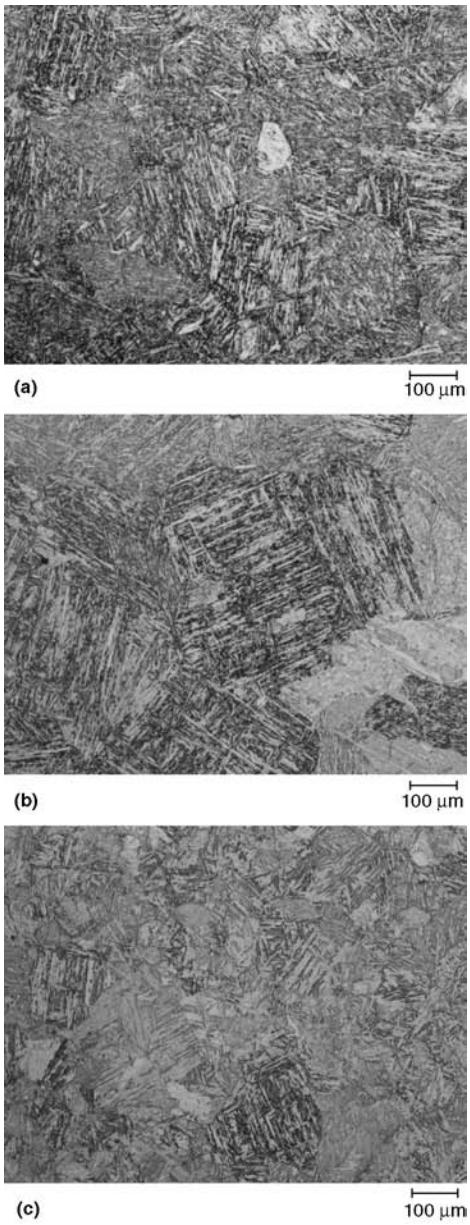

Fig. 51 Martensitic microstructure of EP 428 (revealed using Vilella's reagent) in the (a) as-heat-treated condition, and after 100,000 h at (b) 350 °C (660 °F) and (c) 500 °C (930 °F) service. Used as blades in electric power generators in Russia

but the δ-ferrite does not stand out as well. Figure 59 shows the appearance of δ-ferrite on transverse and longitudinal planes in AM 350. Figure 60 shows the microstructure of AM 355, revealing reverted austenite and ferrite stringers.

The martensitic grades are the most popular precipitation-hardenable stainless grades. They are martensitic after solution annealing and do not retain austenite. Stainless W is a martensitic precipitation-hardenable type. Other more recently developed martensitic precipitation-hardenable grades are 17-4 PH, 15-5 PH, PH 13-8 Mo, Custom 450, and Custom 455, which are capable of strengths to 1380 MPa (200 ksi) or above. Figure 61(a) shows δ-ferrite (5.6%) in a 16.5 cm (6.5 in.) square billet after etching with Murakami's reagent. Figures 61(b) to (g) show 17-4 PH in the solution-annealed condition and after H900, H1025, H1075, H1100, and H1150M tempers (aging treatments). Figure 62(a) shows δ-ferrite in a 20 cm (8 in.) square billet (transverse plane, near the surface) after etching with Murakami's reagent. Figure 62(b) shows a fine δ-ferrite stringer in a smaller wrought bar. The specimen is in the H925 temper condition. Figure 62(c) shows a ferrite-free specimen with a martensitic structure after an H900 temper (41 HRC). Figure 63 shows the microstructure of PH 13-8 Mo in the solution-annealed and aged condition, with a fine martensitic structure. Figure 64(a) shows the structure of Custom 450 in the H1050 temper, while Fig. 64(b) shows it in the H1150 temper condition. Figure 65(a) shows Custom 455 in the solution-annealed condition, while Fig. 65(b) to (f) show it in the H850, H950, H1000, H1050, and H1100 temper conditions.

Stainless W and 17-4 PH contain δ-ferrite stringers in the martensitic matrix (17-4 PH can be made free of ferrite); the other grades are essentially free of δ-ferrite and so have better through-thickness properties. After solution annealing, they are aged at 425 to 455 °C (795 to 850 °F) or at 675 °C (1250 °F). High aging temperatures will produce reaustenitization, which transforms to untempered martensite on cooling to room temperature. Figures 22, 23, and 61(a) show δ-ferrite in 17-4 PH, while Fig. 24 and 59 show δ-ferrite in AM 350.

The austenitic precipitation-hardenable grades have the lowest usage. The austenite matrix in these alloys is very stable, even after substantial cold working. These grades are the forerunners of superalloys. The most common austenitic precipitation-hardenable grade is A-286 (illustrated in the article "Metallography and Microstructures of Heat-Resistant Alloys" in this Volume).

Alloy CB-7Cu-1 (Table 3) is a cast precipitation-hardening alloy similar to wrought 17-4 PH (Table 1). It is essentially martensitic in the solution-treated and aged conditions. It is generally solution treated at approximately 1040 °C (1900 °F) and aged at 480 to 620 °C (900 to 1150 °F) for maximum strength and resistance to corrosion.

The duplex stainless steels (Ref 51 to 53) were developed as a result of studies of superplasticity. They are usually very fine-grained microduplex structures with a composition centered on 26Cr-6.5Ni (IN-744). The very fine grain size improves strength and toughness, and their superplastic nature promotes hot workability. They exhibit good strength and corrosion resistance.

Thermomechanical processing is required to produce the fine duplex structure. During soaking for hot working, the second phase is dissolved. During hot working, it precipitates and stabilizes the grain size of the recrystallized matrix. The microduplex structure results only when second-phase precipitation precedes or occurs during recrystallization.

Service exposure at 370 to 540 °C (700 to 1005 °F) results in an increase in strength but loss of toughness. Sigma phase will form in IN-744 from exposure to temperatures between 550 and 800 °C (1020 and 1470 °F). Cold working enhances subsequent σ-phase formation. Other examples of duplex stainless steels include AISI

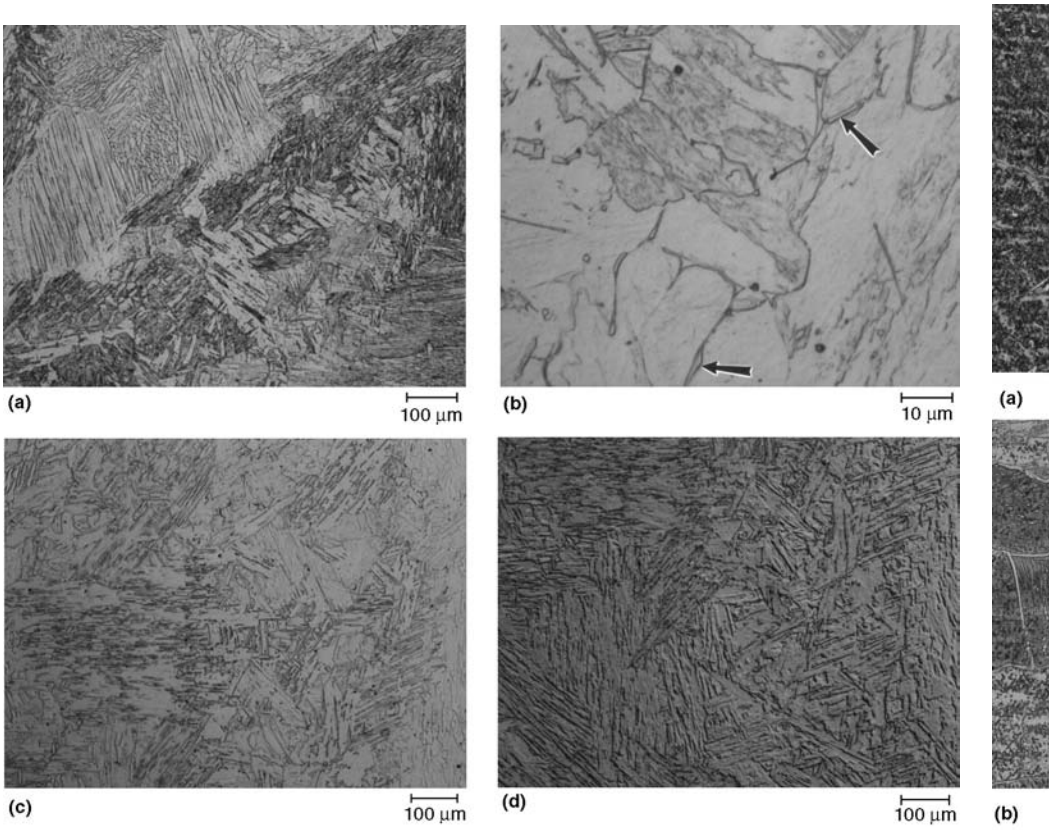

Fig. 52 Martensitic structure of as-cast CA-6NM stainless steel containing some δ-ferrite (see arrows in b). (a) and (b) Etched with Ralph's reagent. (c) and (d) Etched with 15 HCl-10 acetic acid-10 HNO_3. (d) Same field as (c) but viewed with Nomarski differential interference contrast

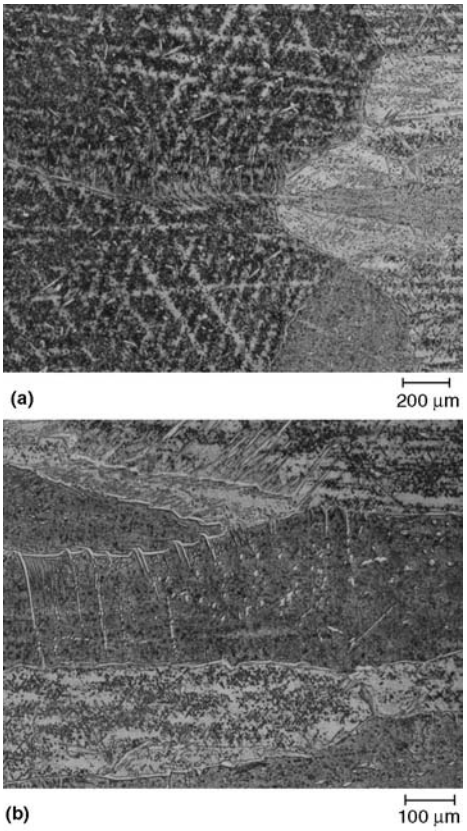

Fig. 53 Martensitic structure of as-cast CD-4MCu (295 HV) etched with waterless Kalling's reagent. There appears to be ferrite in the interdendritic boundaries.

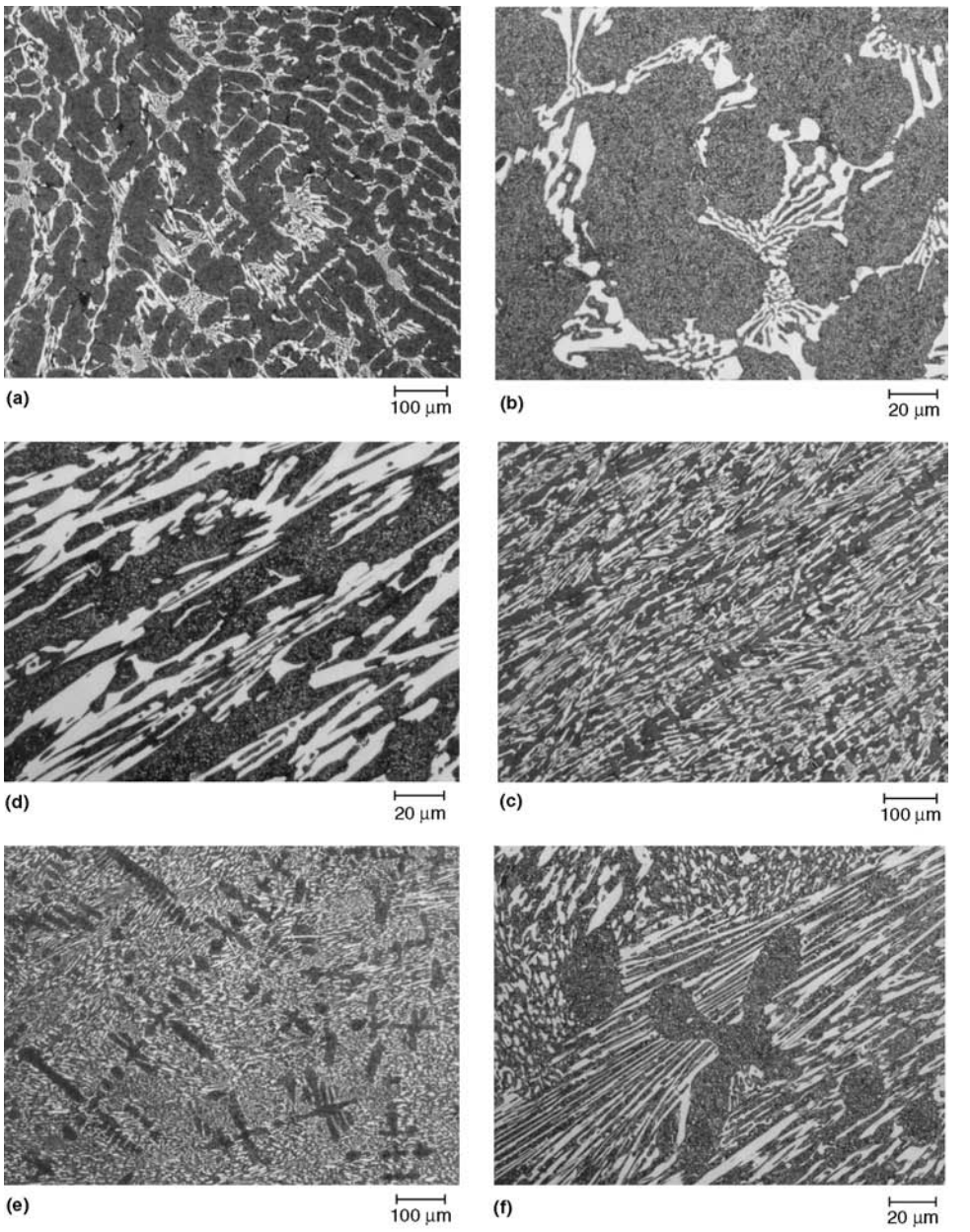

Fig. 54 Martensitic microstructure of Spanish cast high-chromium white irons. (a) and (b) Fe-2.21C-0.92Mn-0.54Si-12.65Cr-0.3Ni-0.70Mo-0.11V at 670 HV. (c) and (d) Fe-3.10C-0.75Mn-1.03Si-18.59Cr-0.22Ni-1.96Mo at 657 HV. (e) and (f) Fe-2.84C-0.67Mn-0.48Si-25.92Cr-0.21Ni-0.14Mo at 643 HV. All etched with Beraha's sulfamic acid (No. 4) reagent

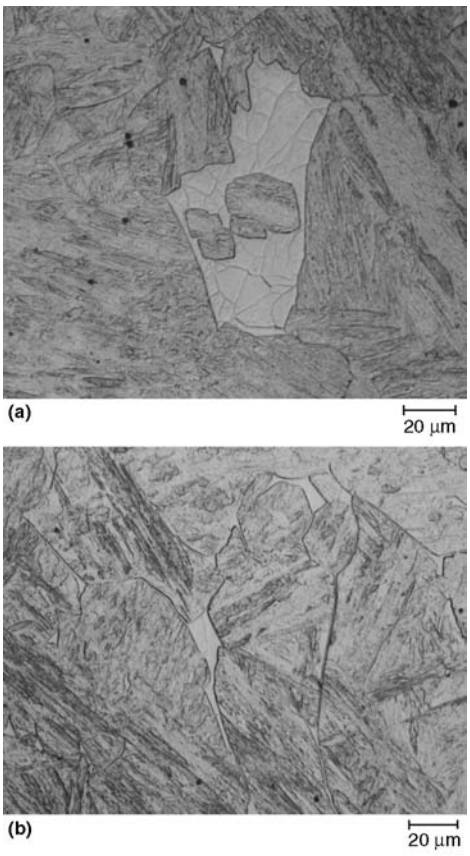

Fig. 55 Martensitic microstructure, with δ-ferrite, in as-cast 410 stainless steel (441 HV). Etched with Vilella's reagent

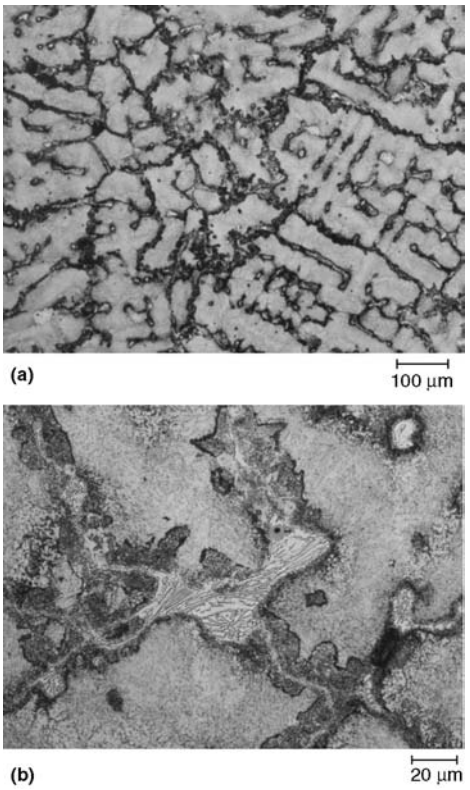

Fig. 56 As-cast microstructure of 440C (560 HV), with a martensitic matrix and a eutectic carbide constituent in the interdendritic regions. Revealed using Ralph's reagent

329, alloy 2205, 7-Mo PLUS, Ferralium alloy 255, and 44LN. Figures 66(a) and (b) show the microstructure of type 312 stainless steel in the annealed condition, while Fig. 66(c) to (e) show a bar after being removed from high-temperature exposure that broke because of embrittlement due to σ formation. Figure 67(a) shows the microstructure of solution-annealed alloy 2205 duplex stainless steel, while Fig. 67(b) and (c) show the precipitation of σ phase after 2 and 8 h at 800 °C (1470 °F). Figure 68 shows the microstructure of alloy 255 (Ferralium) in the annealed condition. The microstructure of 7-Mo PLUS duplex stainless steel is illustrated in Fig. 25.

Alloy CD-4MCu is a cast duplex-phase alloy that, in the solution-treated condition, consists of up to 65% ferrite and 35% austenite. It contains molybdenum and copper. It is normally used only in the solution-treated condition. After solution treating at temperatures above 1040 °C (1900 °F) and quenching in water, oil, or air (depending on casting shape and intended service), it has excellent corrosion resistance and approximately twice the strength of CF-8, an austenitic alloy that normally contains less than 15% ferrite. Other cast duplex stainless steels, as well as

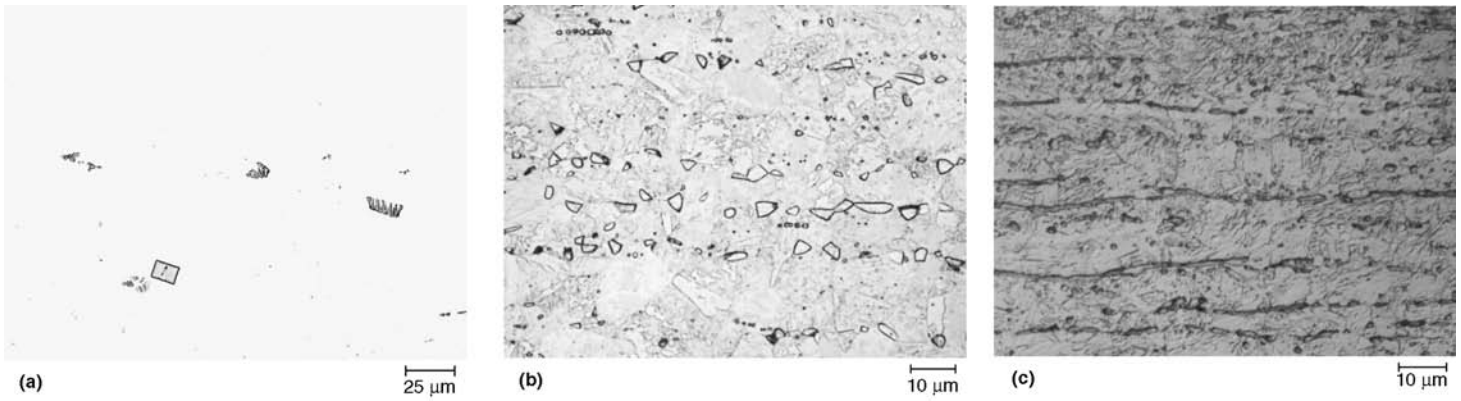

Fig. 57 Microstructure of 17-7 PH stainless steel (193 HV). (a) Nitrides viewed on an as-polished surface. (b) Delta-ferrite and martensitic matrix in specimen shown in (a). Etched with Vilella's reagent. (c) Delta-ferrite stringers and martensitic matrix of a different specimen. Etched with modified Fry's reagent

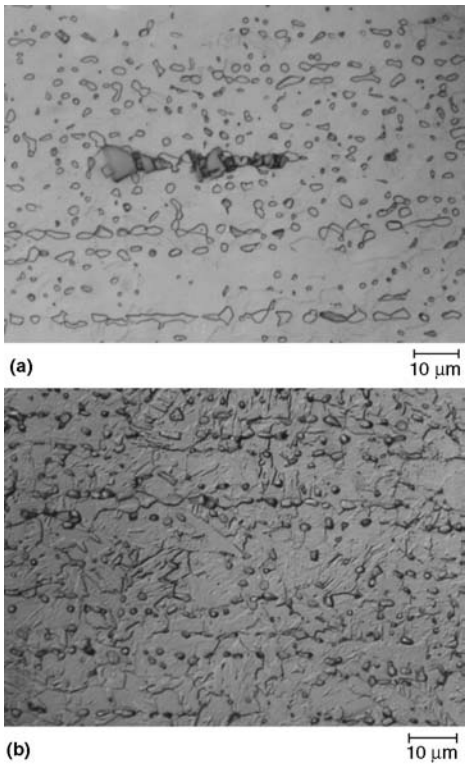

Fig. 58 Microstructure of PH 15-7 Mo stainless steel (360 HV) etched with waterless Kalling's reagent. (a) Light etch showing the δ-ferrite stringers and a nitride stringer. (b) Heavier etch to reveal the martensitic matrix

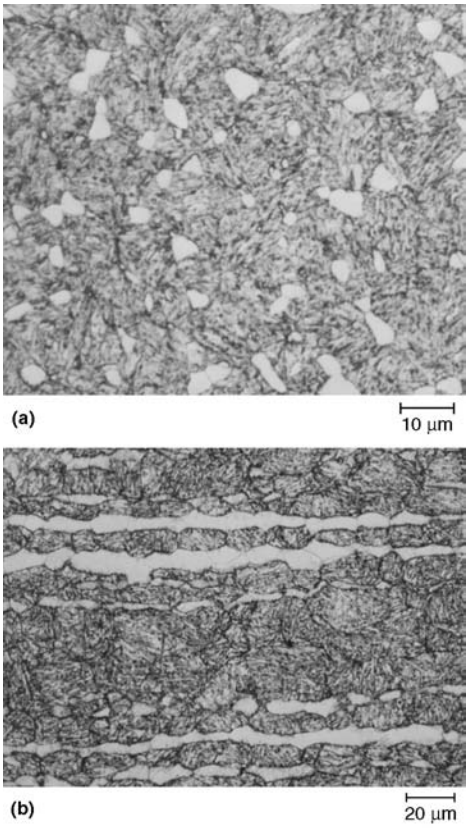

Fig. 59 Microstructure of AM 350 stainless steel etched with modified Fry's reagent, showing the difference in appearance of δ-ferrite in a martensitic matrix on (a) transverse and (b) longitudinal planes

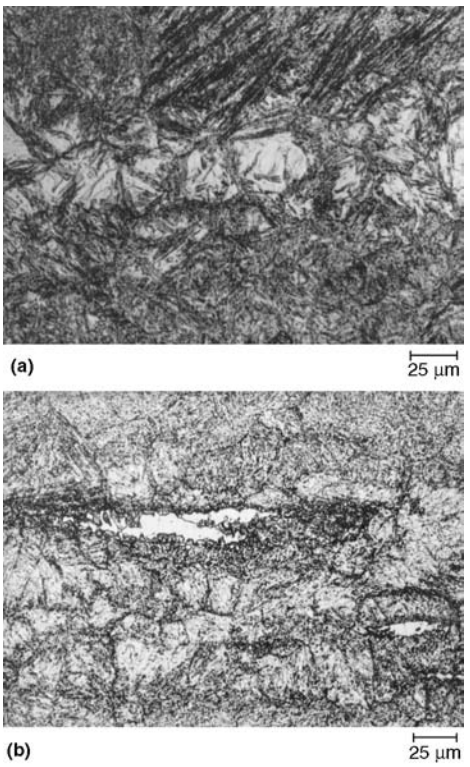

Fig. 60 Microstructure of as-hot-worked AM 355 stainless steel etched with glyceregia, showing (a) reverted austenite in a segregated area and (b) delta-ferrite in a martensitic matrix

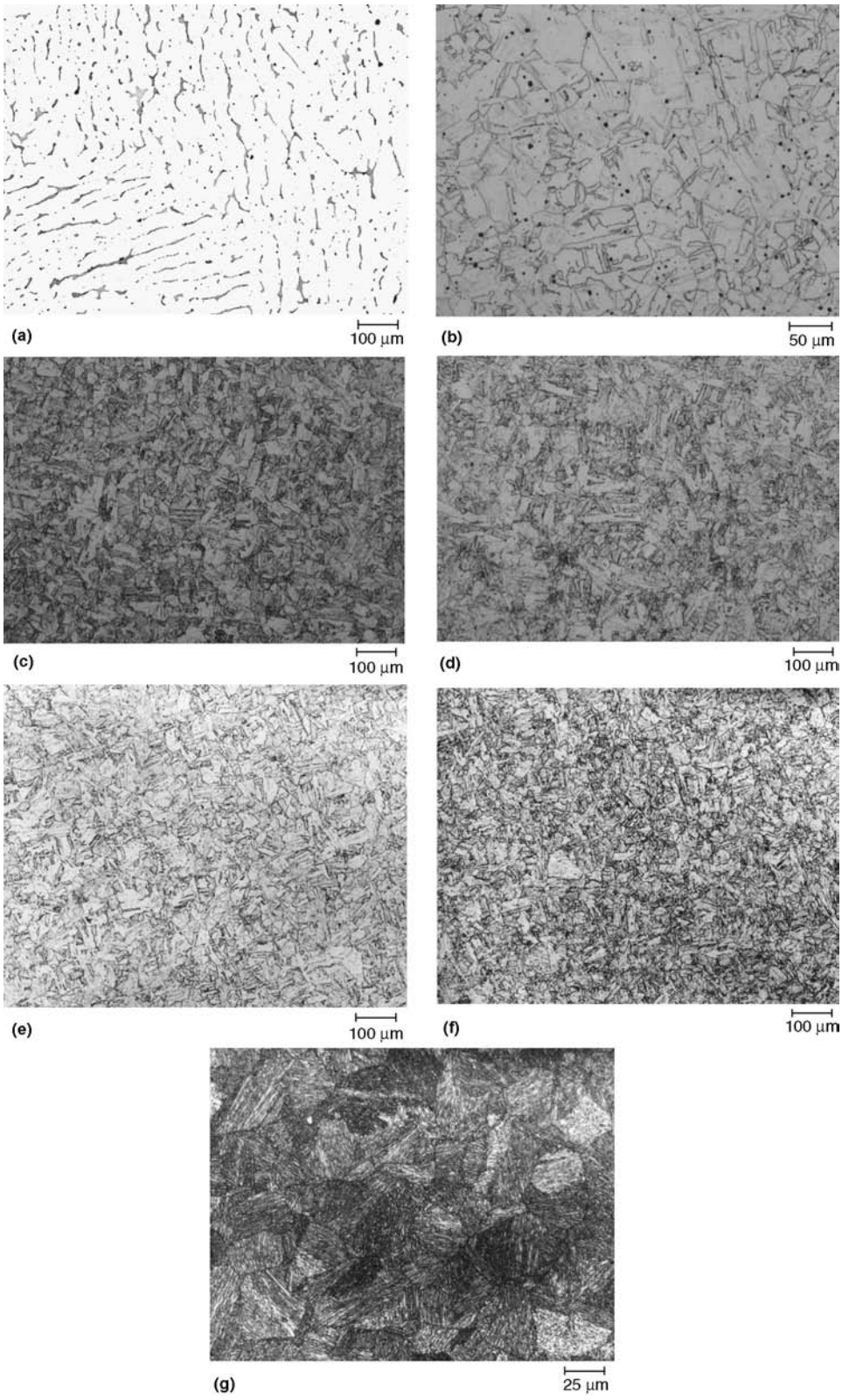

Fig. 61 Microstructure of 17-4 PH stainless steel. (a) Delta-ferrite (5.6%) revealed using Murakami's reagent (2 min at 100 °C, or 210 °F) on a transverse plane from a 16.5 cm (6.5 in.) square billet. (b) Martensitic matrix of a solution-annealed specimen. (c) H900 temper (430 HV). (d) H1025 temper (383 HV). (e) H1075 temper (359 HV). (f) H1100 temper (333 HV). (g) H1150 temper containing martensite and reverted austenite. (b) to (d) Etched with modified Fry's reagent. (e) to (g) Etched with Ralph's reagent

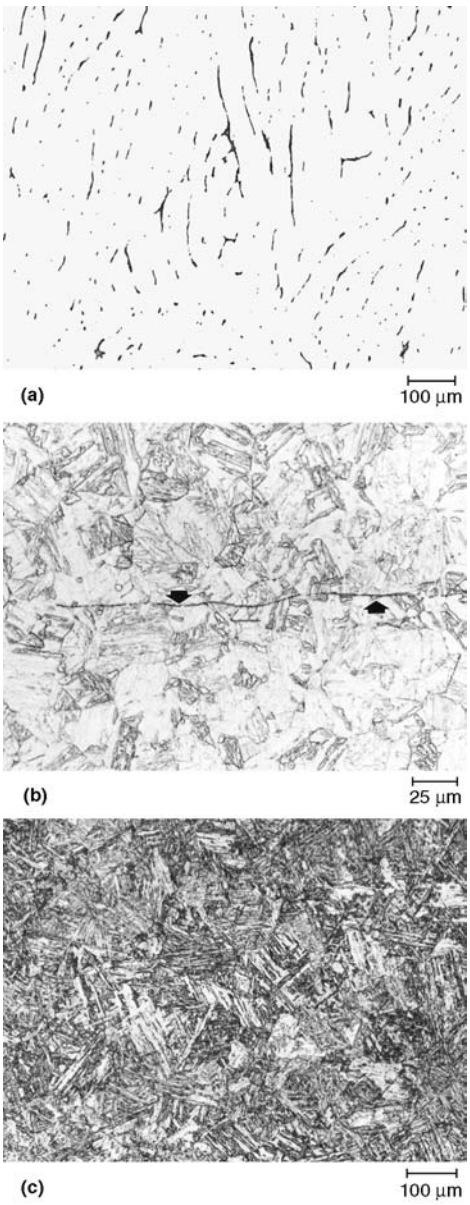

Fig. 62 Microstructure of 15-5 PH stainless steel. (a) Delta-ferrite on a transverse plane from a 20 cm (8 in.) square billet, near the surface. Revealed using Murakami's reagent (2 min at 100 °C, or 210 °F). (b) Delta-ferrite stringer (arrows) in a martensitic matrix on a bar (longitudinal plane) after solution annealing and aging (H925 temper). Revealed using modified Fry's reagent. (c) Martensitic matrix (41 HRC) of a solution-annealed and aged (H900 temper) bar etched with Vilella's reagent

CD-7MCuN, are covered in ASTM A 890. The microstructure of cast duplex stainless steel is shown in Fig. 14.

Maraging Steels. Maraging steels do not contain chromium and do not have stainless characteristics (Table 11). However, they are strengthened by precipitation hardening and have microstructures somewhat similar to precipitation-hardened stainless steels, as discussed in this article. These alloys are nearly free of carbon and form a soft, substitutional type of lath martensite with a high dislocation density when solution annealed. Aging precipitates rod-shaped orthorhombic Ni_3Mo and spherical tetragonal FeTi. Naturally, these precipitates are exceptionally small and can only be observed with the transmission electron microscope. These alloys contain approximately 18% Ni, which depresses the M_s temperature to approximately 150 °C (300 °F). The standard alloys contain 8 to 12.55% Co, which appears to contribute strengthening by short-range ordering. Nickel is rejected from the ordered iron-cobalt regions, and this apparently alters the size of the Ni_3Mo precipitates. The nickel-depleted regions are sites for FeTi formation. If the impurity content is kept low, maraging steels will exhibit exceptionally good toughness at very high strength levels. Formation of Ti(C,N) or TiN and Ti_2S in the grain boundaries embrittles these alloys. Several low-cobalt

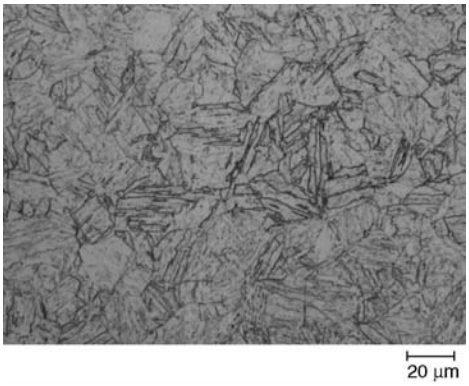

Fig. 63 Martensitic microstructure of PH 13-8 Mo stainless steel etched with modified Fry's reagent

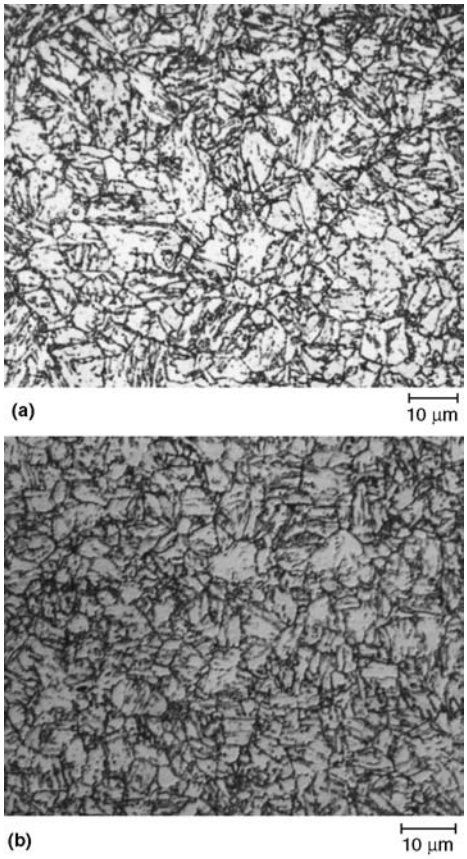

Fig. 64 Martensitic microstructure of Custom 450 stainless steel in the solution-annealed and aged condition. (a) H1050 temper. Etched with modified Fry's reagent. (b) H1150 temper. Etched with waterless Kalling's reagent

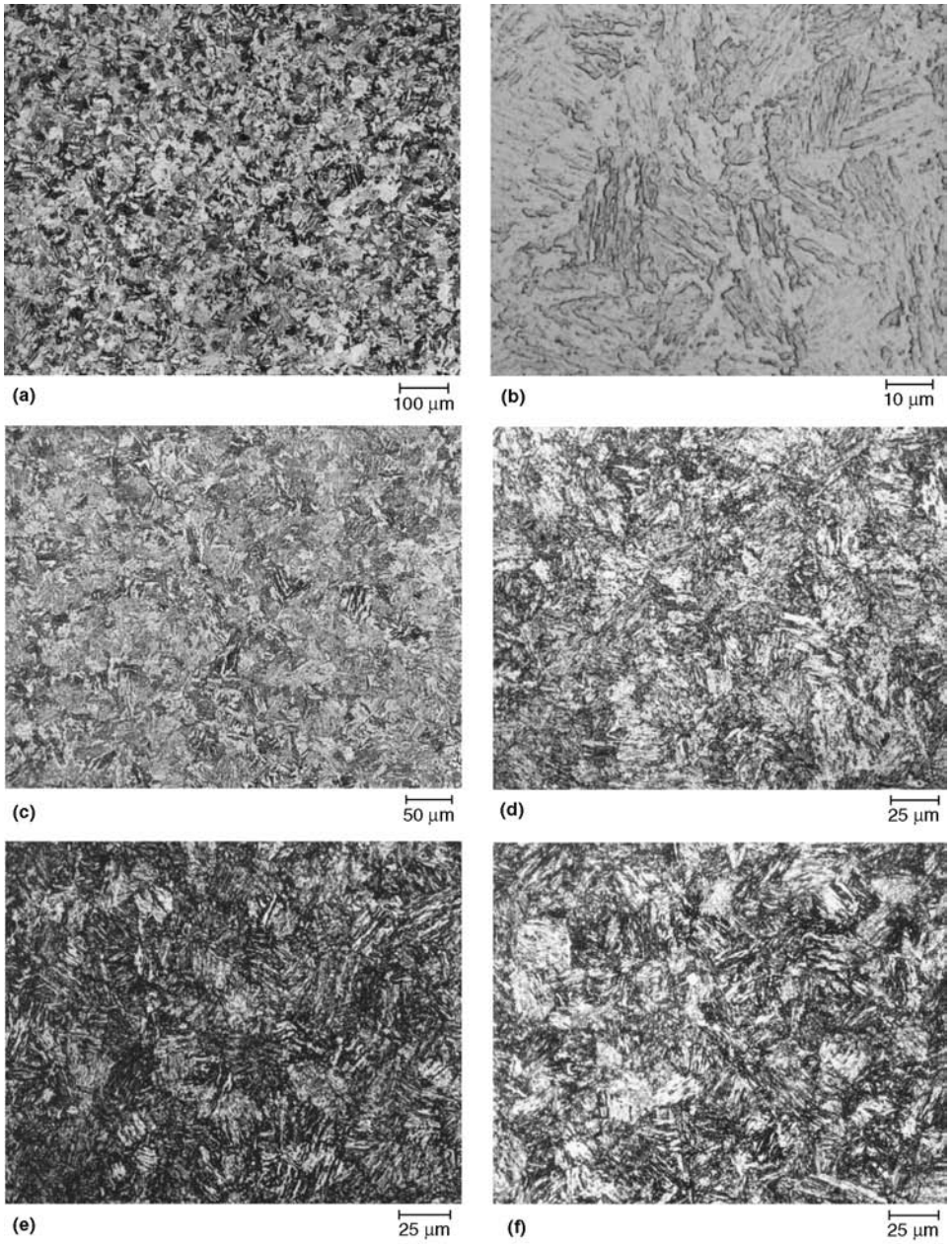

Fig. 65 Martensitic microstructure of Custom 455 stainless steel in the (a) solution-annealed condition (281 HV), etched with Vilella's reagent, and in the solution-annealed and aged conditions. (b) 900 temper (530 HV). Etched with modified Fry's reagent. (c) H950 temper (451 HV). (d) H1000 temper (446 HV). (e) H1050 temper (436 HV). (f) H1100 temper (396 HV). (c) to (f) Etched with Ralph's reagent

and cobalt-free maraging grades have also been developed.

Figures 69(a) and (b) show the microstructure of 18Ni250 maraging steel in the solution-annealed and the solution-annealed and aged conditions. Figures 70(a) and (b) show the microstructure of low-residual 18Ni250 maraging steel in the solution-annealed and the solution-annealed and aged conditions. Figure 71 shows the microstructure of solution-annealed and aged 18Ni300 maraging steel. In each case, the lath martensitic structure is more visible after aging. Figure 72 shows the microstructure of solution-annealed and aged T-250 maraging steel, a cobalt-free grade. The prior-austenite grain boundaries can be revealed in the solution-annealed condition but not after aging. The precipitation-hardenable stainless steels act in a similar manner. The best etchant is electrolytic aqueous 60% nitric acid, but electrolytic aqueous 10% CrO_3 also works.

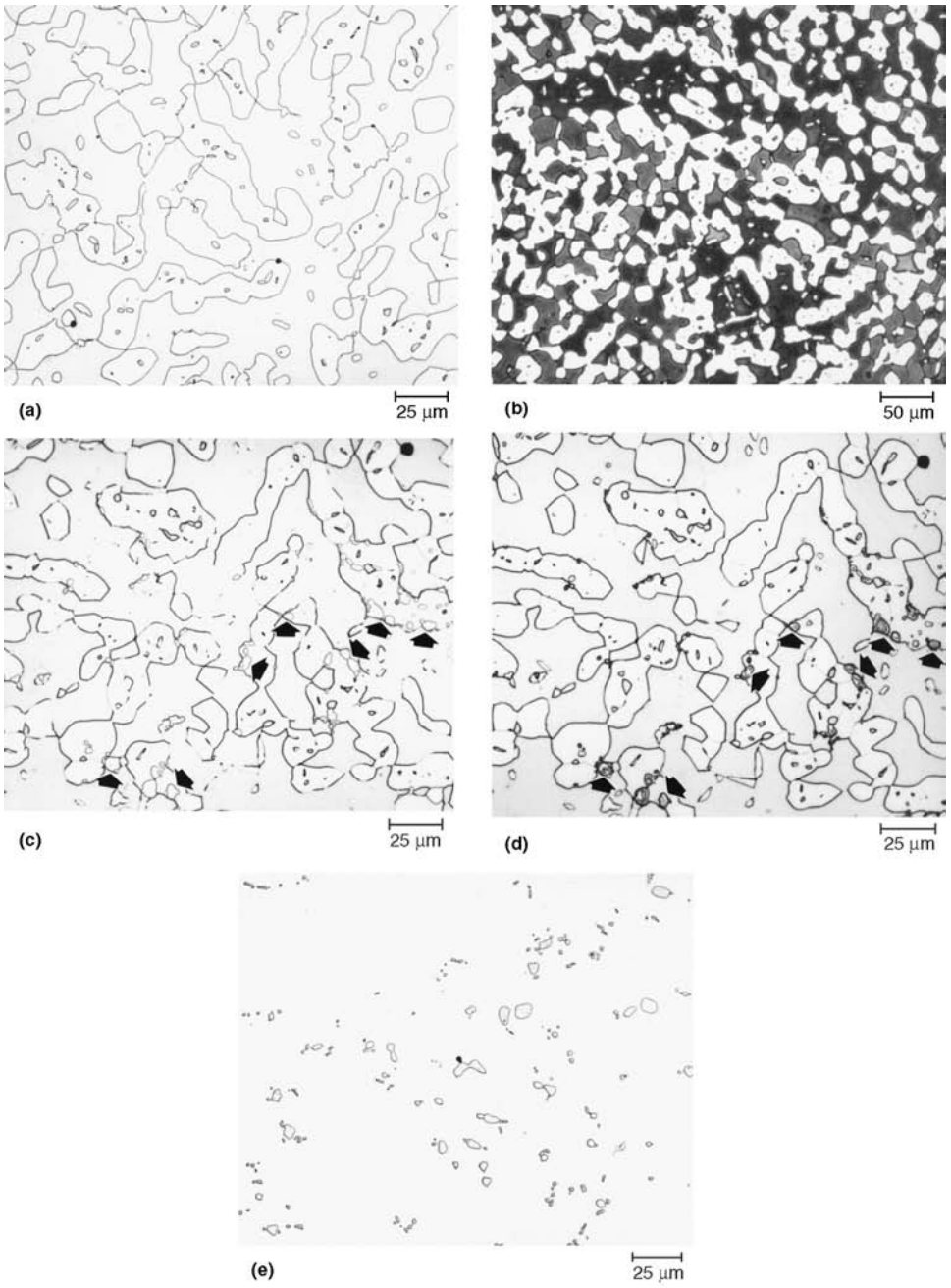

Fig. 66 Ferrite-austenite microstructure of type 312 stainless steel used for welding. (a) and (b) show a solution-annealed bar etched with (a) ethanolic 15% HCl, which reveals the phase boundaries, and (b) Beraha's tint etch, which colors the ferrite. (c) to (e) show the structure of a bar after high-temperature exposure, where σ phase has precipitated. (c) Etched with aqueous 60% HNO_3 at 1 V dc to reveal the phase boundaries (arrows point to particles of σ). (d) Specimen etched as in (c) and given a second electrolytic etch with aqueous 20% NaOH at 2 V dc to color the σ particles. (e) The specimen repolished and etched with concentrated NH_4OH at 6 V dc to color the σ blue

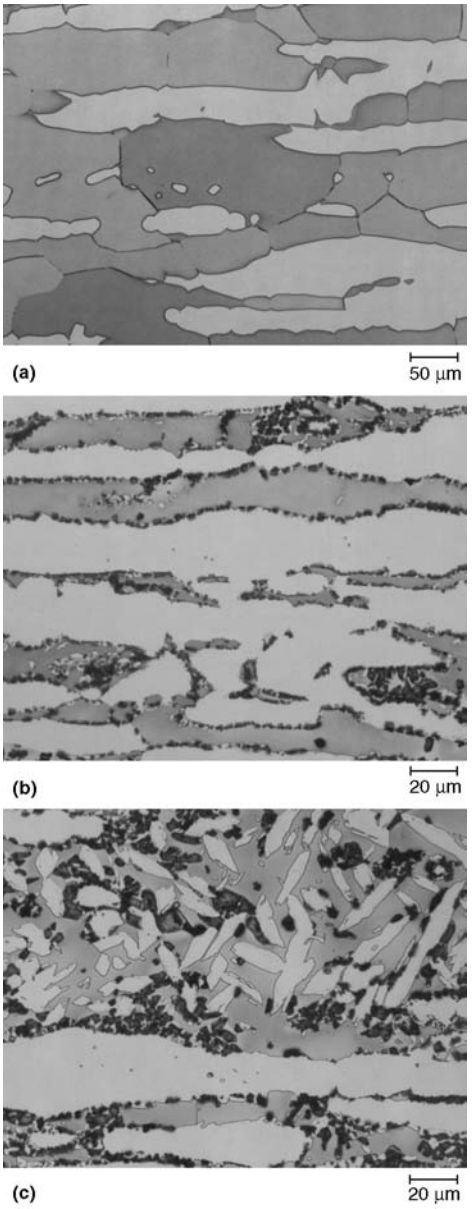

Fig. 67 Ferrite-austenite grain structure of 2205 duplex stainless steel etched with aqueous 20% NaOH at 3 V dc for 15 s to color ferrite. (a) Solution annealed at 1200 °C (2190 °F). (b) After high-temperature exposure at 800 °C (1470 °F) for 2 h, producing σ phase (dark spots). (c) After 8 h at the same temperature

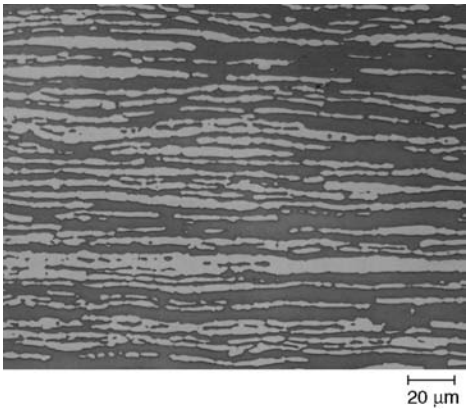

Fig. 68 Ferrite (dark) and austenite in alloy 255 (Ferralium) duplex stainless steel etched with aqueous 20% NaOH at 3 V dc for 3 s

Table 11 Nominal compositions of commercial maraging steels

Grade	Composition(a), %					
	Ni	Mo	Co	Ti	Al	Nb
Standard grades						
18Ni(200)	18	3.3	8.5	0.2	0.1	. . .
18Ni(250)	18	5.0	8.5	0.4	0.1	. . .
18Ni(300)	18	5.0	9.0	0.7	0.1	. . .
18Ni(350)	18	4.2(b)	12.5	1.6	0.1	. . .
18Ni(Cast)	17	4.6	10.0	0.3	0.1	. . .
12-5-3(180)(c)	12	3	. . .	0.2	0.3	. . .
Cobalt-free and low-cobalt bearing grades						
Cobalt-free 18Ni(200)	18.5	3.0	. . .	0.7	0.1	. . .
Cobalt-free 18Ni(250)	18.5	3.0	. . .	1.4	0.1	. . .
Low-cobalt 18Ni(250)	18.5	2.6	2.0	1.2	0.1	0.1
Cobalt-free 18Ni(300)	18.5	4.0	. . .	1.85	0.1	. . .

(a) All grades contain no more than 0.03% C. (b) Some producers use a combination of 4.8% Mo and 1.4% Ti, nominal. (c) Contains 5% Cr

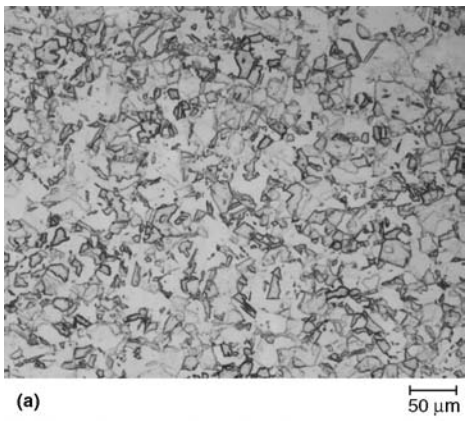

Fig. 69 Martensitic microstructure of 18Ni(250) maraging steel in the (a) solution-annealed condition (305 HV) and the (b) solution-annealed and aged condition (523 HV). Revealed using modified Fry's reagent

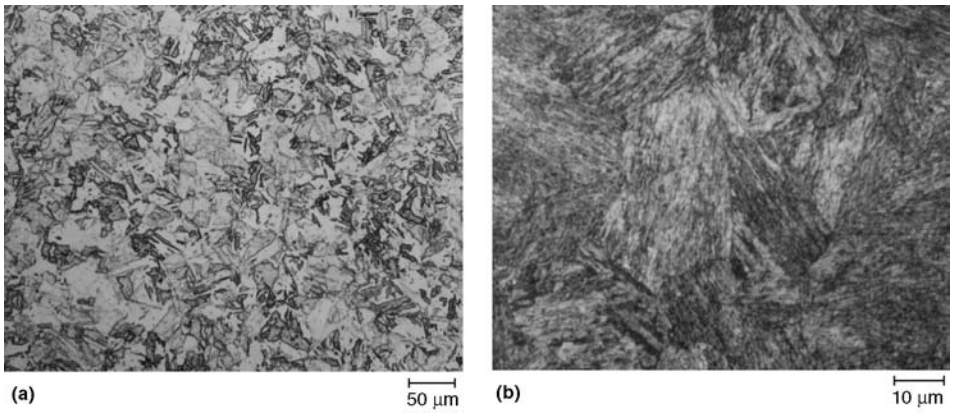

Fig. 70 Martensitic microstructure of low-residual 18Ni(250) maraging steel in the (a) solution-annealed condition (319 HV) and the (b) solution-annealed and aged condition (565 HV). Revealed using modified Fry's reagent

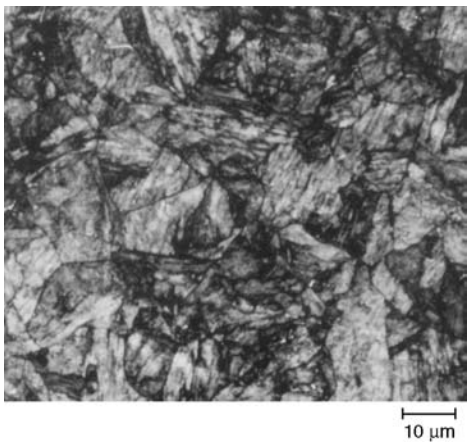

Fig. 71 Martensitic microstructure of solution-annealed and aged 18Ni(300) maraging steel (596 HV). Etched with modified Fry's reagent

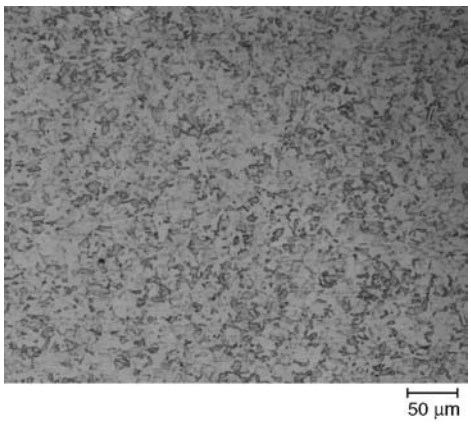

Fig. 72 Martensitic microstructure of solution-annealed and aged cobalt-free Vascomax T-250 maraging steel (535 HV). Etched with modified Fry's reagent

REFERENCES

1. G.F. Vander Voort, *Metallography: Principles and Practice*, McGraw-Hill, 1984. Reprinted by ASM International, 1999
2. F.C. Bell and D.E. Sonon, Improved Metallographic Etching Techniques for Stainless Steel and for Stainless Steel to Carbon Steel Weldments, *Metallography*, Vol 9, 1976, p 91–107
3. J.M. Stephenson and B.M. Patchett, Grain-Boundary Etches for Austenitic and Ferritic Ni-Cr-Mo Corrosion-Resistant Alloys, *Sheet Met. Ind.*, Vol 56, 1979, p 45–50, 57
4. J.J. Gilman, Electrolytic Etching—The Sigma Phase Steels, *Trans. ASM*, Vol 44, 1952, p 566–600
5. E.J. Dulis and G.V. Smith, Identification and Modes of Formation and Re-Solution of Sigma Phase in Austenitic Chromium-Nickel Steels, in STP 110, ASTM, 1951, p 3–37
6. R.J. Gray, Magnetic Etching with Ferrofluid, *Metallographic Specimen Preparation*, Plenum Press, 1974, p 155–177
7. D. Peckner and I.M. Bernstein, Ed., *Handbook of Stainless Steels*, McGraw-Hill, 1977
8. A.L. Schaeffler, Constitution Diagram for Stainless Steel Weld Metal, *Met. Prog.*, Vol 56 (No. 11), Nov 1949, p 680–688
9. W.T. DeLong et al., Measurement and Calculation of Ferrite in Stainless Steel Weld Metal, *Weld. J.*, Vol 35 (No. 11), Nov 1956, p 521s–528s
10. W.T. DeLong, A Modified Phase Diagram for Stainless Steel Weld Metals, *Met. Prog.*, Vol 77, Feb 1960, p 98–100B
11. H.F. Reid and W.T. DeLong, Making Sense out of Ferrite Requirements in Welding Stainless Steels, *Met. Prog.*, Vol 103, June 1973, p 73–77
12. C.J. Long and W.T. DeLong, The Ferrite Content of Austenitic Stainless Steel Weld Metal, *Weld. J.*, Vol 52, July 1973, p 281s–297s
13. S. Mayerhofer and H. Kohl, Statistical Analysis of the Delta Ferrite Content of Austenitic Steels, *Berg Hüttenmänn. Monatsh.*, Vol III (No. 9), BISI 5304, 1966, p 443–453
14. W.T. DeLong, Ferrite in Austenitic Stainless Steel Weld Metal, *Weld. J.*, Vol 53, July 1974, p 273s–286s
15. H.A. Meijer, Quantitative Analysis of Ferrite in Austenitic Stainless Steel, *Br. Weld. J.*, Vol 13, Jan 1966, p 12–17
16. F.C. Hull, Delta Ferrite and Martensite Formation in Stainless Steels, *Weld. J.*, Vol 42 (No. 5), May 1973, p 193s–203s
17. L.S. Aubrey et al., Ferrite Measurement and Control in Cast Duplex Stainless Steels, in STP 756, ASTM, 1982, p 126–164
18. M.T. Leger, Predicting and Evaluating Ferrite Content in Austenitic Stainless Steel Castings, in STP 756, ASTM, 1982, p 105–125
19. L. Pryce and K.W. Andrews, Practical Estimation of Composition Balance and Ferrite Content in Stainless Steels, *J. Iron Steel Inst.*, Vol 195, Aug 1960, p 415–417
20. C.M. Hammond, The Development of New High-Strength Stainless Steels, in STP 369, ASTM, 1965, p 47–53
21. R.B. Gunia and G.A. Ratz, The Measurement of Delta Ferrite in Austenitic Stainless Steel, *Weld. Res. Counc. Bull.*, No. 132, Aug 1968
22. L.A. Brough, The Effects of Processing on Delta Ferrite Measurement, *J. Mater. Energy Syst.*, Vol 5 (No. 1), June 1983, p 36–42
23. W.L. Johns et al., Percent Delta Ferrite Determination in Type 304 Stainless Steel Weldments, *Microstruct. Sci.*, Vol 2, 1974, p 13–22
24. G.M. Goodwin et al., A Study of Ferrite Morphology in Austenitic Stainless Steel Weldments, *Weld. J.*, Vol 51, Sept 1972, p 425s–429s
25. C.B. Post and W.S. Eberly, Stability of Austenite in Stainless Steels, *Trans. ASM*, Vol 39, 1947, p 868–890
26. A.J. Griffiths and J.C. Wright, "Mechanical Properties of Austenitic and Metastable Stainless Steel Sheet and Their Relationships with Pressforming Behaviour," Publication 117, Iron and Steel Institute, 1969, p 51–65
27. R. Stickler and A. Vinckier, Morphology of Grain-Boundary Carbides and Its Influence on Intergranular Corrosion of 304 Stainless Steel, *Trans. ASM*, Vol 54, 1961, p 362–380
28. J.T. Gow and O.E. Harder, Balancing the Composition of Cast 25 Per Cent Chromium-12 Per Cent Nickel Type Alloys, *Trans. ASM*, Vol 30, 1942, p 855–935
29. F.C. Hull, Effects of Composition on Embrittlement of Austenitic Stainless Steels, *Weld. J.*, Vol 52, 1973, p 104s–113s
30. R. Franks et al., Experiments on Etching Procedures for the Identification of the Sigma Phase in Austenitic Chromium-Nickel Stainless Steels, *Proc. ASTM*, Vol 53, 1953, p 143–169, 177–180
31. A.J. Lena, Sigma Phase—A Review, *Met. Prog.*, Vol 66, Sept 1954, p 122–128
32. W.E. White and I. LeMay, Metallographic Observations on the Formation and Occurrence of Ferrite, Sigma Phase, and Carbides in Austenitic Stainless Steels, *Metallography*, Vol 3, 1970, p 35–50, 51–60
33. K.W. Andrews and P.E. Brookes, Chi Phase in Alloy Steels, *Met. Treatment Drop Forg.*, July 1951, p 301–311
34. P.K. Koh, Occurrence of Chi Phase in Molybdenum-Bearing Stainless Steels, *Trans. AIME*, Vol 197, 1953, p 339–343
35. J.S. Kasper, The Ordering of Atoms in the Chi-Phase of the Iron-Chromium-Molybdenum System, *Acta Metall.*, Vol 2, May 1954, p 456–461
36. J.G. McMullin et al., Equilibrium Structure in Fe-Cr-Mo Alloys, *Trans. ASM*, Vol 46, 1954, p 799–811
37. F.L. Ver Snyder and H.J. Beattie, The Laves and Chi Phases in a Modified 12Cr Stainless Alloy, *Trans. ASM*, Vol 47, 1955, p 211–230
38. B. Weiss and R. Stickler, Phase Instabilities during High Temperature Exposure of 316 Austenitic Stainless Steel, *Met. Trans.*, Vol 3, April 1972, p 851–866
39. H. Hughes and S.R. Keown, Precipitation of a Transition Intermetallic Compound (R-Phase) in Steels, *J. Iron Steel Inst.*, Vol 206, March 1968, p 275–277
40. D.J. Dyson and S.R. Keown, A Study of Precipitation in a 12% Cr-Co-Mo Steel, *Acta Metall.*, Vol 17, 1969, p 1095–1107
41. J.K. Lai and J.R. Haigh, Delta-Ferrite Transformation in a Type 316 Weld Metal, *Weld. J.*, Vol 58, Jan 1979, p 1s–6s
42. H.T. Beattie and W.C. Hagel, Intermetallic Compounds in Titanium-Hardened Alloys, *Trans. AIME*, Vol 209, July 1957, p 911–917
43. K.W. Andrews and H. Hughes, discussion of paper "Aging Reaction in Certain Superalloys," *Trans. ASM*, Vol 49, 1957, p 999
44. J.J. Demo, *Structure, Constitution, and General Characteristics of Wrought Ferritic Stainless Steels*, STP 619, ASTM, 1977
45. R.H. Thielemann, Some Effects of Composition and Heat Treatment on the High Temperature Rupture Properties of Ferrous Alloys, *Proc. ASTM*, Vol 40, 1940, p 788–804
46. K.J. Irvine et al., The Physical Metallurgy of 12% Chromium Steels, *J. Iron Steel Inst.*, Vol 195, Aug 1960, p 386–405
47. K.J. Irvine et al., Controlled-Transformation Stainless Steels, *J. Iron Steel Inst.*, Vol 192, July 1959, p 218–238
48. A. Kasak et al., Development of Precipitation Hardening Cr-Mo-Co Stainless Steels, *Trans. ASM*, Vol 56, 1963, p 455–467
49. B.R. Banerjee et al., Structure and Properties of PH15-7Mo Stainless, *Trans. ASM*, Vol 57, 1964, p 856–873
50. H.L. Marcus et al., Precipitation in 17-7PH Stainless Steel, *Trans. ASM*, Vol 58, 1965, p 176–182
51. R.C. Gibson et al., Properties of Stainless Steels with a Microduplex Structure, *Trans. ASM*, Vol 61, 1968, p 85–93
52. S. Floreen and H.W. Hayden, The Influence of Austenite and Ferrite on the Mechanical Properties of Two-Phase Stainless Steels Having Microduplex Structures, *Trans. ASM*, Vol 61, 1968, p 489–499
53. H.D. Solomon and T.M. Devine, "Duplex Stainless Steels—A Tale of Two Phases," paper 8201-089, presented at the 1982 ASM Metals Congress (St. Louis, MO), 1982